SEISMIC REFRACTION INVESTIGATION OF THE SHALLOW SUBSURFACE OF THE LOWER RIO SALADO, NORTHWEST OF SAN ACACIA, NEW MEXICO

by

Steven P. Zody

submitted in partial fulfillment of requirements for the degree of

Master of Science

in Geology

New Mexico Institute of Mining and Technology

Fall 1988

ABSTRACT

The Rio Salado is an ephemeral tributary of the Rio Grande in central New Mexico. Hydrologic studies have found that the elevation of the water table along the Rio Salado declines 38 meters in approximately 4 kilometers. The water table has been mapped through the interpretation of seismic refraction data. Approximately 4.8 km of the channel was investigated by 48 seismic refraction profiles. Data were aquired using 12 geophones per profile, generally with geophone spacings of 2 to 6 meters. Seismic lines were run as reversed profiles, and a sledge hammer and metal plate were used as a seismic source. Three horizons were detected and are interpreted to be an upper, highly attenuative (Q - 10), dry alluvial layer with a velocity of 250–350 m/sec and a thickness of 1.5–2.0 meters; partially saturated alluvium with a velocity of 1100–1600 m/sec and a thickness of 1.5–10 meters; and the aquifer with a velocity of 1900–2300 m/sec. The thickness of the aquifer could not be determined but probably exceeds 20 meters. The water table exhibits two sudden and significant elevation drops along the lower Rio Salado. The gradient of the water table increases to approximately 18 m/km and 14 m/km, respectively, at these two locations. The projected location of the Loma Blanca fault beneath the Rio Salado channel coincides with a water table elevation decline and supports the conclusion that the fault crosses the channel. The water table begins to drop roughly 300 meters west of the fault because it parallels the paleotopography of the Santa Fe Group rocks across the fault scarp beneath the alluvial section. The second elevation drop is approximately 3300 meters downstream. Here the dimensions of the aquifer increase as a result of previous erosion of the Santa Fe Group along the Rio Grande flood plain.

ACKNOWLEDGEMENTS

I would like to thank my committee members, Dr. Dave Johnson and Dr. John MacMillan, and especially Dr. John Knapp who served as the advisor of this thesis. I would like to thank Dr. Dan Stephens for bringing to my attention the need for a project of this nature along the Rio Salado. A number of people provided support and assistance during the course of the study : Mr. Ted Stans allowed access to the Sevilleta National Wildlife Refuge; Don Marshall, Julio Montano, Tracey Spence, and Jim Gridley each volunteered a day as field assistants; Dr. John Hawley and Dr. Allan Sanford offered insights to a number of questions; and Don Marshall offered valuable assistance in generating computer programs to plot the data. A special thank you goes out to my wife, Jacki, who provided field assistance, moral support, and a great deal of patience while at the same time working on research of her own. Financial support for this project was provided by the New Mexico Tech Geoscience department, Mobil Oil Corporation, the New Mexico Geological Society, and the Richard Matuszeski Graduate Research Fund.

TABLE OF CONTENTS

LIST OF FIGURES

LIST OF TABLES

INTRODUCTION

Introduction

The Rio Salado is an ephemeral stream in central New Mexico flowing roughly eastward to the Rio Grande (Figure 1). Although there have been geologic and hydrologic studies of the Rio Salado area (Stephens, 1988; Havlena, 1988; Machette, 1978; Evans, 1963), the subsurface along the lower Rio Salado has not been extensively investigated. Hydrologic studies in the area (Stephens, 1988; Havlena, 1988) have in fact spawned more questions about the area. It is the objective of this study to offer some explanations about the shallow subsurface geology of the eastern extent of the Rio Salado. Specifically, depth to the water table has been mapped based upon information obtained from shallow seismic refraction work. Refraction data has been combined with available hydrologic data to show that there are permanent steps in the water table that may be correlated to known geologic features. Indirectly, abrupt changes in the depth to the water table can be used to indicate where faults pass beneath the Rio Salado channel.

Seismic refraction exploration techniques have historically been used for subsurface studies where depths of investigation are greater than 50 meters. These techniques have been practically applied in the petroleum and minerals industries and have been used for crustal studies. Only in recent years has considerable attention been given to utilizing seismic refraction for studies to depths of 25 meters. Refraction methods have been employed to a small degree for engineering site investigations and for hydrologic studies over the past two or three decades, but the practical and

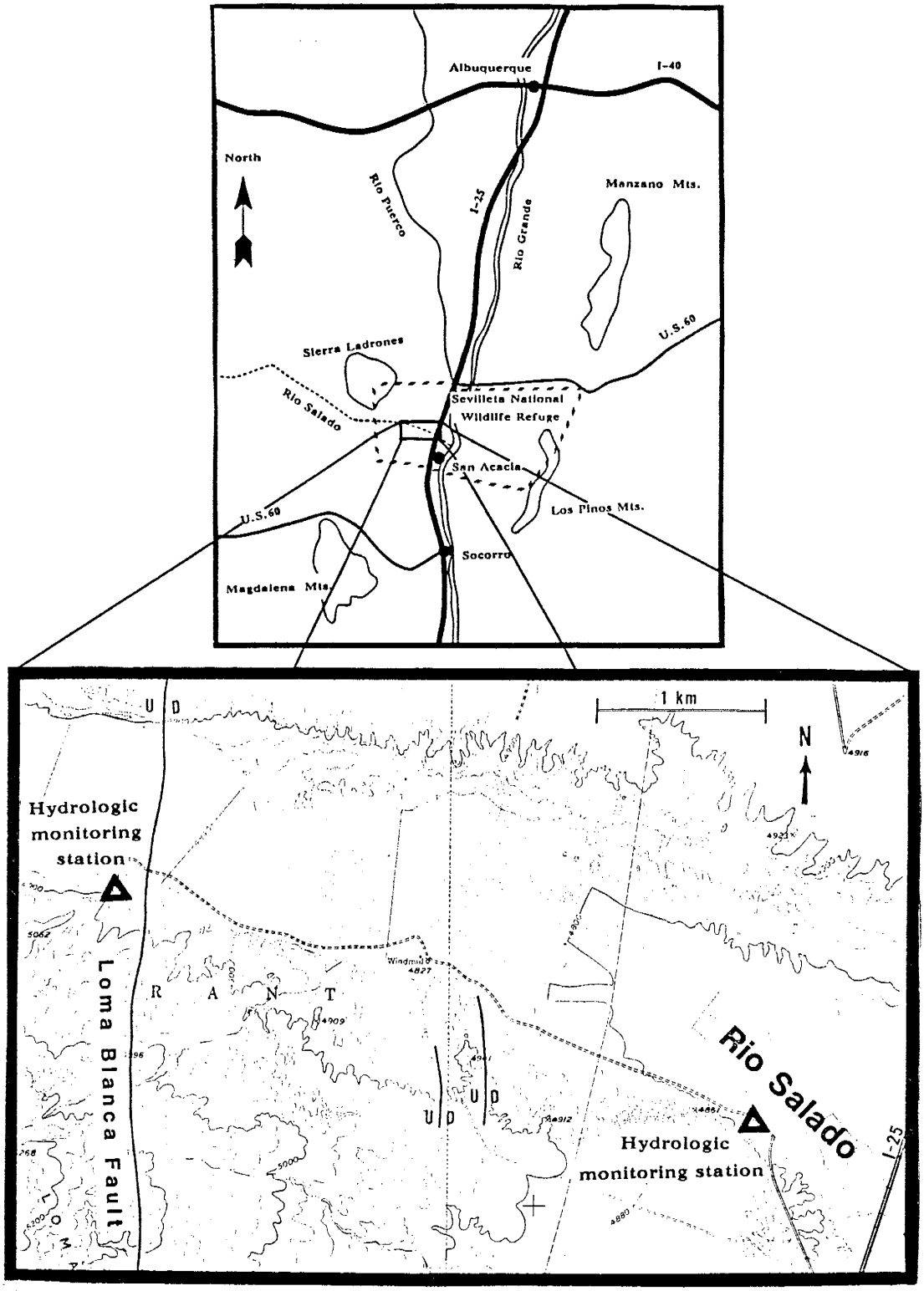

Figure 1 : Location of the study area and the two hydrologic monitoring sites.

economic potential of these applications has only begun to be fully realized. In many shallow investigations, explosives are not required as a seismic source. A metal plate struck by a sledge hammer will provide a sufficient energy source. Survey lines for shallow studies can generally be less than 200 meters and often less than 100 meters. High quality, portable field equipment is constantly being improved so field surveys can be conducted and moved with relative ease. Taking these factors into account, seismic refraction surveys aimed at delineating shallow horizons can be conducted by only one to three workers in an expeditious and inexpensive manner.

In hydrologic studies, the seismic refraction method has most often been utilized to map buried channels (Eaton, 1974; Eaton and Watkins, 1967; Warrick and Winslow, 1960; Pakisar and Black, 1957; Johnson, 1954). Investigations of this nature have been most common in glacial deposits of the Midwest and the East. The targets of these studies are glacially scoured valleys which have since been filled with sediments that act as good aquifers. Even in this type of exploration, the depth of investigation is commonly greater than 150 meters.

Determining depths to the water table is another application of refraction techniques. This procedure has become more widely used in recent years. It is an excellent method of mapping the water table. Where shallow investigations are applicable, aquifers are generally composed of unconsolidated sands and gravels. Marked velocity contrasts occur at the boundary of the saturated and unsaturated sediments which is ideal for the seismic refraction method. Groundwater studies by Haeni (1986), Mazzaferro (1984), and Morrissey (1983) have been very successful as a result of incorporating refraction data into projects. The results of seismic interpretations were used to design exploratory drilling programs. Then seismic

data, drilling data, and previously existing data were integrated to map the water table and bedrock. Map data were then used for a groundwater flow model of the aquifer.

Seismic refraction is also well suited for investigations of variations in water table elevations. The occurrence of increased hydraulic gradients which cause depths to water to vary, seems to be a common situation about which relatively little has been written (Phillips, 1988, personal communication; Stephens, 1988, personal communication; Czarnecki, 1988, personal communication). Hydraulic gradient increases have been documented in Nevada by Winograd and Thordarson (1975). In this case, the features are very large scale. The study encompasses a number of basins and depths of investigation are on the order of 600 meters. Depth to water varies by as much as 130 meters, and the elevation of the water table ranges from 720 to 780 meters above mean sea level. Czarnecki (1987) identified similar large scale features in southwestern Nevada. Winograd and Thordarson (1975) and Czarnecki (1987) found in their studies that water table variations are due to extremely complex structural and hydrologic environments in which they occur. Olmsted, Loeltz, and Irelan (1973) recognized water table variations of approximately 10 meters in southwestern Arizona. A fault cutting the aquifer was determined to be the factor controlling the water table in this area. The existence of fault gouge and mineralization along the fault prohibit groundwater from moving across the zone causing variable depths to water.

Groundwater discrepencies of this nature have also been documented along the Rio Salado in central New Mexico (Stephens, 1988). Two monitoring stations were utilized to acquire hydrologic data along the Rio Salado in this study (Figure 1). Rio Salado alluvium, the principal shallow

water aquifer, was monitored during the investigation. It was discovered that depth to the water table was significantly different between the two monitoring stations. At the western location, the water table was detected approximately 1 meter below the channel, whereas at the eastern site it was located 9 meters below the channel. No information was available between the two sites (a distance of approximately 4 kilometers) to help explain this phenomenon. Stephens suggested that this might be due to the Rio Salado alluvium being thicker on the downthrown side of the Loma Blanca fault, which is located just east of the western site.

An efficient approach to this problem is utilization of seismic refraction exploration techniques, since in the geologic setting of the Rio Salado unconsolidated Rio Salado alluvium is acting as the aquifer. The alluvium is composed primarily of sands and gravels, therefore, a significant velocity contrast occurs at the boundary of the unsaturated alluvium and the saturated alluvium. In addition to delineating water table depths, refraction data are useful for interpretation of subsurface characteristics which may affect the water table. The purpose of this study was to aquire and interpret refraction data in the Rio Salado channel so that the water table could be mapped and conclusions drawn about the parameters controlling water levels.

In general, seismic exploration techniques have been underutilized in hydrologic and shallow subsurface geologic investigations. It is the intent of this study to not only answer the questions applicable to the Rio Salado, but also to illustrate the usefulness and efficiency of the seismic refraction method in obtaining shallow water table data. This data may then be interpreted so that geologic inferences can be made. These are methods which may be employed prior to more expensive and time consum-

ing procedures such as drilling or excavation. The utilization of seismic exploration techniques in the early stages of an exploration or research program can often determine the feasability and/or assist in determining optimum sites for subsequent exploration strategies.

The Rio Salado

The Rio Salado is an ephemeral tributary of the Rio Grande, flowing from west to east through the Sierra Ladrones and Lemitar Mountains and entering the Rio Grande north of San Acacia, New Mexico. The area of interest is that portion of the Rio Salado approximately 4.5 kilometers west of the confluence on the Sevilleta National Wildlife Refuge (Figure 1).

In the region of interest, the Rio Salado channel is straight and distinctly braided. Its width to depth ratio is relatively large as the channel width is commonly greater than 200 meters and the channel depth ranges between 1 and 2 meters. Quaternary sands and gravels are the predominant sediments in the Rio Salado channel. The channel is flanked on the south by other Quaternary alluvial sands and silts and by outcrops of axial stream deposits and piedmont slope/alluvial flat deposits of the Tertiary/Quaternary Santa Fe Group (Machette, 1978). The northern side of the channel is primarily eolian deposits. Some of these sediments have been stabilized by mesquite vegetation and some sediments are currently active. Within the areas of active eolian sedimentation along the northern side of the channel, a large dune system occurs. The general surface geology of the area is illustrated in Figure 2.

Flow in the Rio Salado is fairly rare as the channel is dry an

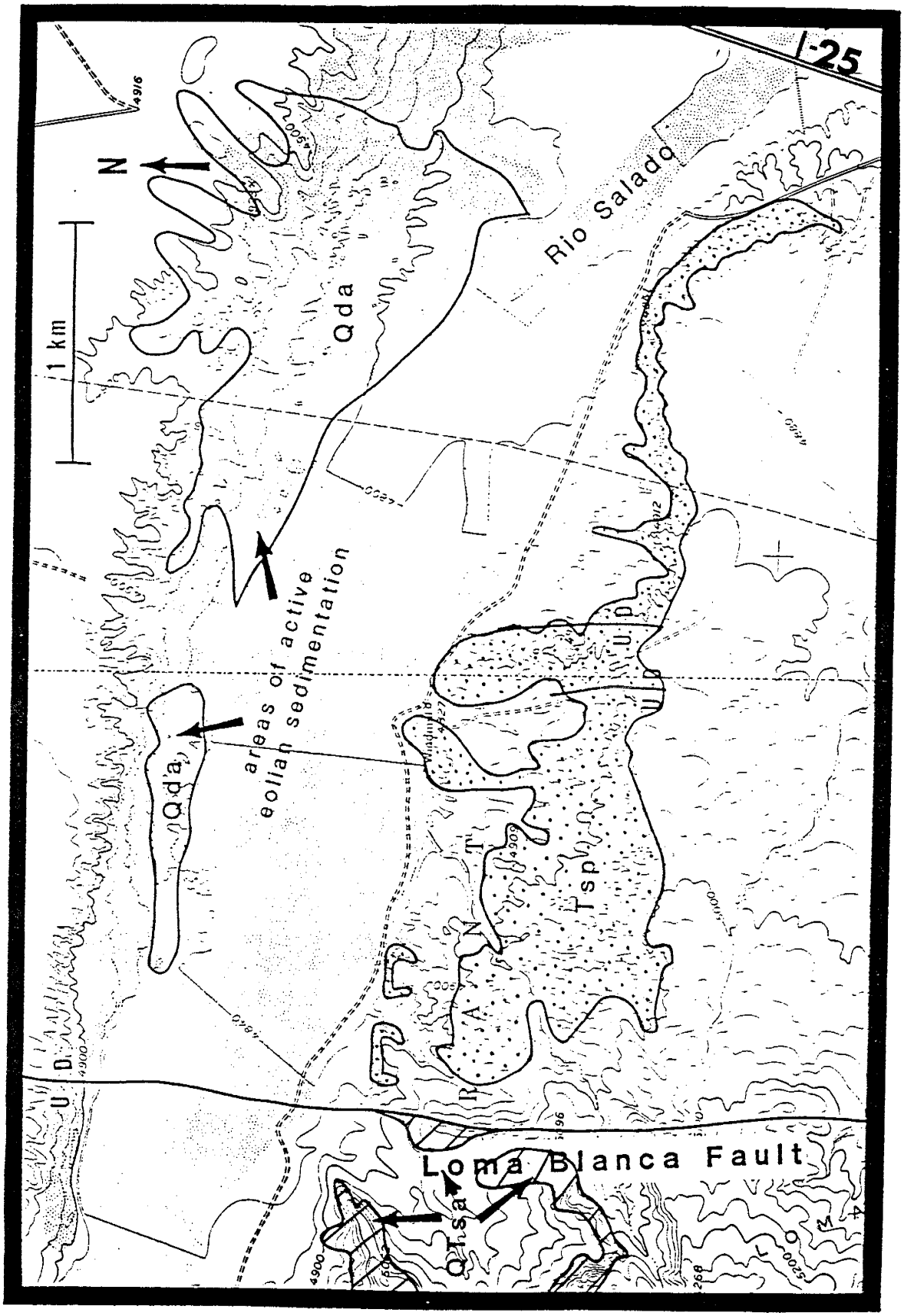
25
N
1 km
Rio Salado
Qda
areas of active
eolian sedimentation
Qda
Tsp
Loma Blanca Fault

average of 320 days per year (Stephens, 1988). When there are flow events, they are usually of low volume. Stream discharge generally occurs in narrow, meandering channels within the main channel. Low flow events create a small meandering subsystem which often cuts local channels up to 0.5 meter deep. Since flow events can be created or dissipated very quickly, meanders are frequently cut off and the meandering subsystem will migrate within the main channel. During large flow events, the channel will be transformed back to a relatively uniform surface as the highly competent waters grade the previous depositional and/or erosional features.

Since the channel is dry almost ninety percent of the year, eolian sedimentation is a prevalent process. Localized channels serve as depositional sites for wind blown sediments during dry periods. Much of the surface sediment is transported from the channel to the active dune fields to the north of the Rio Salado. The configuration of the channel surface is altered quite regularly, but most of the morphological changes are relatively minor and are dependent on the frequency and intensity of flow events and intensity and direction of the wind. Although fluvial and eolian depositional features are evident, the Rio Salado is currently in a stage of degradation (Havlena, 1988; Denny, 1941).

The Loma Blanca fault crosses the Rio Salado in the western part of the study area. Oriented almost directly north-south, the fault intersects the channel at approximately a right angle. The throw on the Loma Blanca fault is down to the east and believed to be greater than 30 meters (Machette, 1978). Two small faults have also been mapped by Machette on the south side of the channel near the central portion of the study area. Similar to the Loma Blanca, these are normal faults oriented approximately north-south and are downthrown to the east. As mapped, however, these

faults terminate before reaching the Rio Salado. Approximately 2.5 kilometers west of the study area is the Loma Pelada fault zone. This normal fault (down to the east) is hypothesized to have a displacement of at least 305 meters, indicated by the fact that Tertiary rocks of the Santa Fe Group are now found adjacent to Quaternary rocks of the Santa Fe Group (Evans, 1963).

Figure 3 illustrates the generalized stratigraphic column of upper Cenozoic deposits in the lower Rio Salado region. Denny (1940 and 1941) was responsible for much of the pioneering work in describing the geology of the area. He essentially defined and described the Tertiary (1940) and Quaternary (1941) geology of the "San Acacia area." The San Acacia area in his studies includes the southern part of the Albuquerque–Belen basin, the north end of the Socorro basin, and the Snake Ranch Flats (Figure 4).

The Popotosa Formation was initially described by Denny. The formation, which consists of eroded volcanic sediments and small amounts of tuff, was interpreted to represent the transition between Miocene volcanics and Pliocene basin deposits. The Popotosa is an alluvial deposit which was deposited in an enclosed basin under semiarid conditions. Petrologic studies indicate that the depositional site included a playa lake. Denny also concluded from observations of the Popotosa that the Sierra Ladrones were highlands at least as early as Popotosa (late Miocene) time. The Popotosa has since been assigned to the Santa Fe Group (Machette, 1978).

The detailed mapping of the Santa Fe Formation (as referred to by Denny, and generally equivalent to Machette's Sierra Ladrones Formation) was also a significant contribution by Denny. He determined that the formation is composed of alluvial fan and fluvial deposits with at least one contemporaneous andesitic lava flow. Paleontological studies indicate that

Generalized Stratigraphic Column of the Lower Rio Salado Area

(map units after Machette, 1978)

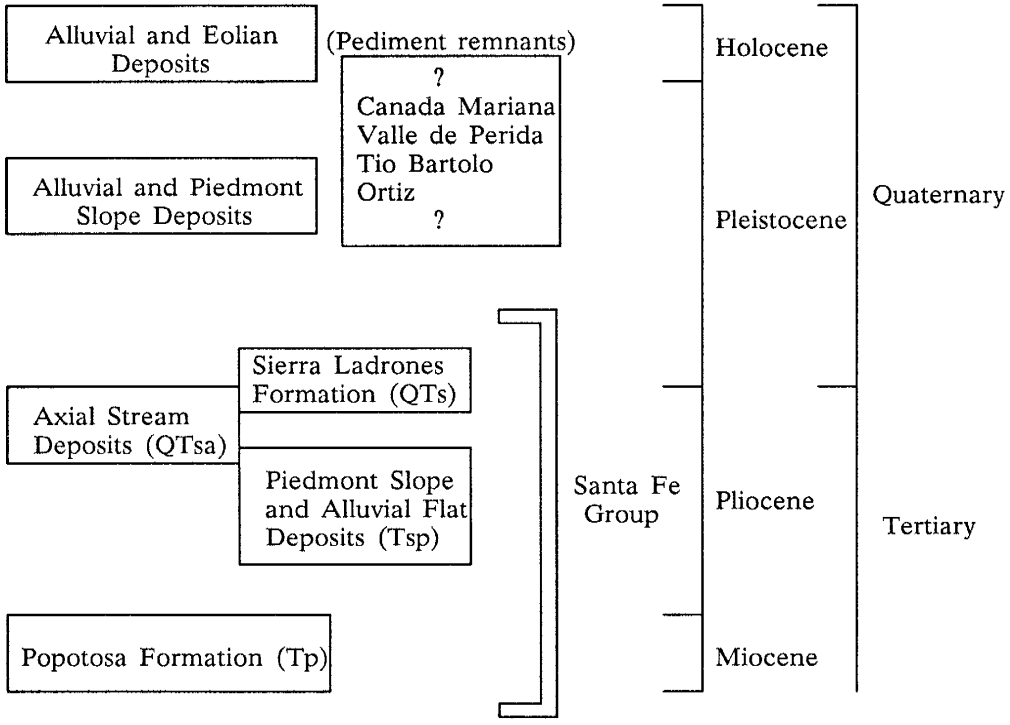

Figure 3 : Stratigraphic column of the study area. Column shows section investigated by Denny (1940 and 1941) and mapped by Machette (1978).

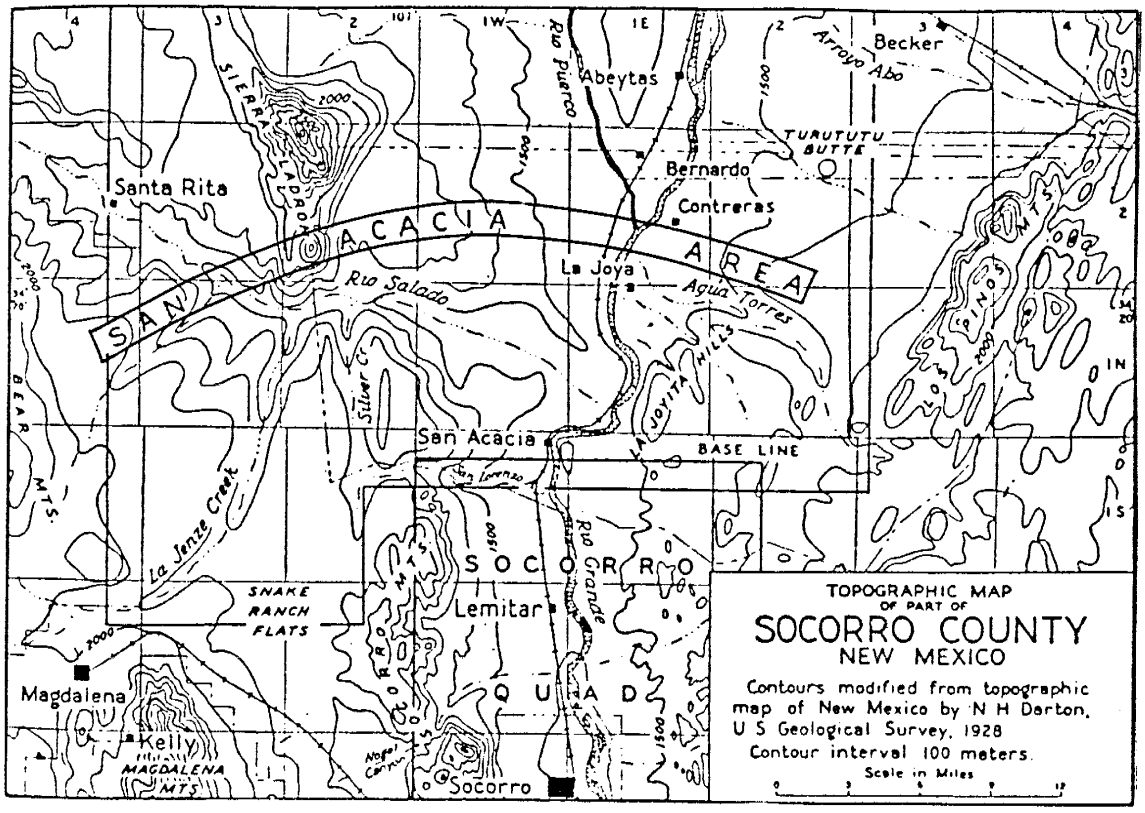

Figure 4 : Map of the San Acacia area within which Denny (1940 and 1941) investigated the Tertiary and Quaternary geology. (From Denny, 1941).

the Santa Fe Formation in the San Acacia area is middle to upper Pliocene in age. Sediments of the Santa Fe Formation were derived from surrounding highlands and deposited in two basins separated by an alluvial divide extending from the Sierra Ladrones to La Joyita Hills.

According to Denny (1941), the Quaternary period in the area was marked by the formation of four pediments. These include (in order of decreasing age) the Ortiz pediment, Tio Bartolo pediment, Valle de Parida pediment, and the Canada Mariana pediment. All formed in response to the Rio Grande lowering its channel during various time periods. Denny did not assign specific ages to the pediment remnants he observed other than indicating all to be post-Santa Fe and to assign the youngest (Canada Mariana) to late Pleistocene.

Denny (1941) inferred that the Rio Salado achieved its present course through piracy. He believed that during Tio Bartolo time, the Rio Salado flowed across the Snake Ranch Flats and to the south of Socorro. A westward cutting stream worked its way through the Sierra Ladron-Socorro Mountain divide during Valle de Parida time and allowed the channel to follow its current path. During Canada Mariana time, the Rio Salado experienced a period of downcutting during which the river eroded deposits of previous arroyos down to at least its present elevation. This was followed by a period of aggradation during which at least 30 meters of sediment was deposited within the channel. Recent times have once again been dominated by erosional processes.

Thick caliche deposits cap the pediment remnants. During the current period of degradation, these resistive layers have lead to the formation of nickpoints (breaks in slope) where tributaries enter the Rio Salado. In addition, the sediments just beneath the caliche layers are generally un-

consolidated and, therefore, easily eroded when exposed along the channel bank. This situation further enhances the development of nickpoints.

Evans (1963) confirmed Denny's (1940) interpretation of the Popotosa Formation through the mechanical analyses of sediments. He states that sediments derived from the Ladron mountain block were transported fluvially to the playas of the Popotosa Formation. A fluvial origin for the Santa Fe Group was also supported by this study.

The sand dunes on the north side of the Rio Salado were also researched by Evans. He observed that the dune sediments are derived from the Rio Salado channel and are multicycle sediments. In studying wind patterns, Evans concluded that the dunes were shaped by southern winds during the summer and by northern winds during the winter. Morphological changes in response to the southern winds were found to be much more dominant than those produced by northern winds.

Hydrologic research was conducted along the Rio Salado by Stephens (1988). This investigation was concerned primarily with evaluating groundwater recharge from ephemeral streams and the effects of unsaturated flow on seepage and recharge. Two monitoring locations were utilized to aquire hydrologic data along the Rio Salado. The Rio Salado alluvium, the principal shallow aquifer, was monitored during the investigation. The direction of groundwater flow was found to be eastward, nearly parallel to the Rio Salado. As previously mentioned, it was also discovered that the depth to the water table varied between the two monitoring sites.

DATA ACQUISTION

Introduction

The majority of the seismic surveys were run in July, August, and September, 1987. Additional data were collected during November, 1987 and February and April, 1988. All lines, with one exception, were run within the Rio Salado channel. One line was run adjacent to the western hydrologic monitoring site so that a direct measurement of depth to water could be compared to the seismic results. This allowed a direct correlation of the water table and seismic velocity data. Approximately 4.8 kilometers of the channel was investigated. Forty-eight lines were run at a total of thirty sites covering the area from the old U.S. 60 bridge to approximately 0.8 kilometers west of the Loma Blanca Fault (Figure 5). The two hydrologic monitoring sites fall within the boundaries of the area of investigation.

Field Procedures

Seismic data was collected using an EG&G ES-1225 Multichannel Signal Enhancement Seismograph. Twelve geophone stations were recorded for each shotpoint. Twenty Hz geophones were used to record ground motion because the surveys were conducted in a highly attenuative environment. The use of higher frequency geophones would not have resulted in significantly different data because in this region only the lower frequency components of the signal are transmitted back to the surface. One-hundred Hz geophones were used when attenuation experiments were made to help

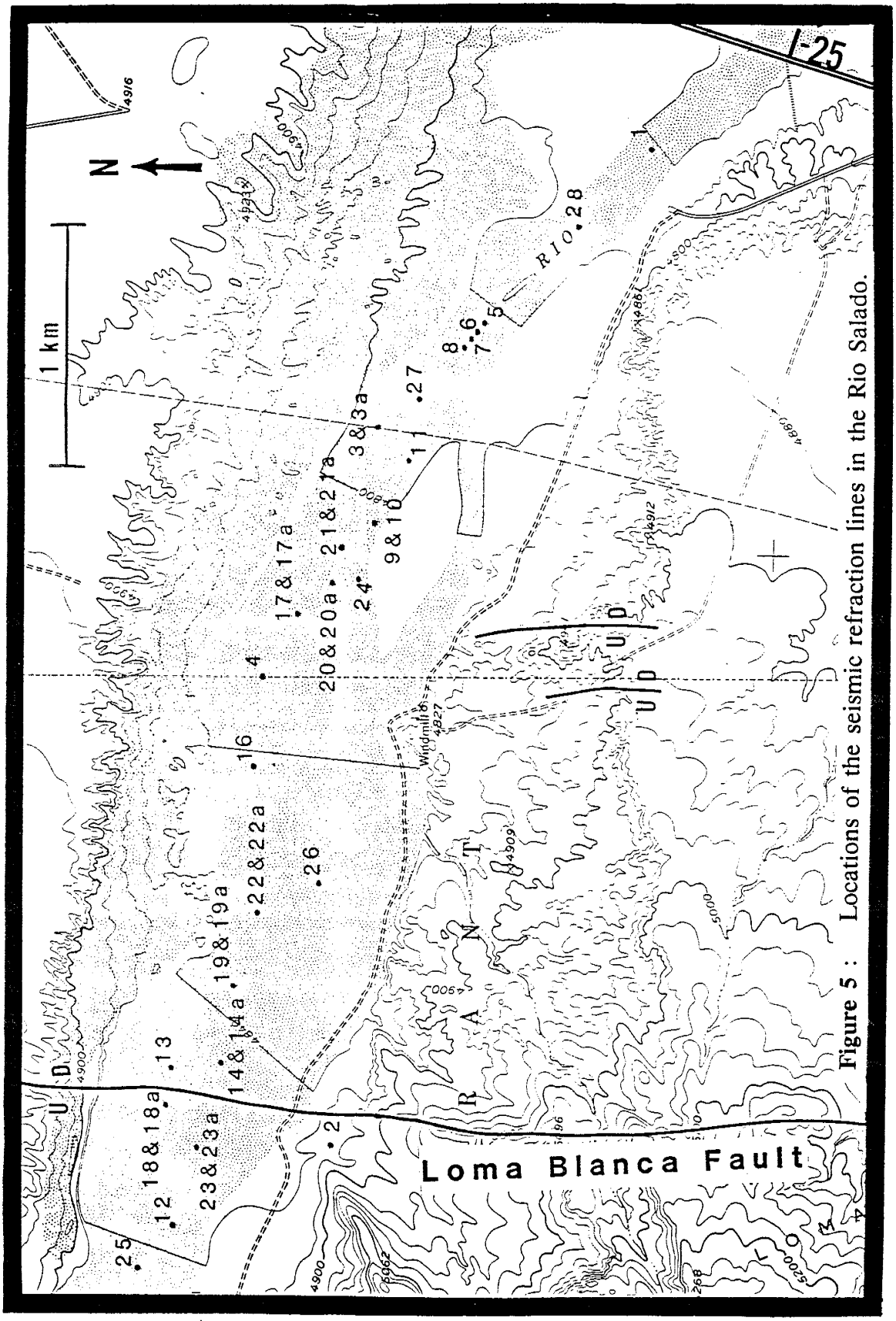

Figure 5 : Locations of the seismic refraction lines in the Rio Salado.

substantiate the energy loss. In these experiments, the geophone spacings and shot offsets were very small, and the objective was to directly observe the loss of the high frequencies with distance.

The energy source to initiate the propagation of seismic waves consisted of striking a metal plate with an eight pound sledge hammer. The plate was placed firmly on the ground surface at all shotpoints to insure that a favorable coupling effect was obtained. A triggering device mounted on the sledge hammer signaled the seismograph to begin recording as soon as the plate was struck. The plate was struck between two and ten times at each shotpoint so that the data could be stacked a sufficient number of times to achieve a high signal to noise ratio. Seismograms were printed in the field directly from the ES-1225.

Data was collected only when the arroyo channel was completely dry. This procedure was followed so that the geophones would function efficiently and so that data collection was restricted to days when the water table was at a relatively stable elevation. Although Stephens (1988) stated that the water table rose in response to a few large runoff events, he also indicated that fluctuations are minimal under normal conditions (personal communication, 1987).

For the most part, field work was conducted when winds were relatively calm to reduce the possibility of noise being introduced into the data. Occasionally winds did pick up during the day. When this occurred, the geophones were placed as far into the ground as possible, and the geophone cables were stabilized with rocks or buried with sand. If wind noise was still introduced into the data, the stacking capabilities of the ES-1225 minimized the effect even further.

As previously mentioned, multiple hammer impacts were pro-

duced at each shotpoint. The signal from each successive impact was stacked, or added, to previous signals from the same shotpoint so that the amplitude of the coherent refracted signal was increased relative to that of the random noise. In the event that the signal from a particular impact was of poor quality at a specific geophone, it was simply rejected and the process continued.

Most seismic lines were run as reversed profiles. Thus, two seismic records were obtained at each line location, one for a shot at each end of the line. The seismogram pair is a record of the signal travelling in opposite directions through the same rock or sediment section. The travel times and derived velocities from each record can be compared to detect dip in the subsurface. The dip calculated from this type of an array represents the apparent dip in the direction of the profile.

Seismic lines run within the Rio Salado channel were run parallel to the channel and as close to the center of the primary channel as possible. Figure 5, showing the line locations, indicates that a number of lines are closer to northern bank of the channel. This distribution was dictated by the fact that portions of the southern part of the channel are heavily populated with salt cedar vegetation. Line locations were kept away from vegetated areas to help minimize noise being introduced into the data. In the event of even slightly windy conditions, the shallow root systems of these plants will vibrate sufficiently to introduce an undesirable signal into the earth. The lines were centrally located in the portion of the channel which is active during runoff events.

Lines were positioned in a manner such that all twelve geophones were on as level a surface as possible. Local channels with banks cut greater than 15 centimeters into the main channel were avoided so that

elevation variations along the line were minimal. In a shallow investigation, elevation differences of as little as 25 centimeters may cause significant travel time variations. Even though the magnitude of travel time variation is on the order of one millisecond or less, the percentage of the total travel time is quite significant relative to a similar error in deeper investigations.

Preliminary Design and Theory

Initial assumptions about the geology and the velocity of the sediments had to be made to design the field surveys. These assumptions were essential to construct theoretical models and, subsequently, optimum seismic surveys to detect the models. Appropriate line lengths, geophone spacings, and record time were derived from the constructed models so that actual field surveys could be conducted in an efficient manner.

It was anticipated that two to four horizons might be encountered via the seismic refraction method (Sanford, personal communication, 1987). These included an upper alluvial layer approximately 1 to 2 meters thick with a velocity of 250–350 meters per second, unsaturated alluvium with a velocity of 600–1000 meters per second, water saturated alluvium 1600–2000 meters per second, and the Santa Fe Group sediments with a velocity of 2300–2500 meters per second.

The simplest subsurface model is the two-layer case consisting of unsaturated alluvium overlying saturated alluvium. Theoretical travel time curves were constructed assuming horizontal dip, V1 = 1000 meters per second, and V2 = 2000 meters per second. Figure 6 illustrates the pair of models which were used for the two-layer case. Each model represents an extreme case for the expected depth to the water table. The travel time

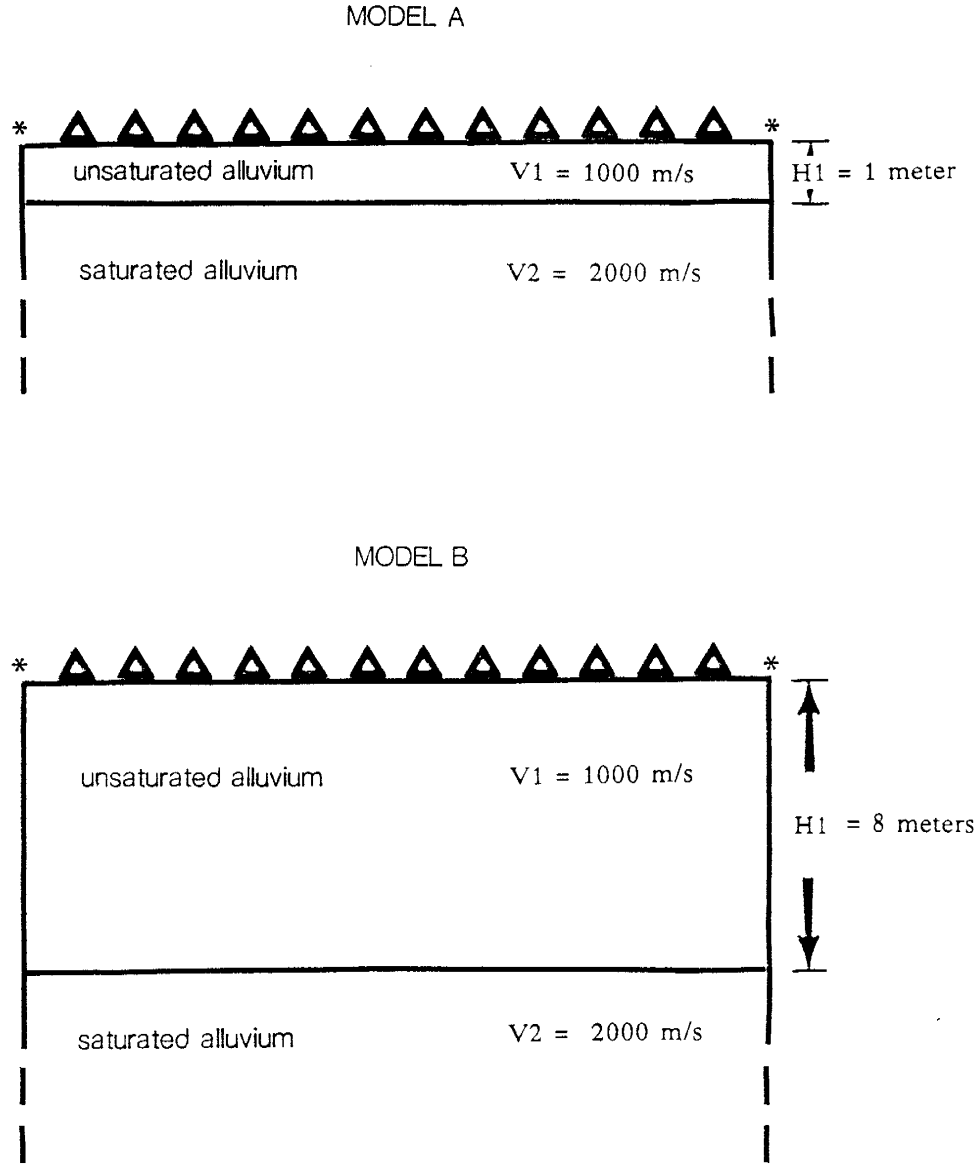

Figure 6 : Geologic Models A and B for which theoretical travel time curves were constructed for the two-layer cases.

curves in Figures 7 and 8 are the expected results from a seismic line with three meter geophone spacings and a three meter shotpoint offset.

For the two-layer case, theoretical travel time curves are constructed by first calculating the model crossover distance (xcross). This is accomplished by plugging the assumed depth to the water table (H), velocity of the first layer (V1), and the velocity of the second layer (V2) into the formula

$$H = 0.5\ [(V2-V1)/(V2+V1)][xcross].$$

The crossover distance is the distance from the shotpoint where the direct wave travelling within the V1 layer and the wave critically refracted from the top of the V2 layer reach the geophone simultaneously. At distances less than this, the wave travelling at V1 reaches the geophone first. At distances greater than this, the wave travelling at V2 reaches the geophone first. Thus, on a travel time curve the two line segments representing the travel times along each of these two paths cross at this distance. Once the crossover distance is known, a line segment having a slope of 1/V1 can be extrapolated from the origin to the crossover distance, and a line segment having a slope of 1/V2 can be extrapolated from the crossover distance to the end of the line. From the travel time curve it can be inferred how many geophones for a given geophone spacing would be expected to detect first arrivals from each layer.

The travel time curve for Model A in Figure 7 indicates that for a geophone spacing of 3 meters only one geophone would detect the direct arrival while the remaining geophones would detect the refracted arrival from the water table because the crossover distance is 3.46 meters. In Model B, where the water table is 9 meters deep, only the last two geophones detect the V2 refracted arrival, whereas the first 10 geophones

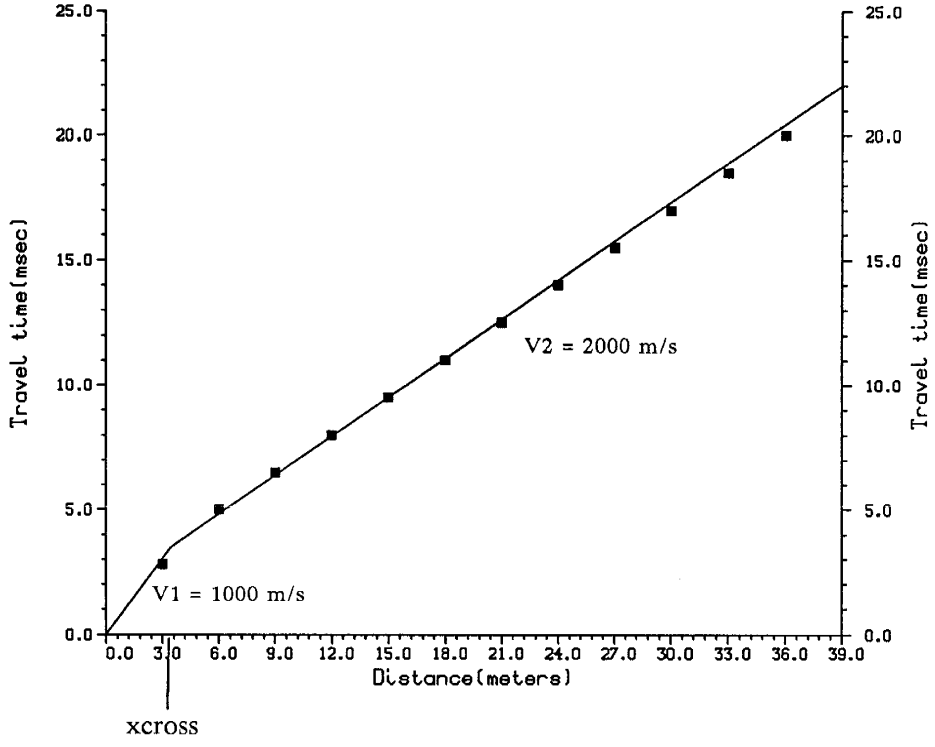

MODEL A

H1 = 1 meter

Geophone Spacing : 3 meters

xcross = 3.46 meters

Figure 7 : Theoretical travel time curve for the detection of Model A with field array consisting of 3 meter geophone spacings and a 3 meter shotpoint offset.

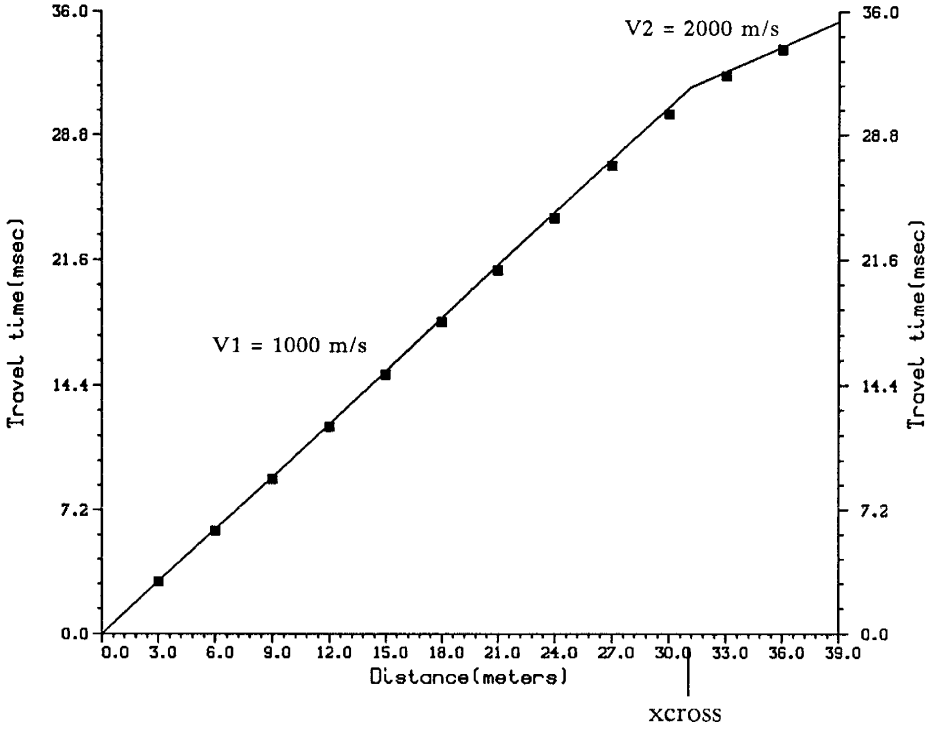

MODEL B

H1 = 9 meters

Geophone Spacing : 3 meters

xcross = 31.2 meters

Figure 8 : Theoretical travel time curve for the detection of Model B with a field array consisting of 3 meter geophone spacings and a 3 meter shotpoint offset.

detect the direct arrival (Figure 8). Again the geophone spacing is 3 meters, but the crossover distance is now 31.2 meters.

The models for the two–layer case indicate that a single geophone spacing would not be appropriate in all cases for the Rio Salado. Even though arrivals from both horizons are detectable on both travel time curves, one velocity dominates in both cases. Any variation in the field of depth, velocity, or dip could result in one horizon being undetected. The lengths of the lines and geophone spacings should vary depending on the expected depths to the water table at a given field location. In areas where a shallow water table is expected, geophone spacings should be kept at two meters or less. Since the crossover distance is only 3.46 meters, a line with geophone spacings of 4 meters would be unable to detect the direct arrival. Conversely, where a deeper water table is expected, geophone spacings should be a minimum of three meters. The crossover distance for a water table depth of 9 meters is 31.2 meters, therefore, if a geophone spacing of 2 meters were used, the total line length would be only 24 meters (since only 12 geophones are being used) and the refracted arrival would go undetected.

It was expected that three horizons would most likely be detected in the Rio Salado so models for a three–layer case were also constructed. Figure 9 illustrates the models. The three geologic horizons used were an upper alluvial layer with a velocity of 300 meters per second, unsaturated alluvium with a velocity of 1000 meters per second, and saturated alluvium with a velocity of 2000 meters per second. Geophone spacings of two and three meters were used for the models. A thickness of one meter for the upper alluvial layer was used in both cases, and thicknesses of one and eight meters for the unsaturated alluvium were used. Dips were assumed to

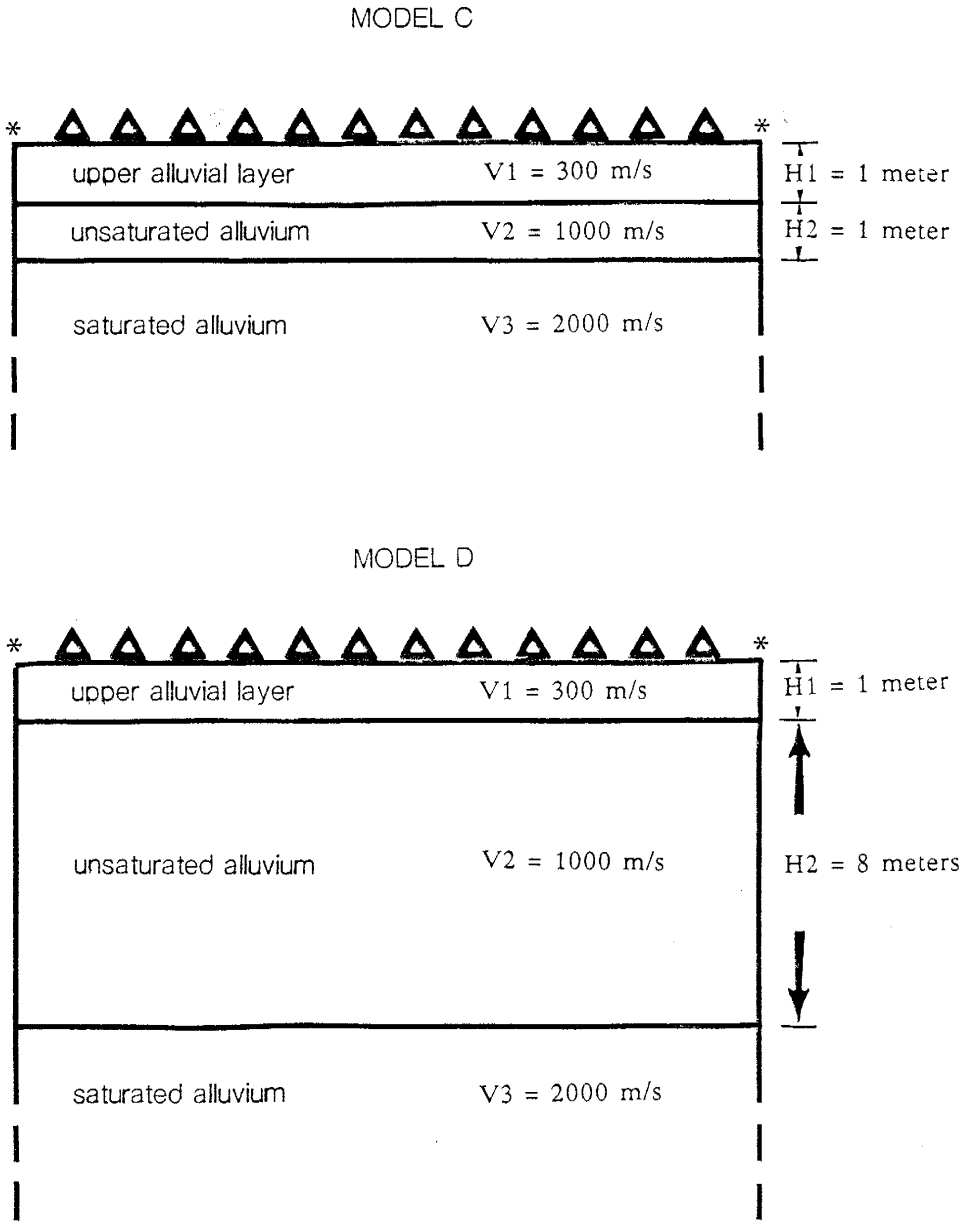

Figure 9 : Geologic Models C and D for which theoretical travel time curves were constructed for the three-layer cases.

be horizontal.

The calculation of theoretical travel time curves becomes more complicated if more than two layers are used. The crossover distance for the V1 and V2 layers can still be calculated in the same manner as the two-layer case, but the crossover distance calculations for the V2 and V3 layers is more complex. Another approach to this problem is to calculate intercept times and then graphically determine the crossover distance. The intercept time for a given horizon is the point on the vertical axis which the line segment representing that horizon on the travel time curve would intersect if projected back to the axis, i.e., the projected travel time for zero offset distance.

The interpretation method outlined by Johnson (1976) was utilized to construct the three-layer travel time curves. The geometry of the system is shown in Figure 10. Intercept times were calculated by working backwards through the depth calculation procedure. Construction of the theoretical travel time curves were simplified by assuming horizontal layers. From Figure 10 :

The critical angle for the V2 layer is $\alpha 1$ given by:

$$\alpha 1 = \arcsin(V1/V2).$$

To calculate the intercept time for the V2 layer:

$$t2 = 2[(H1)\cos(\alpha 1)/V1].$$

For layer 3:

$$\beta 1 = \arcsin(V1/V3).$$

From Snell's law the critical angle is:

$$\beta 2 = \arcsin(V2/V3).$$

To calculate the layer 3 intercept time:

$$t3 = 2[(H1)\cos(\beta 1)/V1 + (H2)\cos(\beta 2)/V2].$$

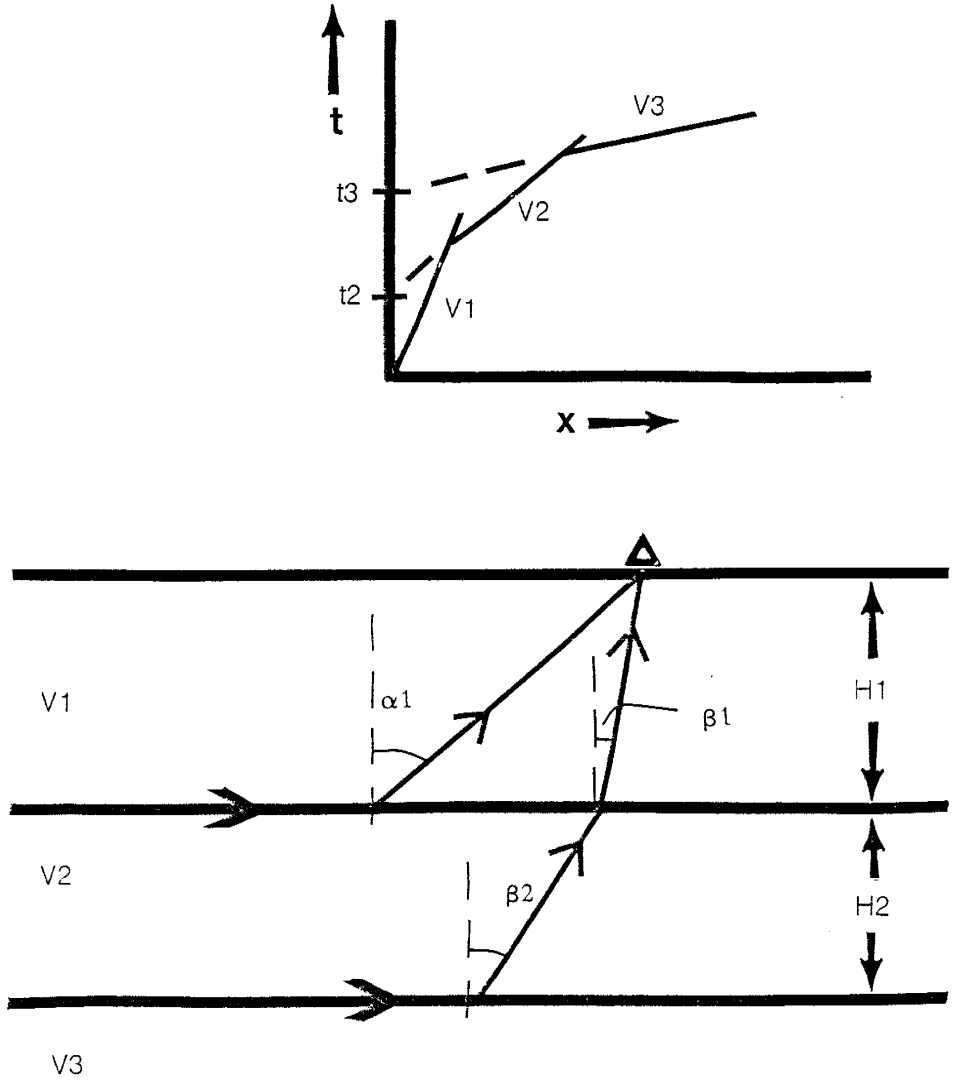

Figure 10 : Geometry of the subsurface as related to refracted raypaths. This system was utilized to construct theoretical travel time curves for the three-layer cases. (Modified from Johnson, 1976).

Once intercept times have been calculated, travel time curves can be constructed by drawing a line segment from the origin with a slope of 1/V1, a line segment from the layer 2 intercept time (t2) with a slope of 1/V2, and a line segment from t3 with a slope of 1/V3. The crossover distances can then be derived by determining where the line segments cross and projecting down to the horizontal axis.

Travel time curves constructed for a line with three meter geophone spacings are shown in Figures 11 and 12 for Models C and D, respectively. In the case of a shallow water table in Model C, the direct arrival is not detected, and the refracted arrival from the unsaturated alluvium is detected only by the first geophone. The remaining geophones detect the refracted arrival from the water table. When the water table is at a depth of nine meters, as in Model D, the first geophone will detect the direct arrival, geophones two through nine will detect the refracted arrival from the unsaturated alluvium, and the last three geophones detect the refracted arrival from the water table.

If the models were to be investigated by a line with 2 meter geophone spacings, the travel time curves would appear as in Figures 13 and 14. For the shallow water table model, signals from the V1 and V2 layers would be detected by the first and second geophones, respectively. The remaining geophones would record the signal transmitted back to the surface from the water table. The first geophone would also record the direct arrival in Model D. In this case, though, all of the remaining detectors would record only the refracted signal from the unsaturated alluvium. Signals from the water table would go undetected.

The models for the three-layer case indicate again that variations

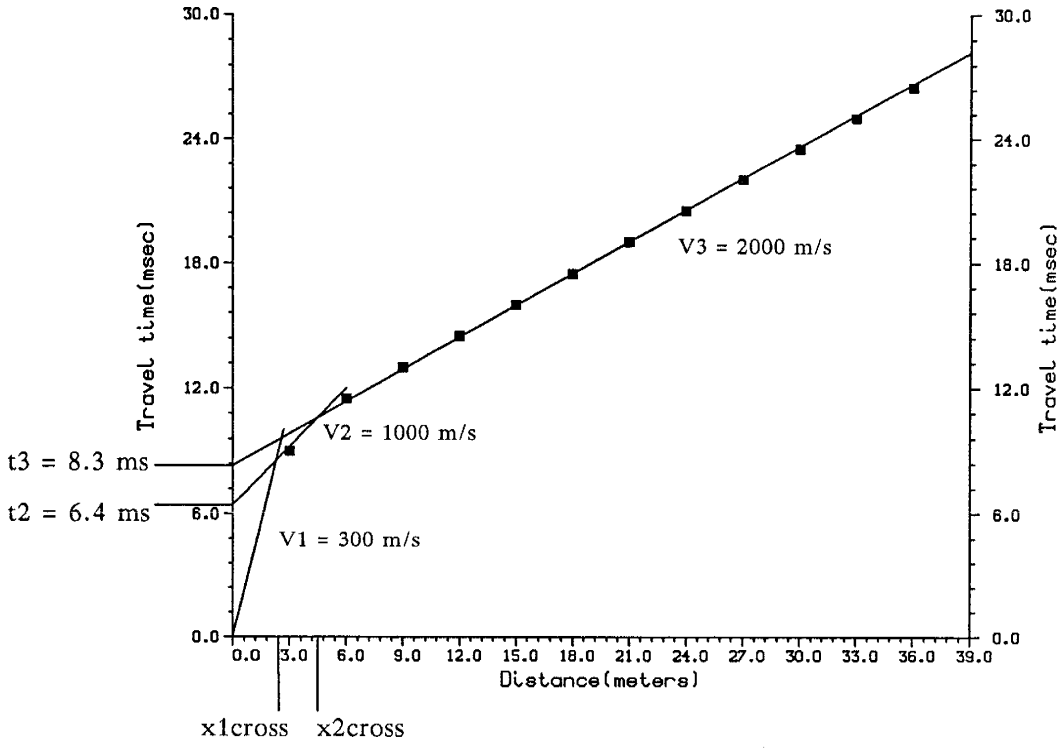

MODEL C

H1 = 1 meter

H2 = 1 meter

Geophone Spacing : 3 meters

x1cross = 2.7 meters

x2cross = 4.8 meters

Figure 11 : Theoretical travel time curve for the detection of Model C with a field array consisting of 3 meter geophone spacings and a 3 meter shotpoint offset.

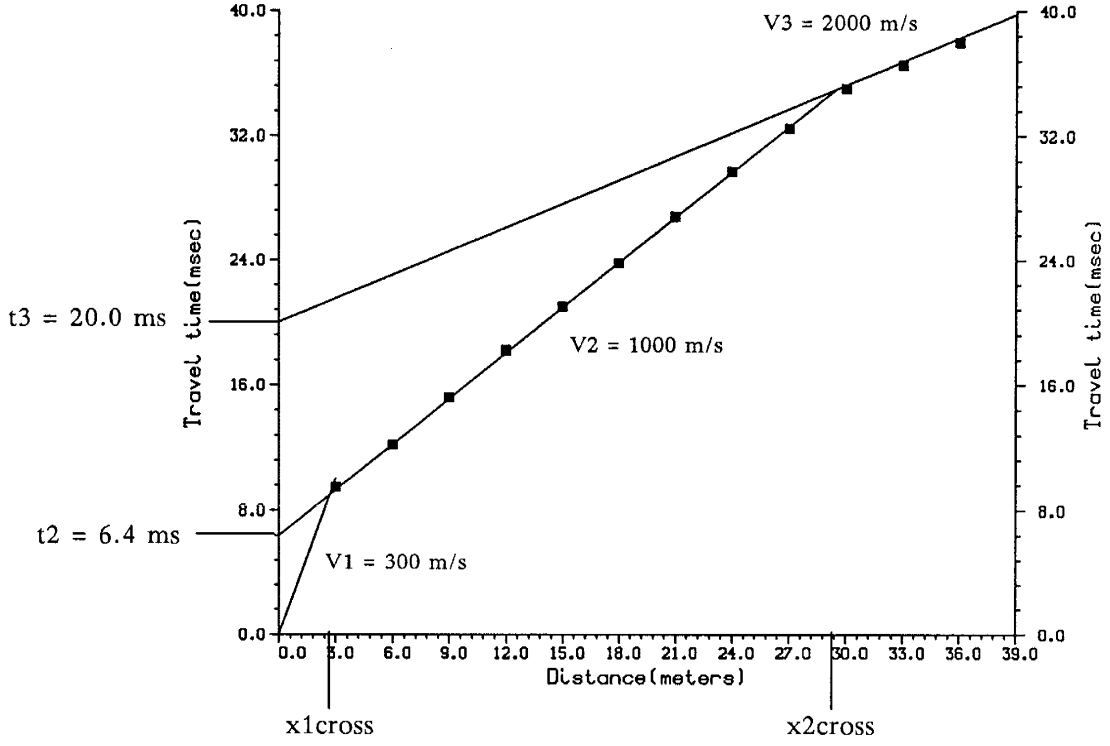

MODEL D

H1 = 1 meter

H2 = 8 meters

Geophone Spacing : 3 meters

x1cross = 2.7 meters

x2cross = 29.3 meters

Figure 12 : Theoretical travel time curve for the detection of Model D with a field array consisting of 3 meter geophone spacings and a 3 meter shotpoint offset.

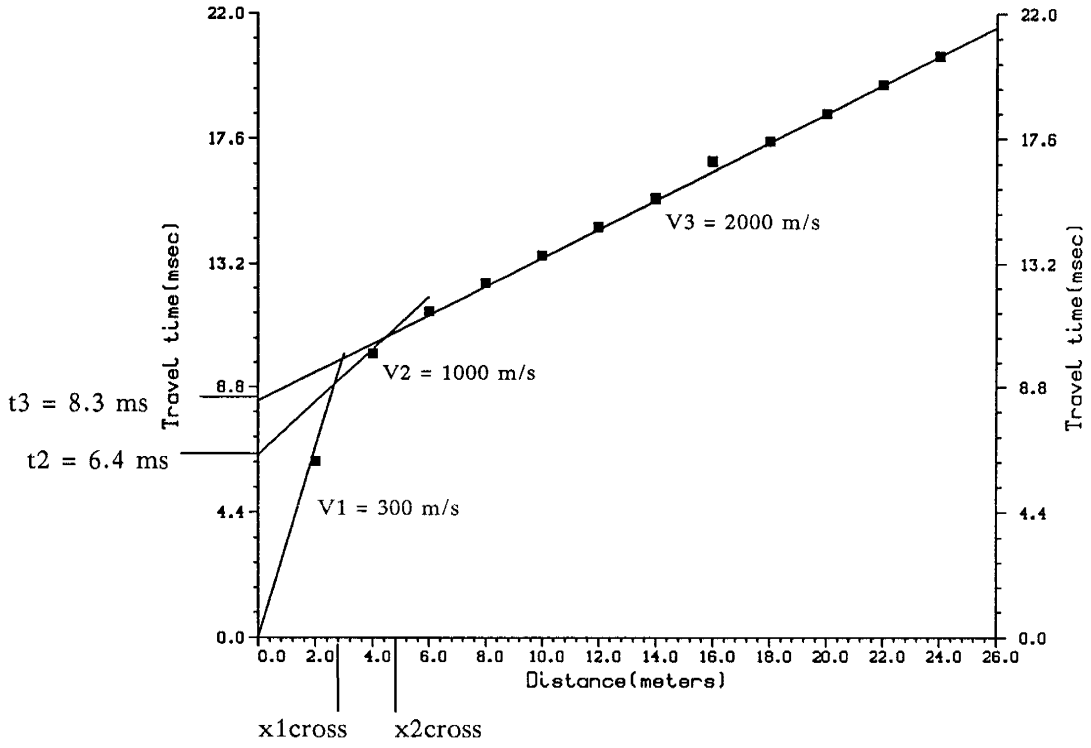

MODEL C

H1 = 1 meter

H2 = 1 meter

Geophone Spacing : 2 meters

x1cross = 2.7 meters

x2cross = 4.8 meters

Figure 13 : Theoretical travel time curve for the detection of Model C with a field array consisting of 2 meter geophone spacings and a 2 meter shotpoint offset.

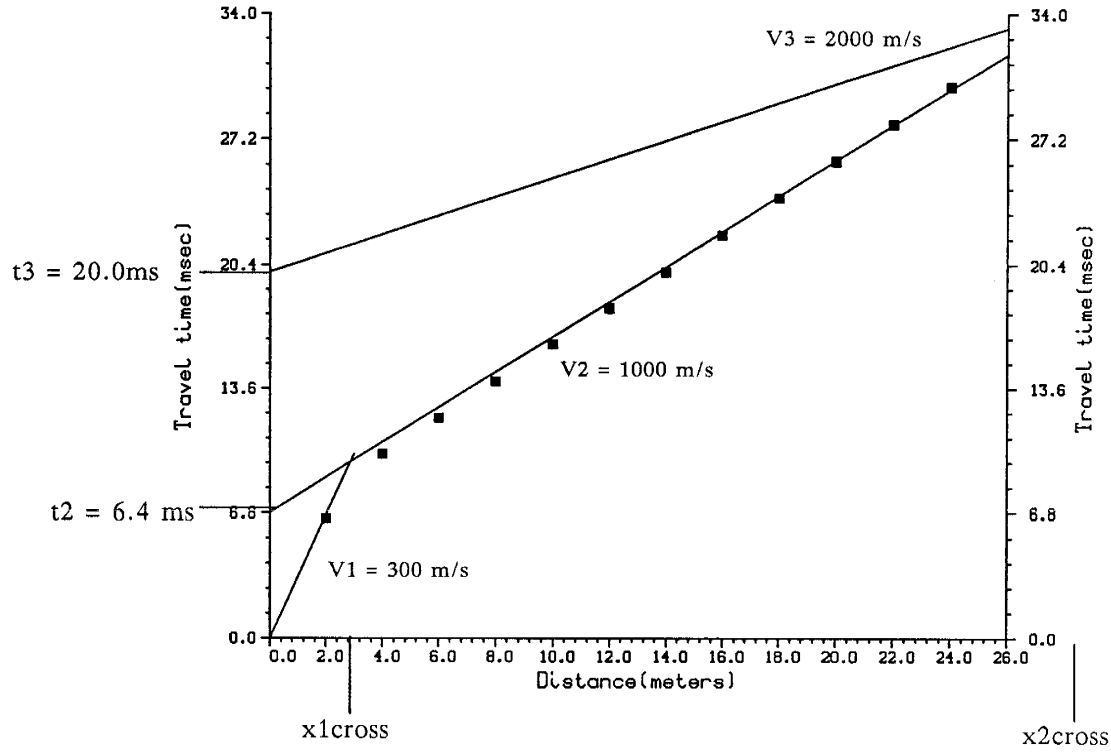

MODEL D

H1 = 1 meter

H2 = 8 meters

Geophone Spacing : 2 meters

x1cross = 2.7 meters

x2cross = 29.3 meters

Figure 14 : Theoretical travel time curve for the detection of Model D with a field array consisting of 2 meter geophone spacings and a 2 meter shotpoint offset.

in the line lengths and geophone spacings may result in a layer being undetected in certain areas of the Rio Salado. In general, the deeper the higher velocity layers the longer the geophone spacing must be to detect them; but the low velocity shallow horizon may go undetected due to the crossover distance being exceeded by larger spacings. Conversely, short spacings are required to detect the direct wave but may cause the deepest horizon to go undetected because the second crossover distance is not achieved by the total line length.

To avoid the potential problem of not detecting layers in the field (since only 12 geophones were used), two lines were often run at the same location but with different line lengths and geophone spacings. The data from both lines were then incorporated into a single travel time curve for the interpretation process as shown in Figure 15. A short line with geophone spacings of 1 to 3 meters was run to detect the direct arrival and a line with geophone spacings of 4 to 10 meters was run at the same location to insure that the water table would be detected. By combining the two data sets, more data points were available for each horizon at each location. If only one line was run for the data set in Figure 15, a limited number of data points would be available for analysis for either the shallowest or the deepest horizon. Because the lines were combined to form one travel time curve, at least three data points are now available for each layer.

Record time can also be derived from observation of the theoretical travel time curves. The record time, or length of time that the seismogram records signals, can be preprogrammed into the ES-1225 prior to each shot. The record time should be as short as possible so that the scale on the seismogram is as large as possible. This allows for a greater degree of accuracy in picking the times of the first arrivals. If, for example, a

FIELD ARRAY

* shotpoints

△ geophone location – 4 meter spacing

□ geophone location – 2 meter spacing

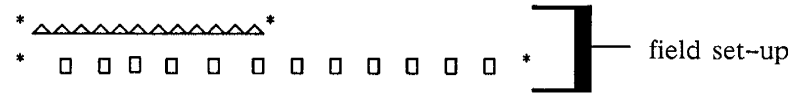

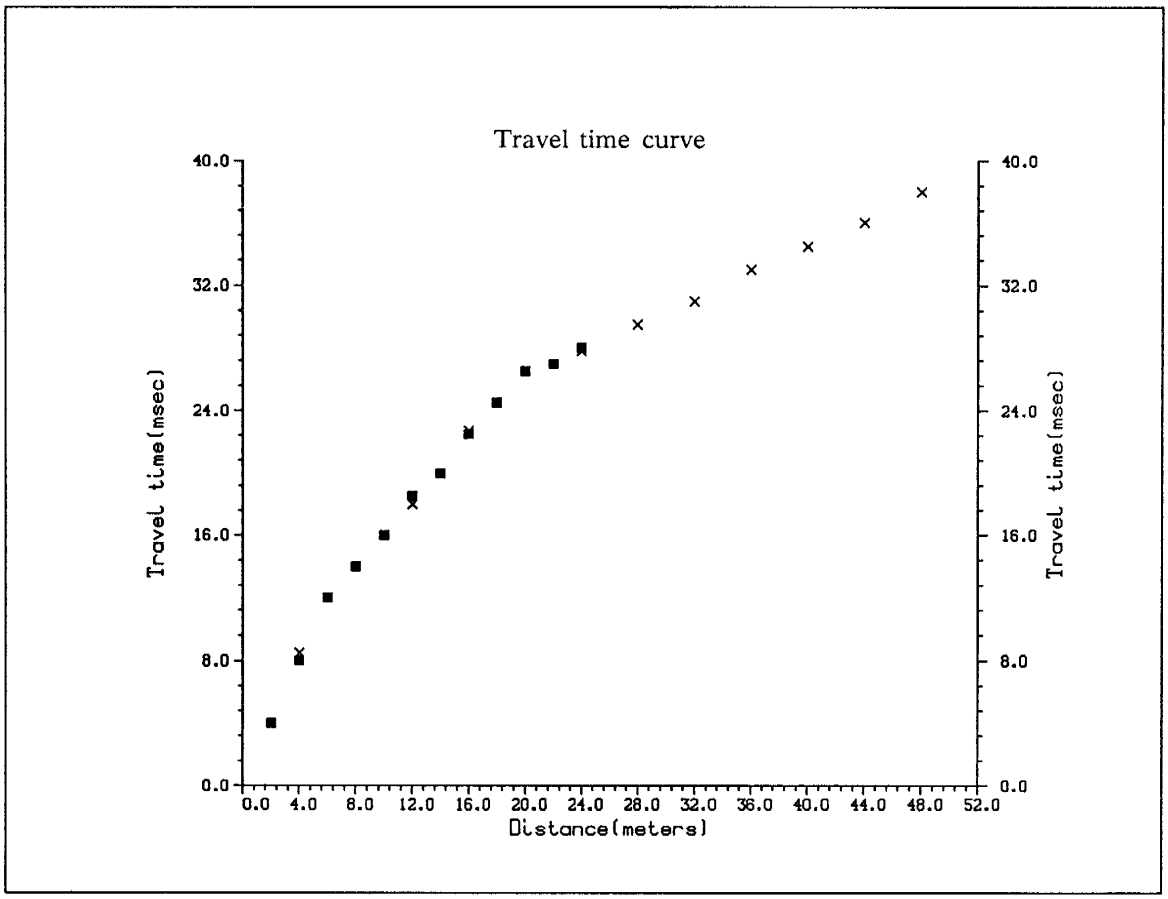

■ data point from line with 2 meter geophone spacing

x data point from line with 4 meter geophone spacing

Figure 15 : Field array and resulting travel time curve when two lines are combined to obtain additional data points for each horizon.

record time was to be chosen for Model C, the travel time curve for the appropriate geophone spacing should be studied. If a geophone spacing of 3 meters was to be used, a record time of 50 milliseconds would be chosen. This value is arrived at by looking at the time at which the signal is detected at the last geophone. In this case, it arrives after approximately 27 milliseconds. If a geophone spacing of 2 meters was used, a record time of 25 milliseconds would be chosen because the last arrival comes in at about 21 milliseconds. The ES-1225 places some limitations on the record time which may be used. Record times are available for 25, 50, 100, and 500 milliseconds, therefore, record times such as 30 or 60 milliseconds may not be used.

INTERPRETATION

Attenuation

Attenuation is the reduction in amplitude of waves produced by reflection and scattering, divergence, and absorption. Significant amounts of energy of the seismic waves propagating in the Rio Salado are lost because of the thick, unconsolidated alluvial section in the area. Because primary energy loss mechanisms are generally intergranular friction and pore fluid flow, attenuation is high as a result of these mechanisms being accentuated in the area.

Attenuation is generally measured by the dimensionless quality factor Q or by the attenuation coefficient α which has units of either inverse length or decibels per wavelength (Hatherly, 1986). These are related by the equation:

$$1/Q = \alpha\, v/\pi\, f$$

where v is velocity and f is frequency. A low Q indicates a highly attenuative environment.

The majority of the attenuation studies which have been conducted have been applied to materials having a Q value greater than 20 (Anderson, 1988). Little work has been done on measuring attenuation in shallow refraction data where Q values are commonly between 5 and 15. Many of the techniques of attenuation measurement which have been documented do not apply to shallow, low Q environments as they do to high Q environments.

It is not the intent of this study to present an exhaustive

discussion on attenuation measurement techniques. An entire study along the Rio Salado could be devoted to this subject. The reader is referred to Anderson (1988), Hatherly (1986), and Kjartansonn (1979), for more detailed discussions concerning attenuation.

Attenuation measurements were made in the Rio Salado to help quantify the nature of acquisition parameters in the area. The attenuation data should also serve as a preliminary data base for future studies in the Rio Salado.

The most suitable attenuation measurement technique for shallow refraction data is based on pulse broadening. This technique assumes that broadening is proportional to attenuation and Q is independent of frequency (Hatherly, 1986). Pulse broadening is related to Q by the equation:

$$\tau = \tau 0 + ct/Q$$

where τ is pulse width, $\tau 0$ is the pulse width of the source pulse, t is travel time, and c is a constant. The problem with this method is the lack of agreement on the value for c. Various authors have used different c values (ranging from 0.29 to 0.773), but the most accepted value seems to be 0.5, which will be used for this study.

Two attenuation experiments were conducted in this study. The lines were positioned such that one was located over a shallow water table, and the other was located where the water table was deeper (Figure 16). The experiments were conducted in this manner to observe whether attenuation effects varied across the region.

At both locations, seismic lines were run with 0.25 meter geophone spacings and 0.25 meter shot offsets so that only the direct wave would be recorded. Two surveys were conducted for each experiment, one with 20 hertz geophones and one with 100 hertz geophones. Two records

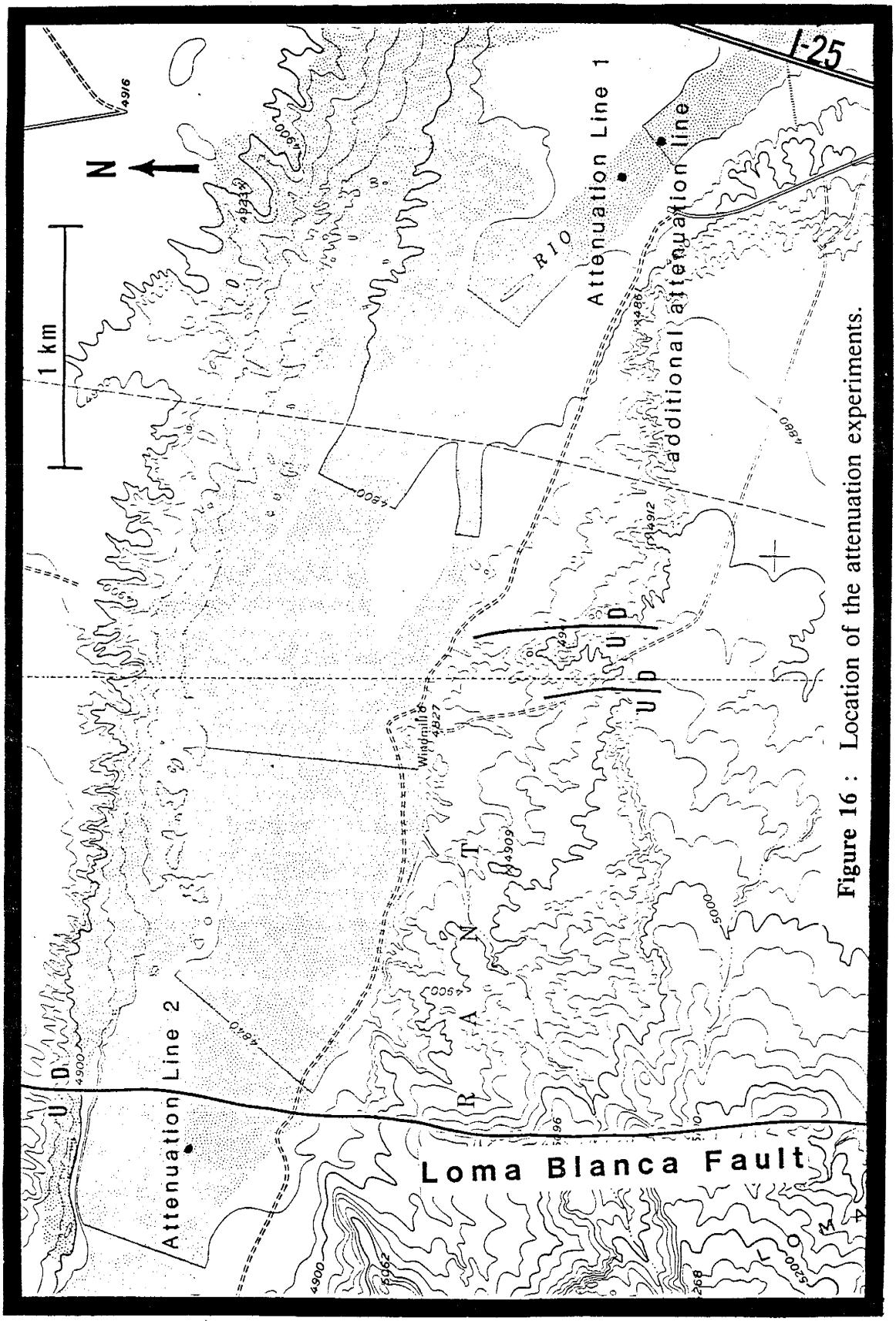

Figure 16 : Location of the attenuation experiments.

were obtained for each set of geophones at each location. The even channels were recorded on one record and the odd channels were recorded on the other in order to prevent the signal record on adjacent channels from overlapping so that accurate measurements could be made.

Travel time versus pulse width was plotted to evaluate attenuation. The first trace was used as a reference point so that all other trace values were plotted relative to the first arrival of the first geophone. Therefore, on the attenuation data plots (Figures 17–20), the first trace was plotted at the origin and the travel times of succeeding traces from the first trace were plotted on the horizontal axis, and the difference in pulse widths from the first trace were plotted on the vertical axis. A least squares line was then fit to the data from which the slope was calculated. The slope of the line is equal to c/Q. A Q value was then calculated using a c value of 0.5.

The calculated Q values ranged from 9 to 14 indicating highly attenuative environments. An additional attenuation survey (Knapp, unpublished class report, 1988) found Q to be 13, slightly higher but still indicating a highly attenuative environment. The location of this line is also shown in Figure 16.

Attenuation Line 1 was run just west of Line 1 where the first refractor was found to be 5.9 meters deep, and the water table was found to be 12.0 meters deep. Running the survey with 20 hertz geophones resulted in a Q of 10, and a Q of 11 was calculated when 100 hertz geophones were used. Attenuation Line 2 was run at the same location as Line 23 where the first refractor was found to be 1.6 meters deep, and the water table was found to be 6.4 meters deep. A Q of 9 was obtained from the 20 hertz

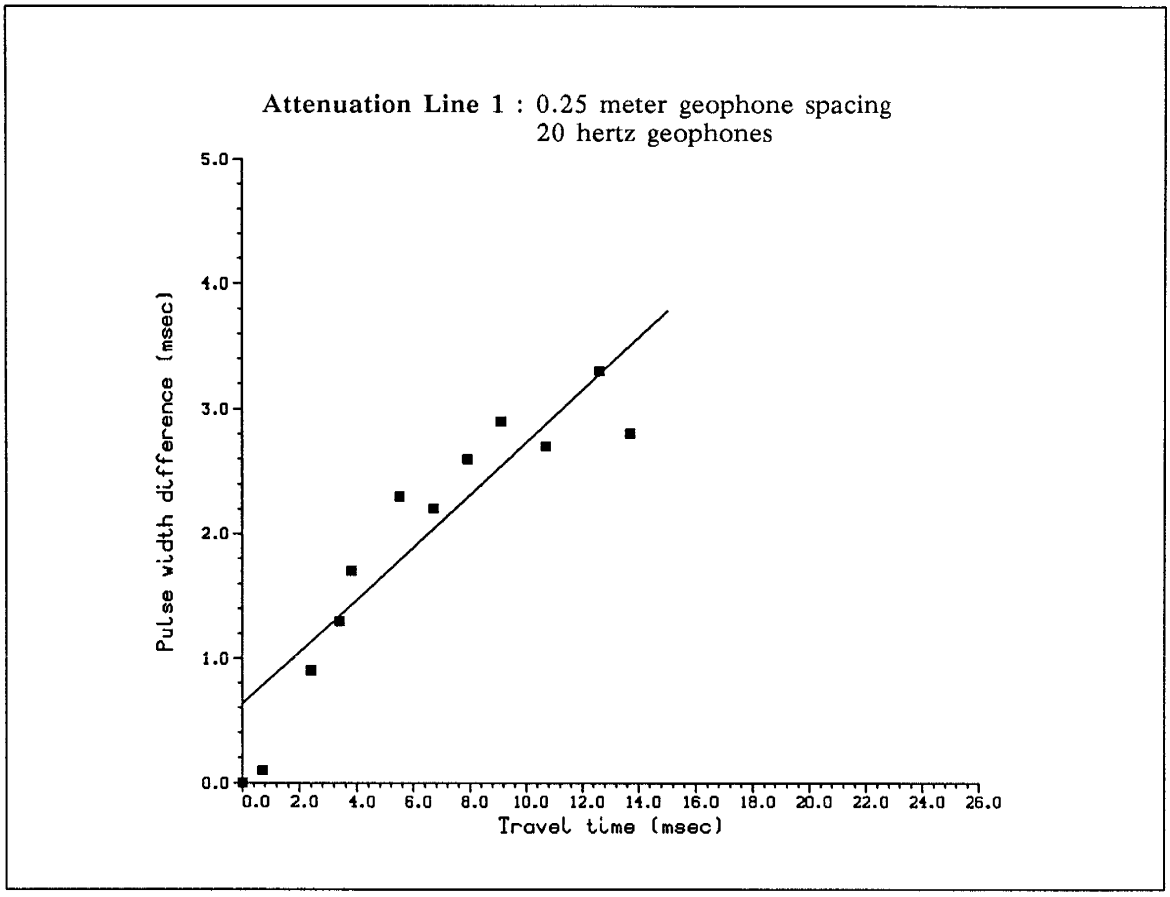

Q = 10

Correlation Coefficient : 0.91

Figure 17 : Plot of Attenuation Line 1 data using 20 hertz geophones. Both pulse widths and travel times are plotted relative to the signal from the first channel.

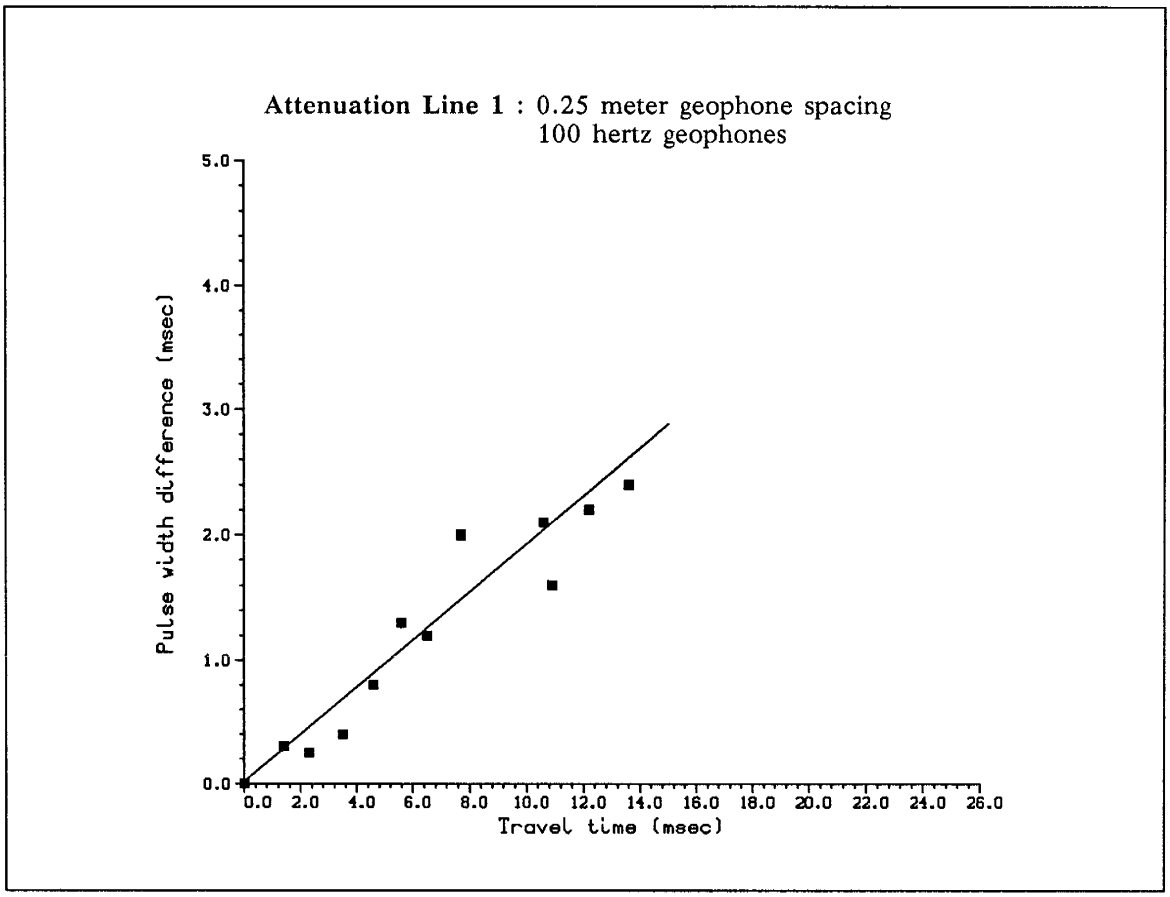

Q = 11

Correlation Coefficient : 0.94

Figure 18 : Plot of Attenuation Line 1 data using 100 hertz geophones. Both pulse widths and travel times are plotted relative to the signal from the first channel.

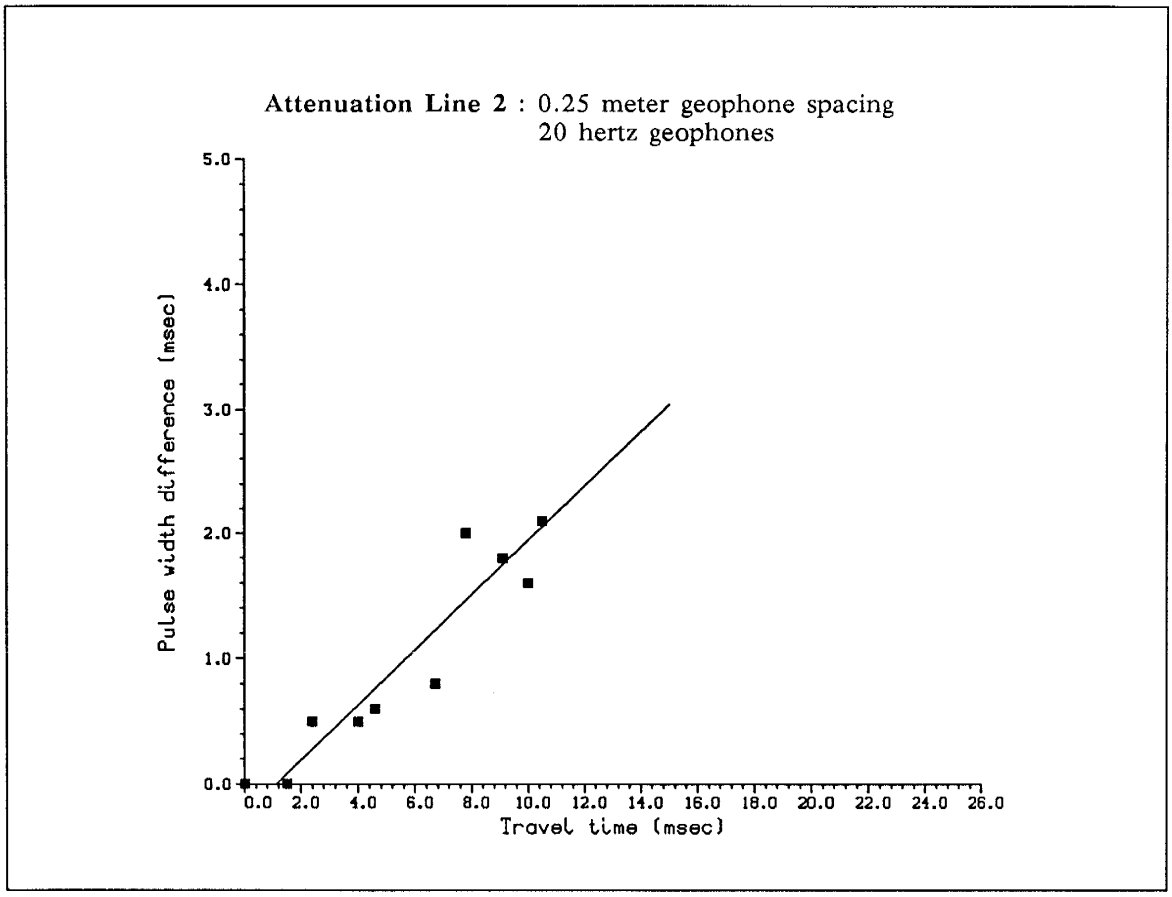

Q = 9

Correlation Coefficient : 0.93

Figure 19 : Plot of Attenuation Line 2 data using 20 hertz geophones. Both pulse widths and travel times are plotted relative to the signal from the first channel.

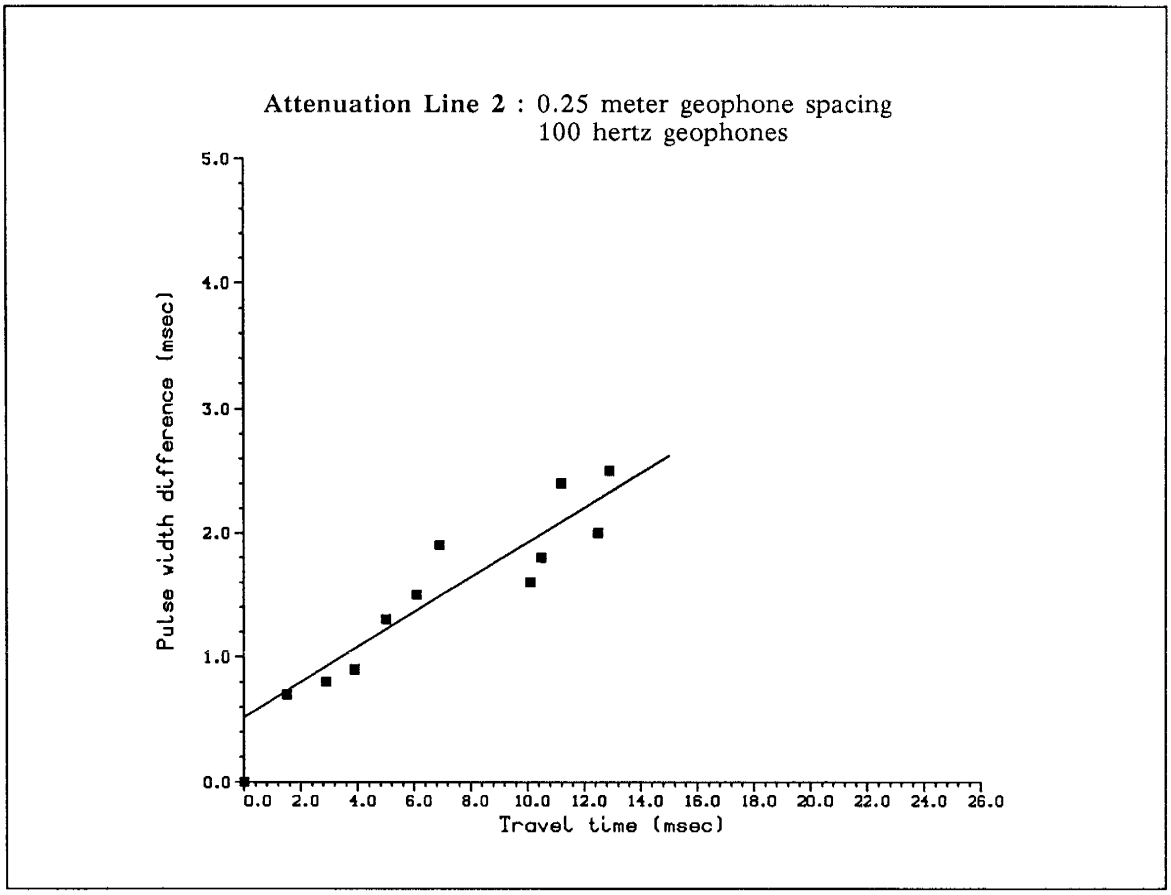

Q = 14

Correlation Coefficient : 0.92

Figure 20 : Plot of Attenuation Line 2 data using 100 hertz geophones. Both pulse widths and travel times are plotted relative to the signal from the first channel.

geophone data and a Q of 14 from the 100 hertz geophone data.

In both cases, data collected from the 100 hertz geophones appears to be of better quality. This may seem contradictory to the statement made in the data acquisition section which indicates 20 hertz geophones are better suited for Rio Salado data collection. This is true for normal data collection surveys where line lengths are much larger. In the case of attenuation lines, however, the total line length is only 3 meters, and maximum travel times are less than 15 milliseconds. The 100 hertz geophones work well for these experiments because the signal has not travelled far from the source and, therefore, has not lost as much energy as it would after being refracted and detected at much greater distances from the source. This also allows more accurate picks of travel times and pulse widths to be made because more components of the signal are recorded.

The data from attenuation Line 1 are somewhat more consistent than the data from attenuation Line 2. This may be due to the differing depths to the first refractor. Some scattering occurs in the data for the far geophones on attenuation Line 2. This could be due to the crossover distance being approached and interference from the refracted signal being incorporated into the data. The crossover distance is not even close to being achieved for attenuation Line 1 so all events should be exclusively from the direct wave. In any case, Q values do not vary significantly over the area.

Attenuation is an important characteristic in the Rio Salado because it can severely affect seismic signals and the ability to interpret the seismic records. This must be kept in mind during the course of the data acquisition process because minor amounts of noise can cause significant interference on a highly attenuated signal. The data must be stacked more

times than usual to insure that high quality records are obtained. Attenuation effects must also be considered throughout the interpretation process. If appropriate measures have not been taken in the field, travel times may not be able to be accurately picked from data which has been severely affected by attenuation.

Interpretive Methods

The primary tool for the interpretation of seismic refraction data is the time-distance graph. Data are plotted in terms of travel time from the source as a function of source-to-receiver distance. These graphs are then used to determine velocities, depths to refracting horizons, and dips of refracting horizons. Each of these plots for the refraction lines conducted in this study are in Appendix A in numerical order from Line 1 to Line 28. Velocity and depth values associated with each line are also presented with each graph. Since the interpretation of each graph will not be discussed in detail, when time distance graphs are mentioned the reader should refer to Appendix A for the appropriate plot.

The construction of effective time-distance graphs requires that accurate time picks be made from the field seismograms. The first break of each channel was picked to the nearest 0.1 millisecond when possible. Because the recording instrument has a fixed number of samples per record, the resolution of the seismograms is dependent on the record length. Since shorter record times can be used for shorter line lengths, more accurate picks can be made. In these instances, where geophone spacings are 3 meters or less and the largest travel time is on the order of 40

milliseconds, the millisecond becomes a relatively large unit. Errors of only a millisecond have the potential to cause significant variations in the interpretation of shallow refraction data. The possibility of an incorrect pick is more likely for increased offset distances because the signal decreases in amplitude and the higher frequency components of the signal are more rapidly attenuated (Northwood, 1967).

Once satisfactory picks were made and the data were plotted on an appropriate time–distance graph, straight line segments were fit (by eye) to the data. This was the most important step in the interpretation process. Each line segment represents a different refracting horizon, and the inverse slope of the line represents the apparent velocity of the horizon. In most cases, the data do not form a perfectly straight line so there is some degree of flexibility in how the lines may be fit to the data. This means that there is a range of velocity values which could feasibly be assigned to a given refractor. Each velocity value would subsequently result in slightly different dip and depth estimates. Velocity values could vary up to 400 meters per second, depth values up to 2 meters, and dip values up to 2 degrees. Values of this magnitude in shallow refraction investigations can result in a large percentage of error. It is imperative, therefore, that there be extreme care and consistency exercised when working with the data. It should also be pointed out that these error estimate values are applicable to this study where the majority of the dip values are relatively minimal. Errors have the potential to be even more severe if large dips are encountered.

Two assumptions were made in the interpretation of the data : 1) refracting horizons are planar – a layer may dip, but there are no discontinuities or any curvature along the refracting horizon; 2) velocity is constant both laterally and vertically within a given layer.

The line segments representing the direct wave were always forced through the origin of the time–distance graphs and were constructed in a such manner that lines from both shot directions had the same slope, fitting the data on both ends of the profile as well as possible. This insured that the velocity of the direct wave (V1) was identical from either end of the profile. Because the least number of data points were generally available from the direct wave, this criterion provided some control in fitting the line segments to the data. This procedure assumes that the direct wave velocity is constant along the length of the profile, and that there are no anomolous features at the shotpoint locations.

To provide additional control on the placement of the line segments of the V2 and V3 layers, reciprocal times were utilized. The reciprocal time is the travel time between common points on reversed refraction profiles. Theoretically, the travel time of the signal must be the same in both directions for a given geologic section (that is, the travel time from a source point at A to a geophone at B must equal that from a source point at B to a geophone at A). In environments where lateral velocity changes or irregular refracting surfaces are present and the reciprocal times are not directly observed, they may be difficult to estimate due to complex travel paths. As long as the refractor is dipping less than 10 degrees, the accuracy of the interpretation should not be affected by minor relief along the refracting horizon (Dobrin, 1976). Dip data to be presented later indicate that in all cases, refractors detected in this study are dipping less than 10 degrees.

To test the assumption that lateral velocity changes are minimal, Line 13 and Line 16 (see Figure 5) were run with two source–to–near–receiver offsets. Both lines were run with 3 meter geophone spacings and 3

meter source-to-near-receiver offsets. In addition, source-to-near-receiver offsets of 6 meters were utilized. When two offset shot positions along the same profile are used, crossover points can be compared to determine if lateral velocity changes are present (Ackerman, Pankratz, and Dansereau, 1986). If no lateral velocity changes are present, the shot to crossover point distances remain constant. Otherwise, the shot to crossover point distances will vary. Both Line 13 and Line 16 exhibit shot to crossover point distances which remain equal for both source-to-near-receiver offsets indicating that no lateral velocity changes are present. This indicates that the assumptions of constant velocity are valid and that the use of reciprocal times is appropriate in the Rio Salado environment. It is especially important for the case of Line 13 because it was run where the Loma Blanca fault is believed to cross the Rio Salado. Because no lateral velocity variations are evident, this implies that the fault does not affect the alluvium at least at depths shallower than 12 meters.

Construction of the line segments representing the second and third horizons (having velocities of V2 and V3, respectively) was accomplished through the use of hypothetical reciprocal times because actual reciprocal times were not observed. In both cases, line segments were fit through the data points interpreted to represent the given horizon from each shot direction. Thus, two line segments representing a single refracting horizon were constructed on each time-distance graph; one related to the apparent velocity from the western shotpoint (Va2 or Va3) and one related to the apparent velocity from the eastern shotpoint (Vb2 or Vb3). The two segments for each refractor were made so that if each one was extrapolated to the far vertical axis (the distance to the opposite shotpoint), they would have equal travel times, or hypothetical reciprocal times. Sufficient control

was established by finding the best fit for each line pair while making sure that hypothetical reciprocal times were preserved.

An example of how this technique was applied to the data is presented in Figures 21 and 22. Figure 21 shows the two seismograms obtained for Line 17a, and Figure 22 illustrates the time-distance graph derived from the seismograms. The line segments for the V1 layer were constructed on the time-distance graph as previously described. The data points from geophones 1-4 for the western shot, and the data points from geophones 1-3 for the eastern shot were interpreted to represent the V2 layer (geophone 1 is to the west, geophone 12 is to the east). A line segment for the data from the western shotpoint (Va2), and a line segment for the data from the eastern shotpoint (Vb2) were constructed so that each fit the respective data points as well as possible, and when each line segment was extrapolated to the far axis, both had a hypothetical reciprocal time of 47 milliseconds. The Va2 and Vb2 lines were also drawn on the seismograms. By continuing these lines on through the last geophone, it can be seen in both cases that the lines would intersect a time of 47 milliseconds one trace beyond the last geophone, or the distance to the far shotpoint. The hypothetical reciprocal time chosen on the time-distance graph is supported by the field data which means that it is a good estimate of the actual reciprocal time. The V3 layer was interpreted in a similar manner with a hypothetical recriprocal time of 37.5 milliseconds which is shown circled in Figure 22.

Depth and dip calculations were conducted once an acceptable time-distance graph was completed. Apparent velocity and intercept time values were taken from the time-distance graphs and used to compute actual velocities, depths, and dips of the refracting horizons. A procedure

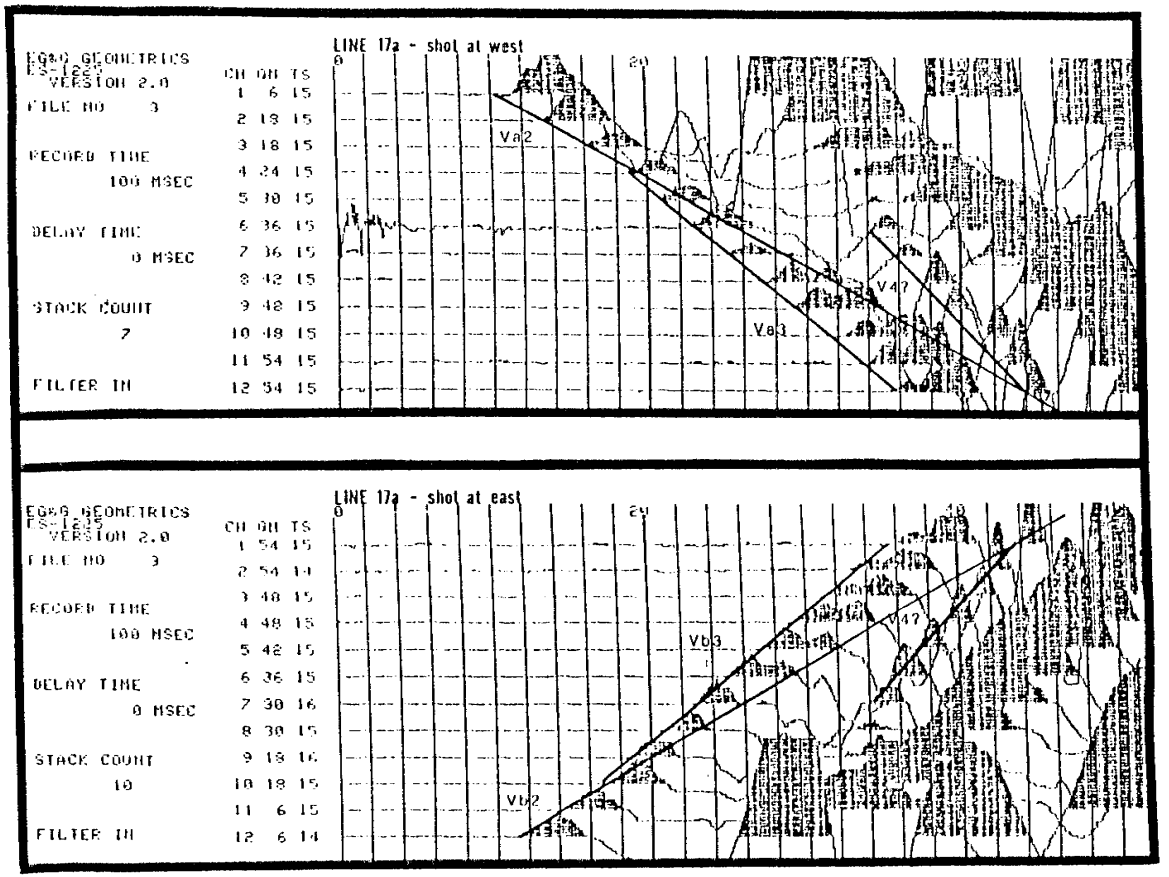

Figure 21 : Seismogram pair obtained for Line 17a. Note that if the V2 line segments are extrapolated to the end of the lines, they would intersect a time of 47 milliseconds, the hypothetical reciprocal time.

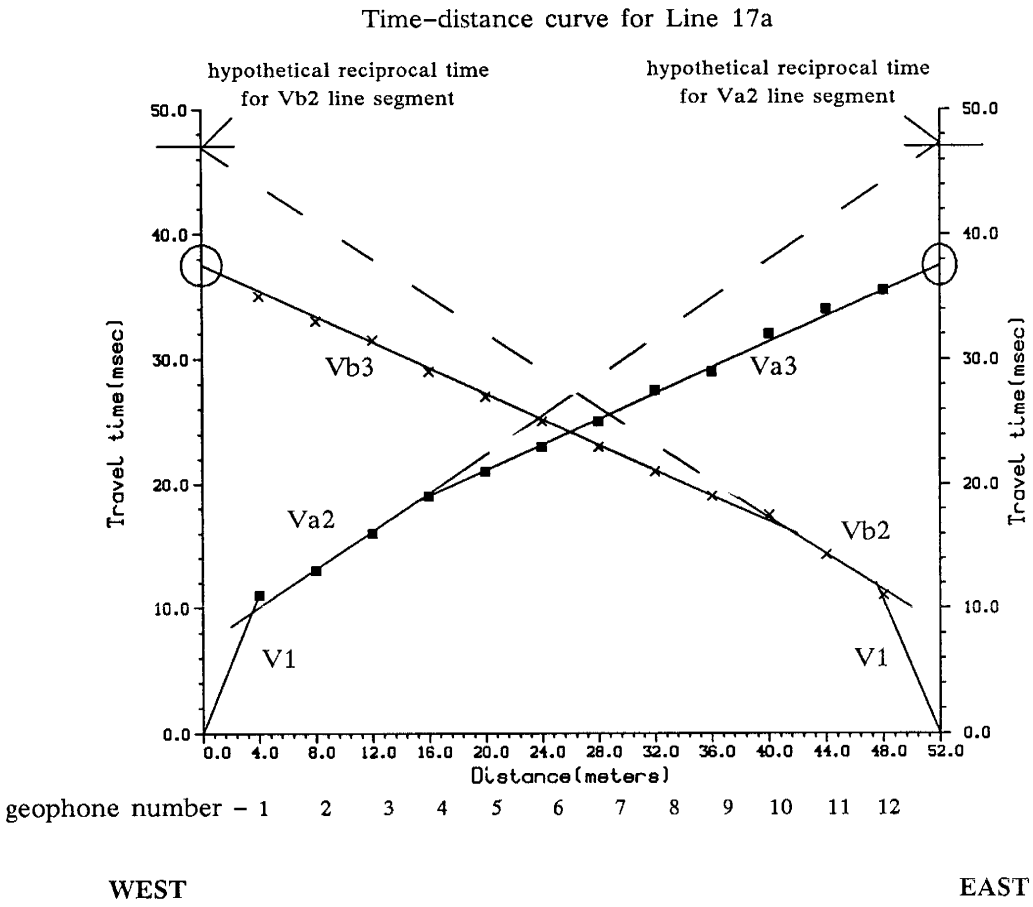

Figure 22 : Example of the construction of a time-distance graph using hypothetical reciprocal times. The Va2 and Vb2 lines are extrapolated to a hypothetical reciprocal time 47 milliseconds, and the Va3 and Vb3 lines are constructed through a hypothetical reciprocal time of 37.5 milliseconds (circled times).

similar to the one used to construct the models in the data acquisition section was used to obtain these values. Horizontal layers were not assumed in the interpretation, however, so the method becomes somewhat more complicated. The method is outlined by Johnson (1976) and the geometry of the system is shown in Figure 23. From Figure 23 :

$$\alpha 1 = \arcsin(V1/Va2)$$

and

$$\beta 1 = \arcsin(V1/Vb2)$$

and

$$a1 = b1 = (\alpha 1 + \beta 1)/2.$$

Thus, for the actual velocity of layer 2:

$$V2 = V1/\sin(a1)$$

and (dip of layer 2)

$$w2 = (\alpha 1 - \beta 1)/2.$$

To calculate the depth of the V2 layer:

$$H1 = [\ V1/(\cos(\alpha 1) + \cos(\beta 1)][t2].$$

For layer 3:

$$\alpha 1 = \arcsin(V1/Va3)$$

and

$$\beta 1 = \arcsin(V1/Vb3)$$

and

$$a1 = \alpha 1 - w2$$

and

$$b1 = \beta 1 + w2.$$

From Snell's Law:

$$P2 = \arcsin[(V2/V1)(\sin(a1))]$$

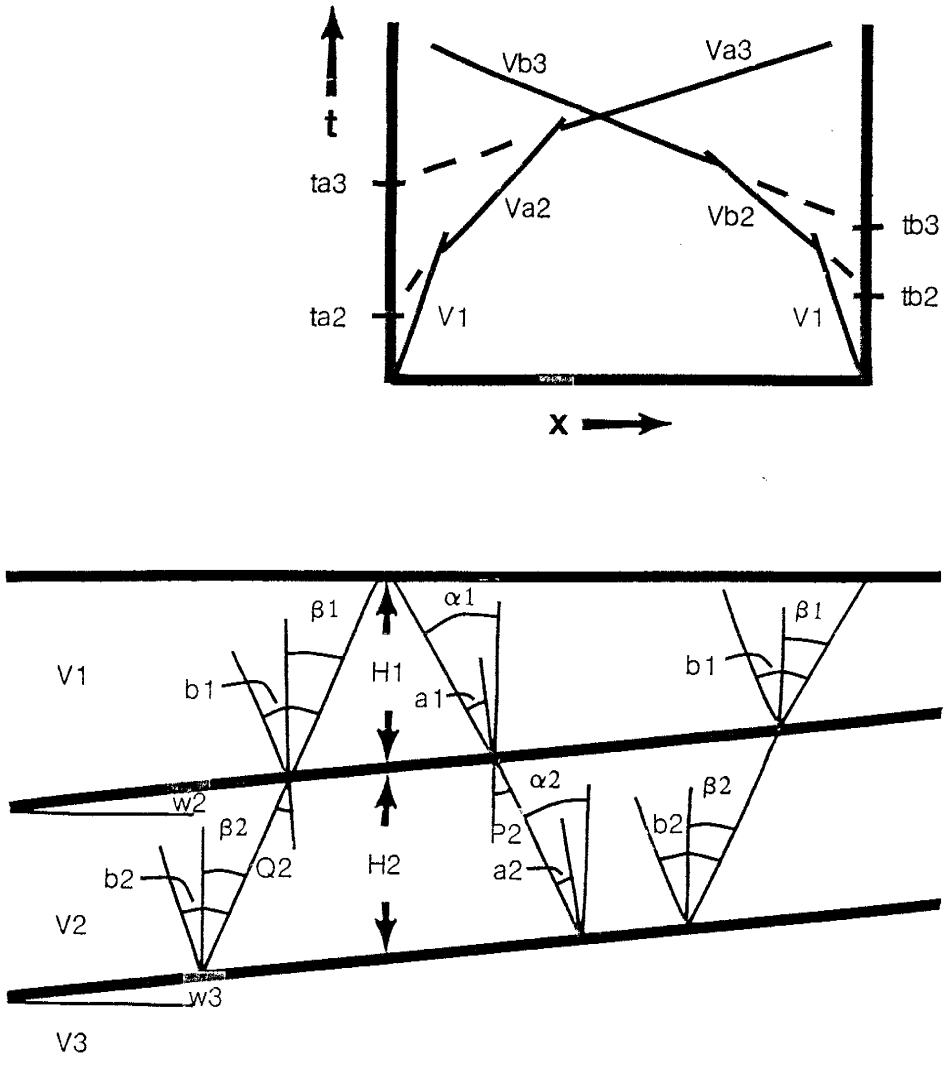

Figure 23 : Geometry of the subsurface as related to refracted raypaths. This system was utilized to calculate dips and depths of refracting horizons in the interpretation process. (Modified from Johnson, 1976).

and

$$Q2 = \arcsin[(V2/V1)(\sin(b1))].$$

Then

$$\alpha 2 = P2 + w2$$

and

$$\beta 2 = Q2 - w2$$

and

$$a2 = b2 = (\alpha 2 + \beta 2)/2.$$

Thus, for the actual velocity of layer 3:

$$V3 = V2/\sin(a2)$$

and (dip of layer 3)

$$w3 = (\alpha 2 - \beta 2)/2.$$

To calculate the depth of the V3 layer:

$$H2 = [V2/(\cos(\alpha 2) + \cos(\beta 2))]\ [t3 - (H1(\cos(\alpha 1) + \cos(\beta 1))/V1].$$

Depths to the V2 and V3 layers were calculated using the average intercept time of the forward and reversed profiles. In most cases, intercept times of a line segment pair varied slightly because small dips (generally < 4 degrees) were detected causing the slopes of the lines to differ only slightly. Due to the fact that this difference would cause depth values to vary by 0.5 meter or less for each profile, the two times were simply averaged to determine an average depth value along each line.

The initial step in the interpretation process was to estimate how many horizons might actually be encountered in the field and the approximate velocity values associated with each horizon. Especially of interest was the velocity of the saturated alluvium. As previously mentioned, three horizons were anticipated with associated velocity ranges of 250–350 meters

per second, 600–1000 meters per second, and 1600–2000 meters per second. The western hydrologic monitoring site was utilized to obtain a direct measurement of the depth to water which could be compared to the refraction data. The depth to water in an observation well was found to be 6.0 meters. Line 2 was run approximately 15 meters from the site of measurement along a dirt road. The line was run on the road so that it would be on a flat surface. Geophone spacings and the shot offset were 2.5 meters. Three distinct horizons were detectable from the time–distance graph. The three associated velocities were calculated to be 285 meters per second, 833 meters per second, and 2000 meters per second respectively. Depths to refracting horizons were found to be 4.1 meters to the first horizon and 5.3 meters to the second horizon. The elevation of the seismic line was estimated to be 0.8 meter lower than that of the observation well so the refractor at a depth of 5.3 meters with a velocity of 2000 meters per second was able to be confidently correlated with the water table, assuming that the water table is flat over this distance. All of the calculated velocities agreed extremely well with the expected values.

Since data for this study were collected over an eight month period from July, 1987 to April, 1988, there was some concern as to whether fluctuations in the water table might occur over this length of time. Any major variations might cause erroneous anomolies to be observed between data collected during differing time periods. Fortunately, this was not the case. Water table elevation data gathered by Stephens (1988) from 19 observation wells at the two hydrologic monitoring sites indicate that only minimal fluctuations occur (see Table 1). Many of the wells were monitored on a weekly basis for up to 18 months from 1985 to 1987. Data

TABLE 1

Observation well data incorporated with seismic refraction data

Well	Period of Measurements	Mean Elevation (m)	σ
U8	9/85 - 4/87	1478.7	0.46
U9	9/85 - 4/87	1479.1	0.50
U10	9/85 - 4/87	1480.1	0.52
U15	9/85 - 3/87	1481.0	0.51
U22	4/86 - 7/86	1481.9	0.15
L1	9/85 - 10/86	1443.5	0.57
L2	9/85 - 3/87	1444.2	0.78
L3	9/85 - 3/87	1444.2	0.74
L4	9/85 - 3/87	1445.9	0.74

from nine of the wells (Figure 24) were incorporated with the seismic interpretation results. The average water elevation values were used with the seismic data when constructing a water table elevation map and cross section. The standard deviation values for all of the well measurements are less than 0.8 meter which is near the accuracy of the refraction data. It was, therefore, concluded that any minimal fluctuations which might occur did not significantly affect the results of the refraction data interpretation. Thus, it is possible to combine data collected at different times.

None of the seismic lines detected more than three horizons because of high attenuation in the Rio Salado. The total thickness of the Rio Salado alluvium could not be determined since the rocks of the Santa Fe Group were unable to be detected. Some minimum thickness estimates can be made, though. By assuming that the crossover distance between the saturated alluvium and the rocks of the Santa Fe Group occurred at the last geophone (in other words, if there was a 13th geophone, it would detect the refracted signal from the Santa Fe Group), and that the velocity of the Santa Fe Group rocks was 2500 meters per second, minimum depth estimates were made for five lines. These are presented in Table 2.

Another approach to estimate the depth to the Santa Fe Group is to study secondary arrivals on the seismograms. Seismograms from four lines have been chosen and are presented in Appendix B. Secondary arrivals (labeled by the V4? branches) can be observed on the later traces having velocities greater than the V3 layer. These may represent refracted signals beginning to arrive from the Santa Fe Group. Assuming that these are in fact from the Santa Fe Group, depths were calculated and are presented in Table 2. Results obtained by this method are probably too deep (Hawley, personal communication, 1988), but it must be kept in mind

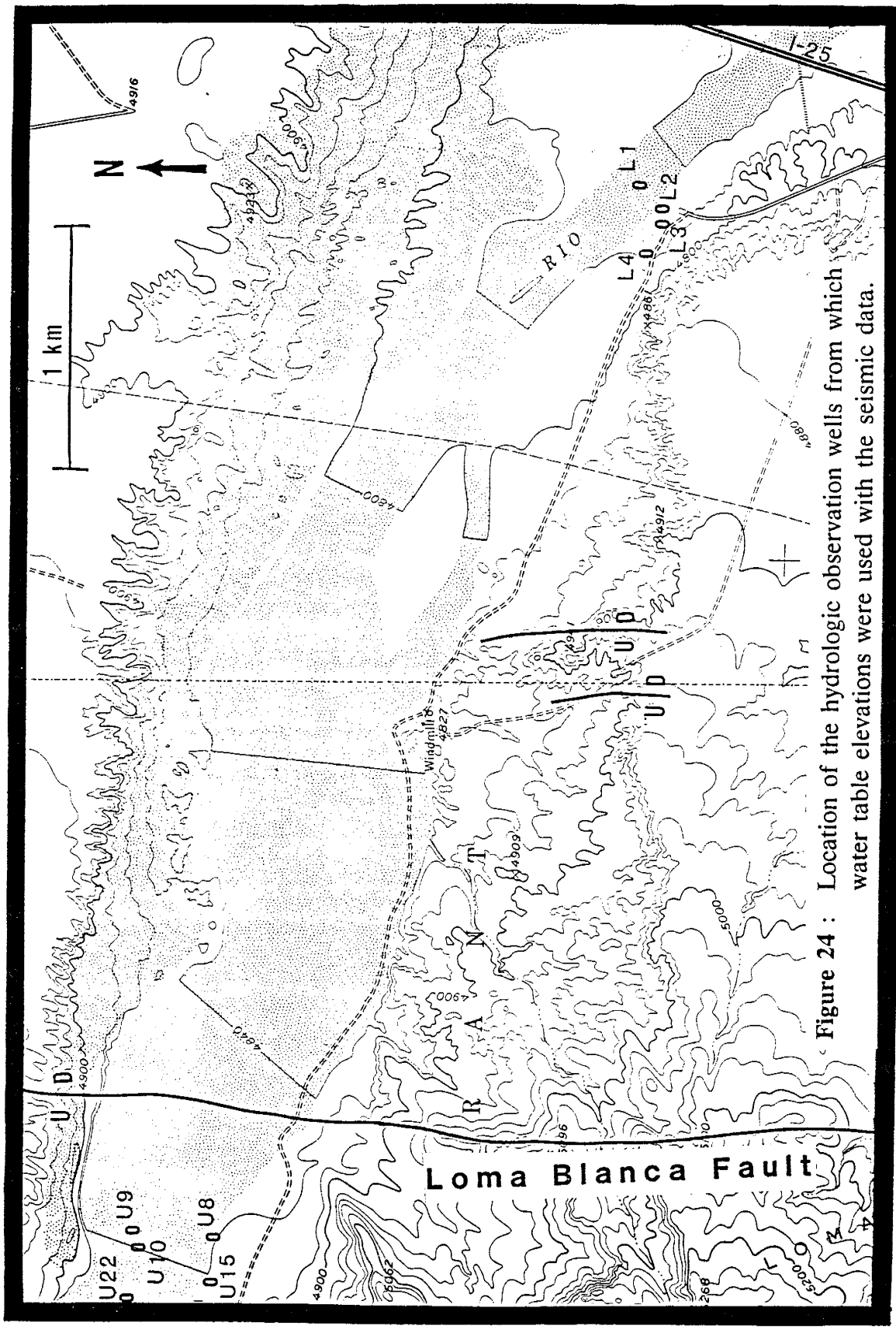

Figure 24 : Location of the hydrologic observation wells from which water table elevations were used with the seismic data.

TABLE 2

-----Depth Estimates to the Santa Fe Group---

Depths obtained assuming the last geophone is at the crossover distance (minimum estimates assuming that V4=2500 m/s)

Seismic line	Depth(meters)
1	23.2
12	8.5
13	11.4
19	17.7
20	17.5

Depths obtained using secondary arrivals (see Appendix B for seismograms)

Seismic line	V4 Velocity(m/s)	Depth(meters)
12	2500	28.4
13	2600	46.4
17a	2388	27.7
1	2185	60.3

that this is purely speculative. The signals arriving after the first arrivals become complex very quickly, so further investigation is required to determine if these arrivals truly represent the Santa Fe Group.

Water table depths interpreted from seismic data were converted to elevations (Figure 25) so that a cross section (Figure 26) and a structure contour map of the water table (Figure 27) could be constructed. Average water table elevation data from a number of hydrologic observation wells were incorporated into these figures with water table elevations derived by the seismic method. Elevations from the observation wells agreed to within ± 1.0 meter with the seismic data indicating accurate measurements were obtained through the seismic refraction method.

The cross section and the contour map illustrate two significant drops in the water table elevation. The first occurs approximately 300 meters west of the postulated position of the Loma Blanca fault. The second case in point occurs approximately 3300 meters downstream where the Rio Salado channel narrows. Other than these two instances, the water table shows a fairly uniform downstream decline in elevation which roughly parallels the surface topography. The elevation of the first refractor (top of layer 2) is also shown in Figure 24. This horizon is a fairly uniform 1.5 to 2.0 meters deep throughout most of the area. It essentially parallels the surface topography except for the extreme eastern part of the area where the upper alluvial layer exhibits a gradual thickening in the downstream direction.

The dip data for the water table are presented in Figure 28. All values are derived from seismic data and, therefore, are apparent dips. In general, the water table dips downstream, or east–southeast. A few locations in the eastern part of the area show slight upstream components of

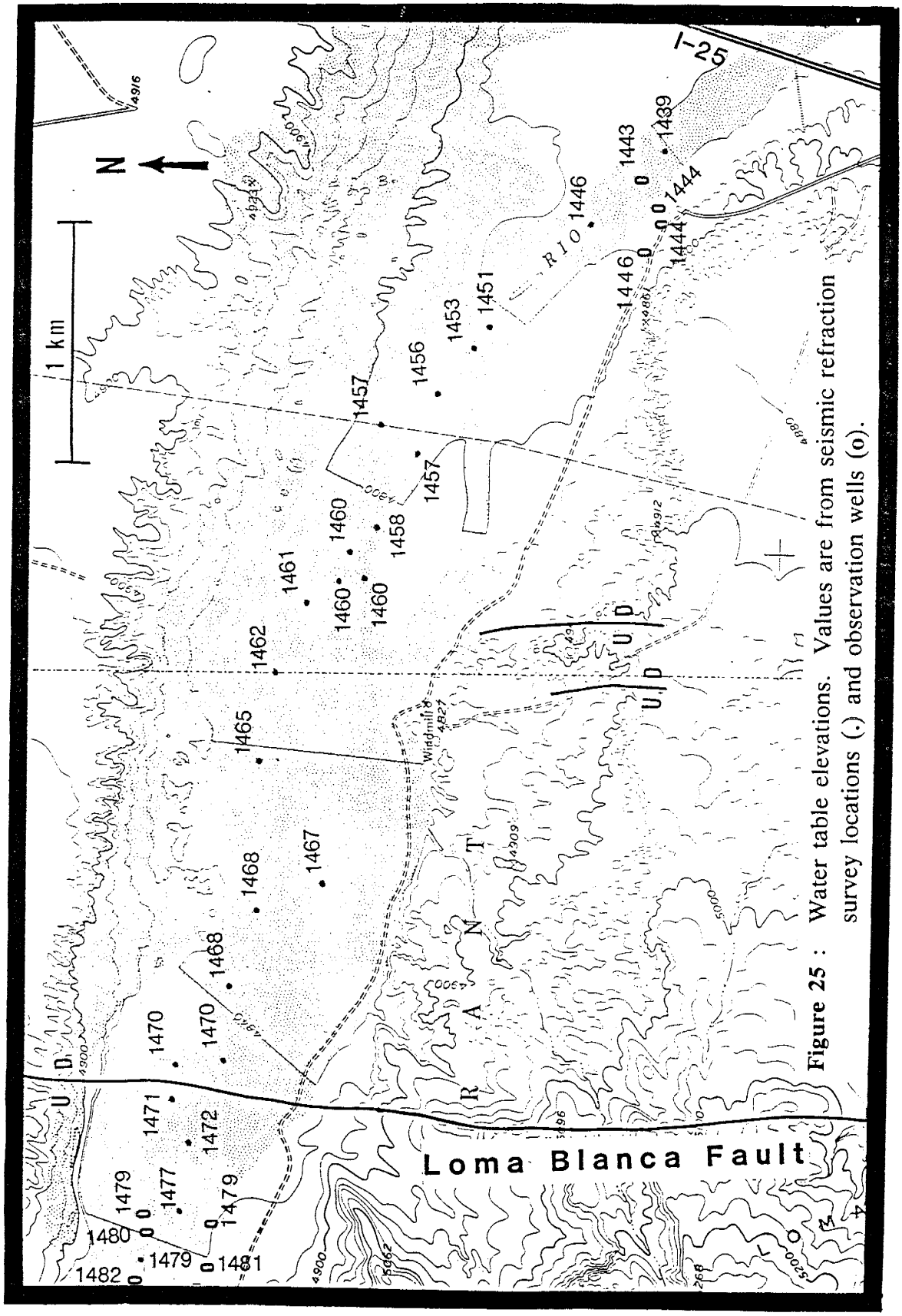

Figure 25 : Water table elevations. Values are from seismic refraction survey locations (.) and observation wells (o).

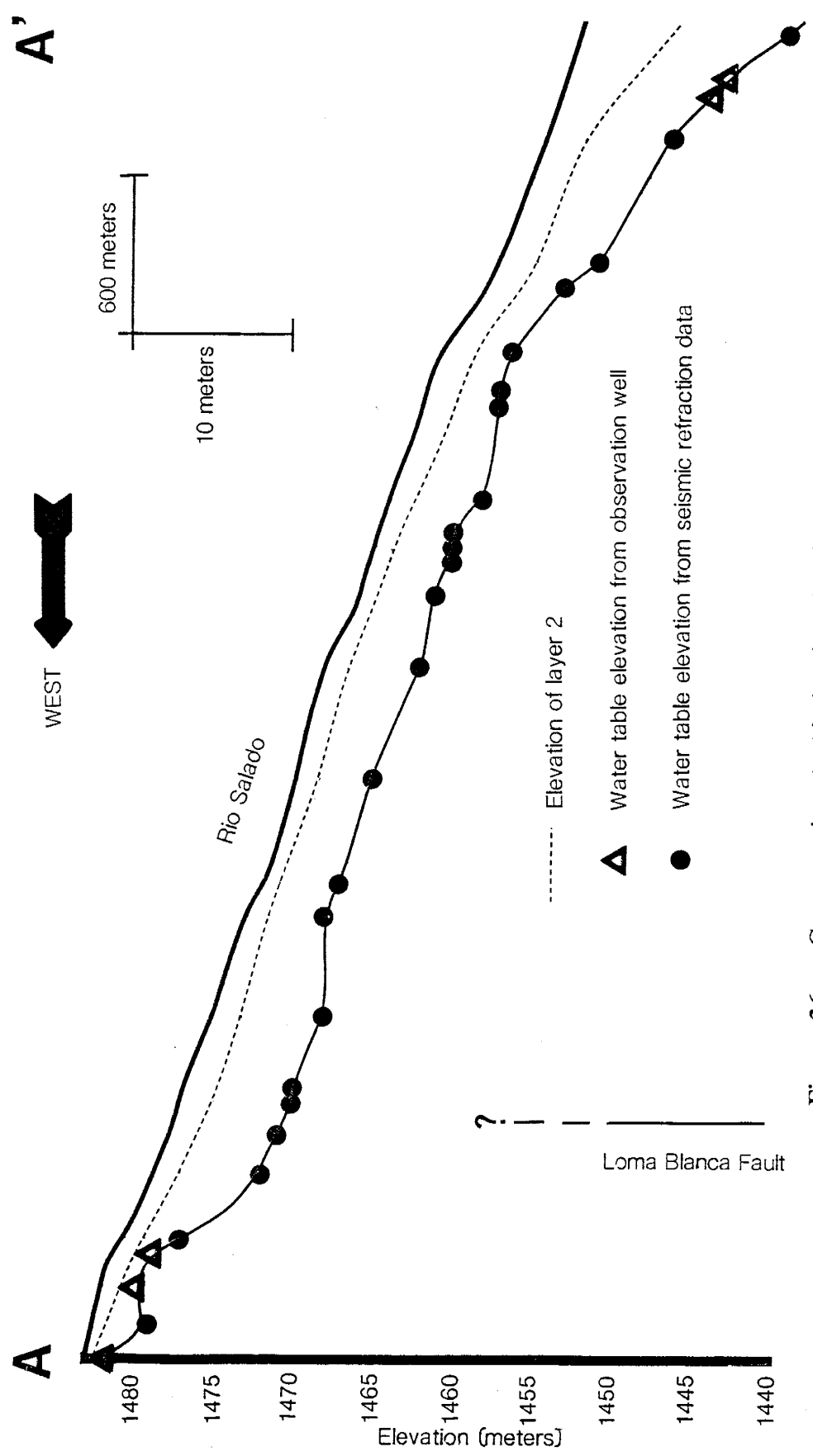

Figure 26 : Cross section A–A' showing the first refracting horizon and the water table relative to the Rio Salado. The cross section is through the center of the channel from A to A' shown in Figure 25.

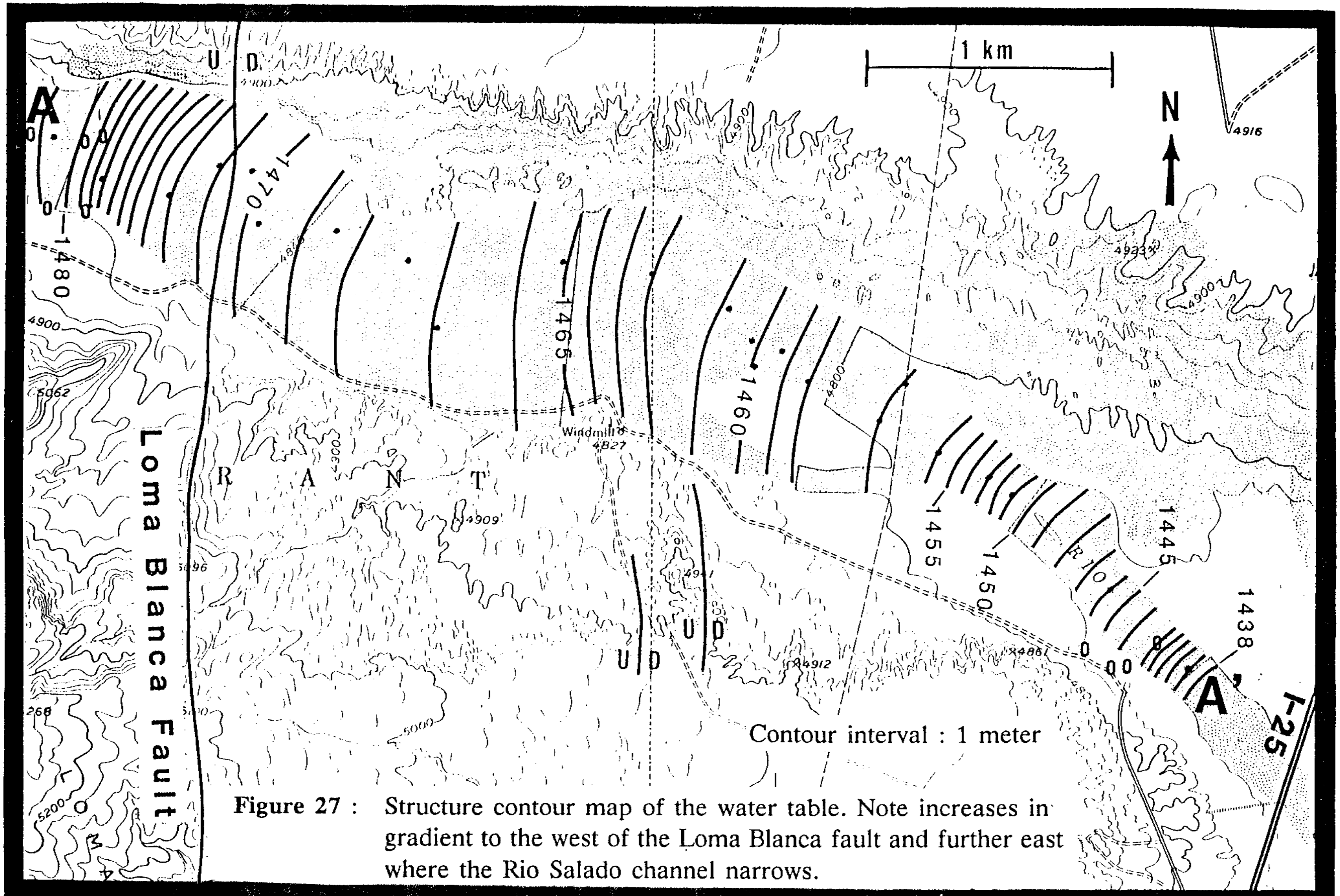

Figure 27 : Structure contour map of the water table. Note increases in gradient to the west of the Loma Blanca fault and further east where the Rio Salado channel narrows.

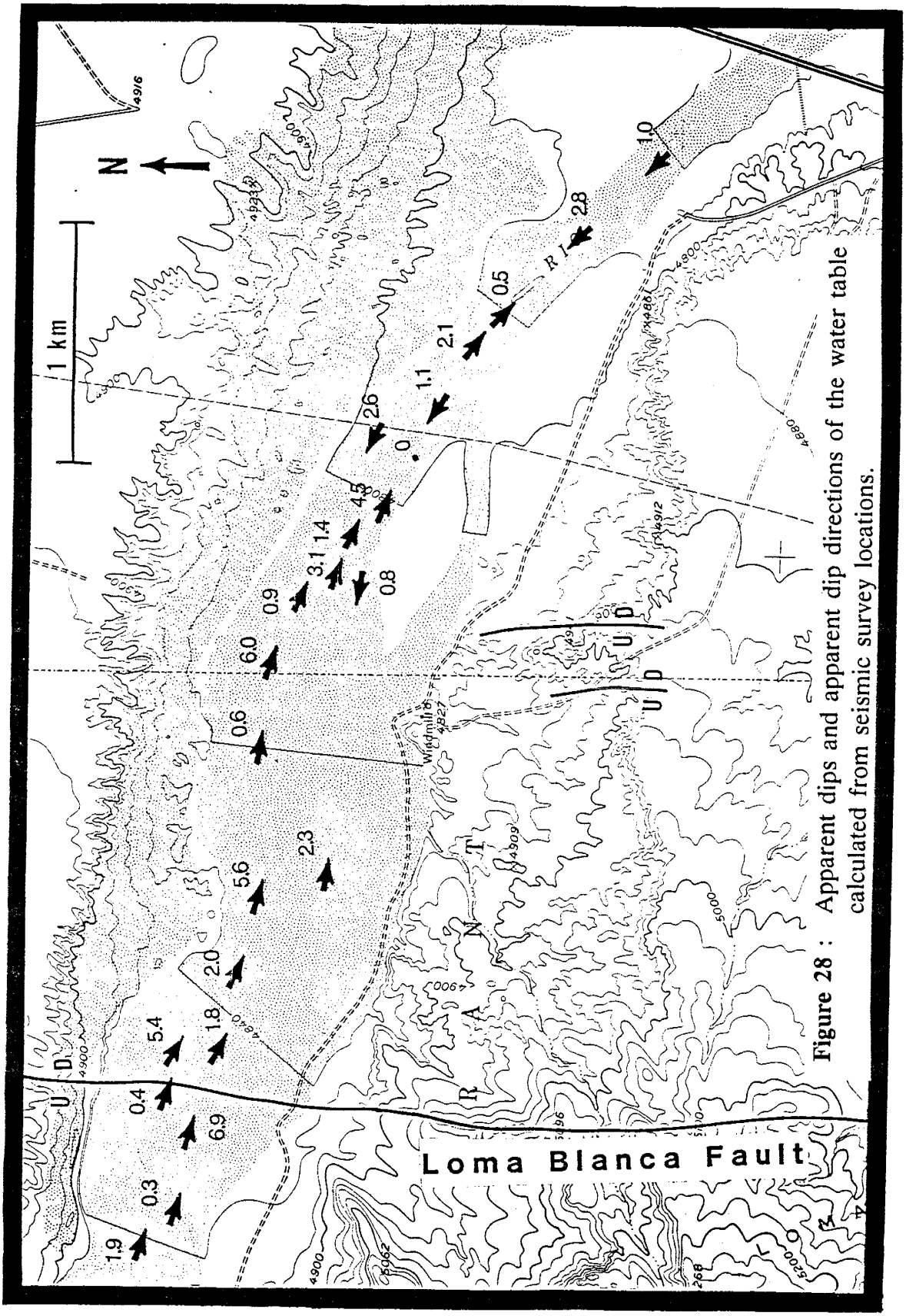

Figure 28 : Apparent dips and apparent dip directions of the water table calculated from seismic survey locations.

dip. Most of the dip values are relatively small, generally being less than 4 degrees. The dip data in this study are difficult to interpret because the calculated dips are relative to the ground surface. An upstream (or western) component might only imply that the layer is just dipping less steeply to the east than the ground surface. Additionally, because the lines are relatively short, any local small-scale variations will be detected and may be misleading when attempting to interpret the dip data on a larger scale.

Conclusions

The results of the seismic refraction data interpretation can be integrated with the known hydrologic and geologic data in the area so that inferences can be made about parameters controlling the water table. Refraction data has already been shown to agree extremely well with available water table data, so these results can be used with a high degree of confidence in reaching additional conclusions about the area.

Three horizons were consistently detected throughout the entire area of investigation. The third, or deepest, horizon has been interpreted to be the aquifer. Seismic results have been compared with direct water table measurements to substantiate this conclusion. The second horizon has been interpreted to be partially saturated alluvium and the first horizon to be highly attenuative dry alluvium. In general, all three horizons are probably geologically homogeneous. That is, all consist of a relatively uniform mixture of Quaternary sands and gravels. The primary differences in the three layers are the amount of water saturation and the degree of compaction. The variation of these characteristics create seismically inhomogeneous lay-

ers which results in the consistent detection of the three layers via the seismic refraction method.

The elevation of the water table generally declines downstream at a gradient of 6–7 meters per kilometer. The Rio Salado flows toward the center of the Rio Grande rift. The Rio Grande rift is characterized by blocks progressively downfaulted toward the center of the Rio Grande Valley, so alluvium most likely exhibits a natural downstream thickening as the flood plain of the Rio Grande is approached and the elevation of the bedrock (Santa Fe Group) declines toward the center of the Rio Grande Valley. The nature of the Santa Fe Group is believed to be the primary controlling factor. Superimposed on this general trend of a downstream water table decline are the two cases where the water table rapidly falls in elevation.

Because the Loma Blanca fault is a dip–slip fault with the east side down, it causes a vertical discontinuity in the Santa Fe Group that forms the base of the aquifer beneath the Rio Salado channel. Consequently, it is likely that these vertical displacements will also be apparent in the depth to the water table. The fault can be easily mapped south of the channel where a clastic dike exists along the north–south trending fault zone. The clastic dike terminates approximately 200 meters south of the channel and the fault has only been inferred to continue across the Rio Salado and northward. The observed, more rapid, water table elevation drop in this region substantiates the existence of the fault and, as will be discussed later, also helps to infer the paleostructure across the fault scarp.

There are a number of hypotheses that could explain why the gradient of the water table increases to approximately 18 meters per kilometer near the Loma Blanca fault. These cases are illustrated in Figure 29. The first (Figure 29a) is simply that the base of the Rio Salado alluvium is

a.

Case of thicker alluvium on downthrown side of fault

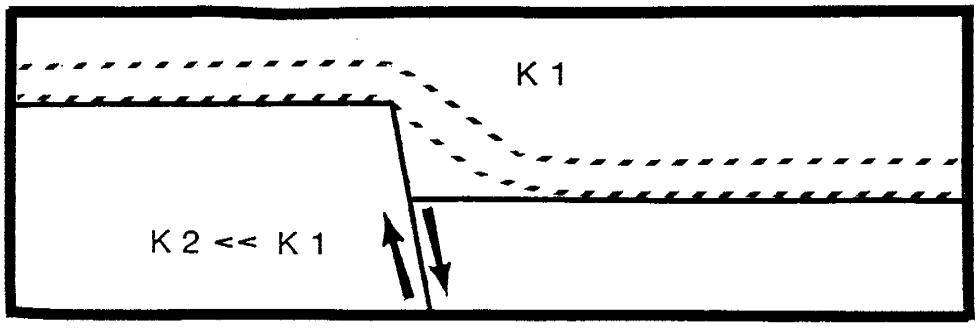

b.

Case of varying K in alluvium

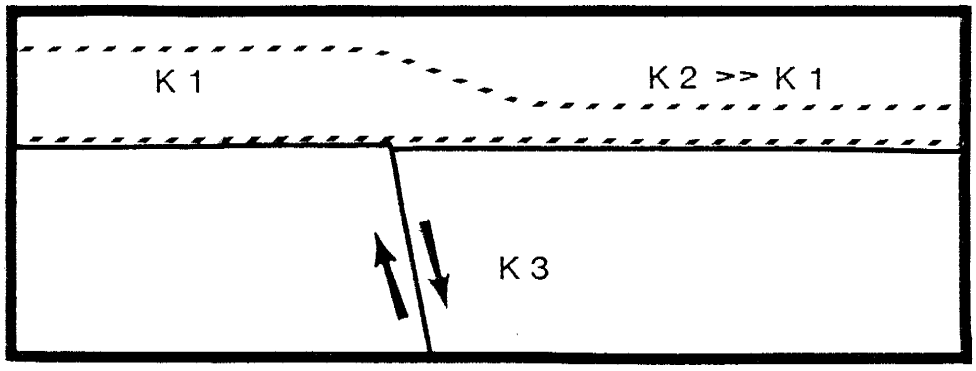

c.

Case of varying K in Santa Fe Group

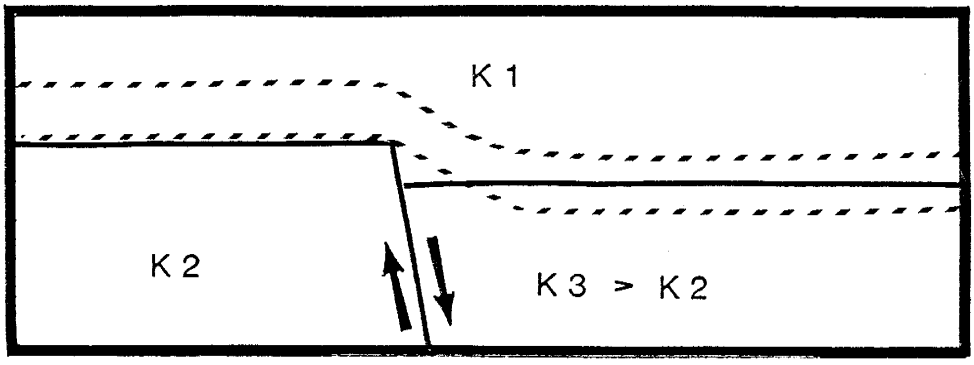

K = hydraulic conductivity

Aquifer limits

Figure 29 : Possible explanations for the water table elevation drop in the region of the Loma Blanca Fault.

d.

Case of fault acting as groundwater barrier

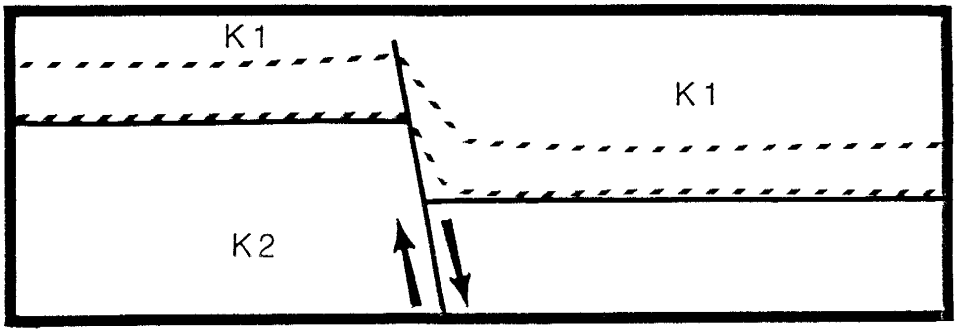

e.

Case of increasing aquifer dimensions

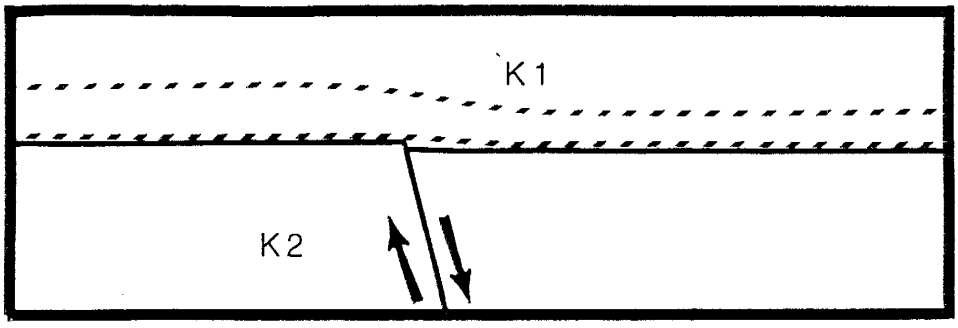

Figure 29, continued

deeper on the downthrown side of the fault. Assuming that the hydraulic conductivity is uniform throughout the aquifer and that the Santa Fe Group is an aquitard, the water table would drop as it crossed the fault.

Another possibility is that there is relatively no relief on top of the Santa Fe Group across the fault and the hydraulic conductivity of the alluvium changes (Figure 29b). For this case, the hydraulic conductivity of the alluvium on the downthrown side of the fault would have to be much greater than that on the upthrown side. This would allow for a greater volume of water to flow through the aquifer east of the fault and cause the water table to drop where the hydraulic conductivity increases. If this is the case and no vertical offset remains at the top of the Santa Fe Group, this hypothesis requires that there be some discontinuity in the alluvium above the fault. Even if this were a significant strike-slip fault penetrating the alluvium, it is difficult to explain geologically why the Quaternary alluvium would be different on opposite sides of the fault.

Hydraulic conductivity variations could also be present within the Santa Fe Group rocks (Figure 29c). If the hydraulic conductivity of the alluvium is constant but increases across the fault within the Santa Fe Group, the base of the aquifer would be in the Santa Fe Group on the downthrown side. Again, the water table would be forced to drop across the fault. This might be likely if the fault juxtaposed rocks of significantly different composition and porosity, but this would require a large vertical throw.

If the fault is cutting the alluvium (Figure 29d), a permeability barrier may exist within the aquifer caused by fault gouge. This would cause a damming effect upstream of the fault leading to a mounding up of the water table.

Another explanation may be that the hydraulic conductivity of the alluvium remains constant, but the lateral extent of the aquifer increases (Figure 29e). This would cause a water table drop because there would be more available space for groundwater flow downstream where the aquifer widens.

The probable cause of the water table drop at this location is a modification of Figure 29a. The latter hypotheses can be discounted because in all probability hydraulic conductivity does not increase across the fault, the fault is not cutting the alluvium, and the lateral extent of the aquifer is probably fairly consistent in this area. There is no evidence from the hydrologic investigations or any other rationale to conclude that the hydraulic conductivity of the Rio Salado alluvium should be anything but uniform. The Santa Fe Group rocks on both sides of the fault are presumably impermeable as they are finer grained and well indurated (Machette, 1978), therefore, the conductivity of these rocks will not affect the elevation of the water table. Also, the Loma Blanca Fault does not juxtapose rocks of radically different ages. Because the throw of the fault is small enough that the Santa Fe Group remains in contact on each side of the fault, there should not be any significant conductivity variations beneath the alluvium. The fault does not extend into the alluvium to create any permeability barriers. The water table would exhibit an even steeper decline in a more restricted area near the fault if the fault zone acted as a barrier. Rocks of the Santa Fe Group (Tsp) outcrop continuously along the southern bank of the channel (Figure 30), indicating that the area within which the Rio Salado alluvium is deposited does not increase laterally.

The rapid decline in the elevation of the water table near the Loma Blanca fault actually begins about 300 meters upstream of the in

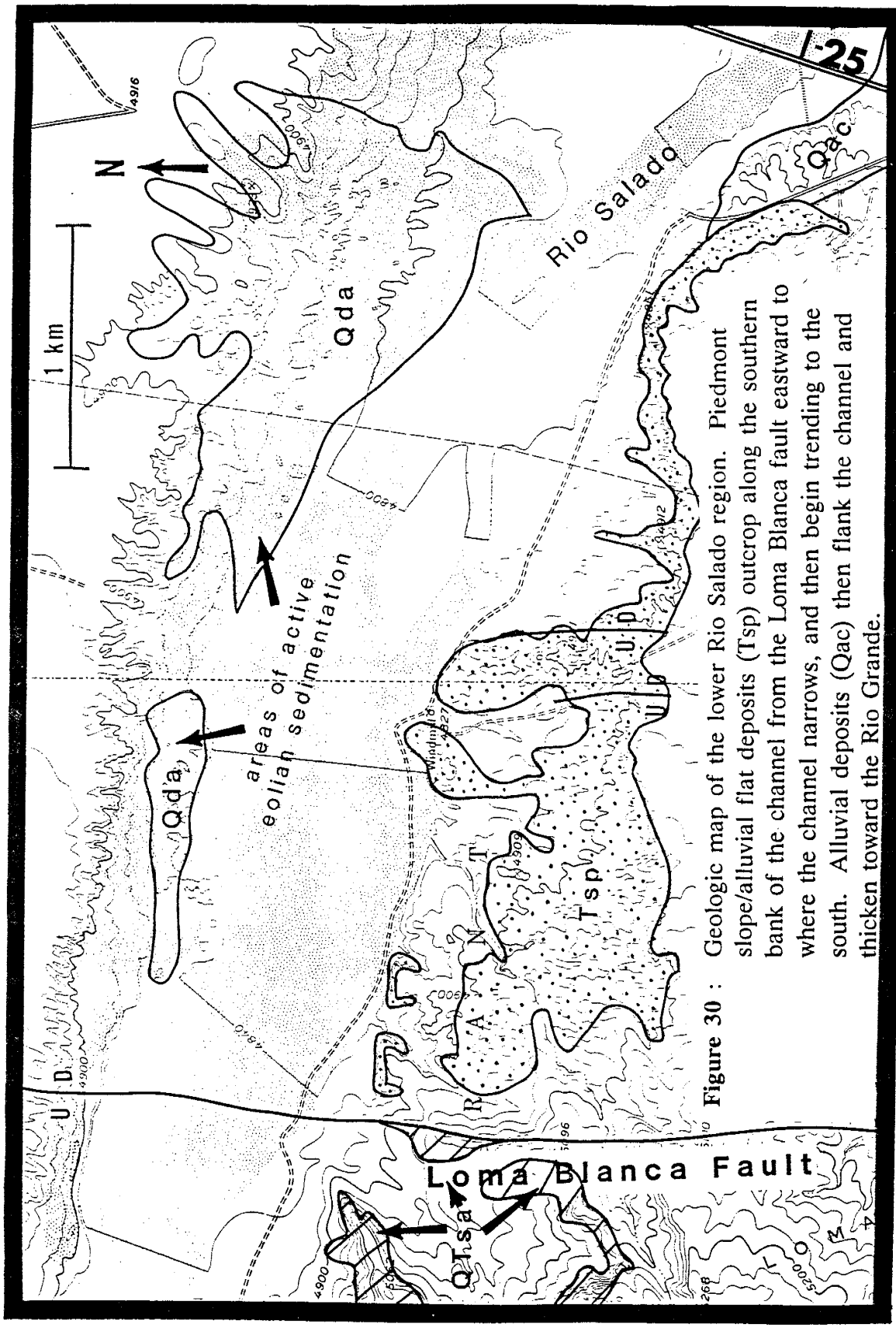

Figure 30 : Geologic map of the lower Rio Salado region. Piedmont slope/alluvial flat deposits (Tsp) outcrop along the southern bank of the channel from the Loma Blanca fault eastward to where the channel narrows, and then begin trending to the south. Alluvial deposits (Qac) then flank the channel and thicken toward the Rio Grande.

ferred position of the fault. This suggests that a slightly more complicated situation exists than that described in the proposed situations given in Figure 29. During a period of exposure sometime in the Quaternary (late Pleistocene?), it is believed that the younger axial stream deposits of the Santa Fe Group which outcrop a short distance away from the fault on the upthrown side (Figure 30) were subject to erosional processes. This resulted in a type of nickpoint feature which created a sloping topography from approximately 300 meters west of the fault to the older piedmont slope and alluvial flat deposits of the Santa Fe Group on the downthrown side. The Rio Salado then deposited alluvium within its channel and buried this feature. The water table is now controlled by the paleotopography of the Santa Fe Group rocks along the buried fault scarp (Figure 31). The water table effectively mirrors the paleotopography of the Santa Fe Group, beginning to drop in elevation where the nickpoint initiates and continues downward toward the fault. At the projected location of the fault, the most extensive drop has already occurred. The Loma Blanca fault controls the water table in the sense that the Santa Fe Group rocks were displaced and the ancient fault scarp was eroded, allowing a deeper alluvial section to be deposited on the downthrown side.

To the east of the Loma Blanca fault the water table elevation gradually declines in the downstream direction, paralleling the elevation of the Santa Fe Group rocks. Here again, the unconfined aquifer is generally controlled by the underlying aquitard rather than surface topography. The two faults south of the channel in the central part of the area probably do not extend beneath the Rio Salado channel because the water table gradient remains fairly uniform across this region.

The character of the Santa Fe Group is believed to be the primary

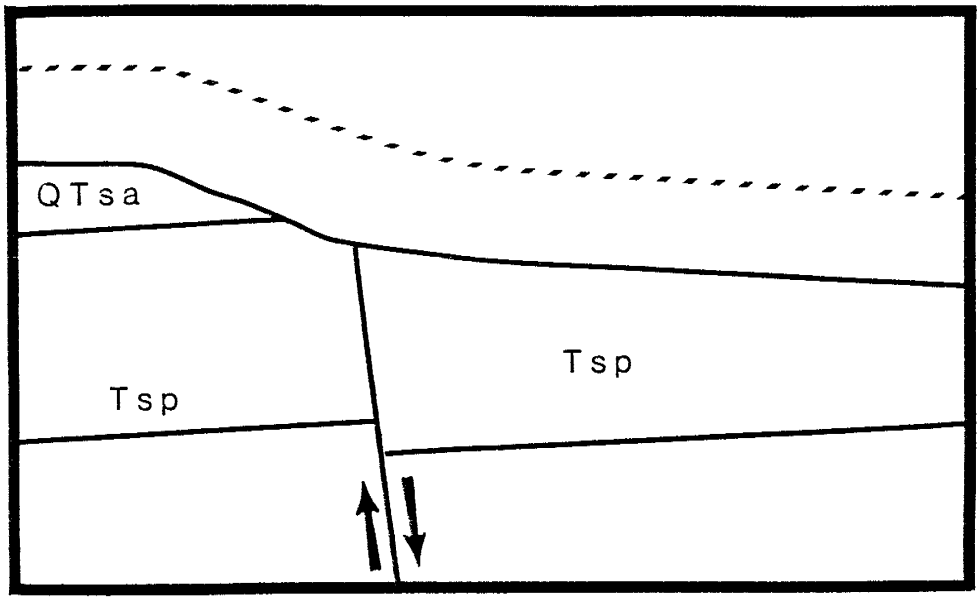

Figure 31 : Proposed geologic model illustrating the factors controlling the water table near the Loma Blanca fault. The water table parallels a nickpoint preserved on the paleotopography of the Santa Fe Group.

controlling factor where the water table exhibits a second increase in gradient (approximately 14 meters per kilometer) roughly 3300 meters east of the Loma Blanca fault. This elevation decline is not as large as the first case, but is evident. This point is approximately 3.5 kilometers from the confluence of the Rio Salado and the Rio Grande. At this location, a significant portion of the Santa Fe Group has probably been removed as a result of the Rio Grande occasionally migrating to the west and the Rio Salado channel experiencing a relatively high degree of erosion in trying to achieve the base level of the Rio Grande. In essence, the basin that has been carved into Santa Fe Group within which the Rio Salado alluvium is deposited has been enlarged laterally and cut deeper in this area. The surface geology in the area presents some evidence to support this theory (Figure 30). The piedmont slope and alluvial flat deposits (Tsp) of the Santa Fe Group outcrop in a narrow east–west trending band almost continuously along the south side of the Rio Salado to the east of the Loma Blanca fault. In the area where the water table gradient begins to increase, the outcrop pattern of these rocks veers to the south which may indicate a widening of the alluvial basin. From this point east to the Rio Grande, the Rio Salado floodplain is broad and flat, and the channel is flanked by silty sand to sandy gravel sized alluvium (Qac) which thickens toward the Rio Grande (Machette, 1978). This would essentially increase the width of the aquifer and cause the water table to drop because there would be an increase in the available space for groundwater flow.

In summary, through the use of seismic refraction data, a number of conclusions have been reached concerning the geologic and hydrologic characteristics of the lower Rio Salado. The water table has been accurately mapped and two significant elevation drops have been documented. The

integration of the seismic refraction data with known hydrologic and geologic data has resulted in evidence supporting the location of the Loma Blanca fault. The nature of the drop in the water table suggests that a nickpoint developed across the fault. From this point downstream, the water table parallels the top of the Santa Fe Group until it reaches a point where the Santa Fe Group has been eroded, allowing the dimensions of the aquifer to increase causing the water table to drop again.

Future Investigations

The Rio Salado presents excellent opportunities for future investigations. One of the primary problems which needs addressed is the depth to the Santa Fe Group throughout the area. At this time, the exact thickness of the alluvial section is unknown. The construction of a structure contour map of the Santa Fe Group would greatly enhance the understanding of the geologic and hydrologic characteristics of the area.

Seismic studies should be continued in the area. Future seismic investigations should employ longer line lengths, additional geophones per line, and a more powerful energy source so that refracted arrivals from the Santa Fe Group can be detected. The detection of the Santa Fe Group could be achieved using the same geophone spacings as in this study, but by adding geophone stations at greater offsets and using more powerful sources to compensate for the great attenuation in the area.

More detailed studies should also be conducted with data from short survey lines or with the data from this study. Secondary arrivals should be closely examined to verify if they actually do correspond to a V4 layer. Time–distance data should also be interpreted in more detail to define more complicated, local structure. For example, the time–distance

graphs of Line 4, Line 24, and Line 26 show that the data, especially from the V3 layer, deviate somewhat from a straight line. This may indicate the presence of local structural variations.

A drilling program should supplement the investigations to obtain direct measurements to the water table as well as the Santa Fe Group. Presently, there are a number of observation wells which have been drilled, but all of them are concentrated in the two hydrologic monitoring areas. This study has shown that accurate results can be obtained through the interpretation of seismic refraction data. Therefore, only a few wells need to be drilled in various locations and seismic surveys can fill the voids between them. A well planned drilling program could be carried out in a relatively inexpensive manner because refraction surveys could also be utilized to monitor water depths as well as delineate various geologic horizons between wells.

REFERENCES

Ackerman, H. D., Pankratz, L.W., and Dansereau, D., 1986, Resolution of ambiguities of seismic refraction traveltime curves : Geophysics, v. 51, pp. 223-235.

Anderson, K. R., 1988, Validation of Q determination techniques in a highly attenuative environment : Geophysical Open-File Report, New Mexico Institute of Mining and Technology.

Czarnecki, J. B., 1987, Characterization of the subregional ground-water flow system of a potential site for a high level nuclear waste repository : Unpublished Ph.D. dissertation, The University of Minnesota.

Denny, C. S., 1940, Tertiary geology of the San Acacia area, New Mexico : Journal of Geology, v. 48, pp. 73-106.

Denny, C. S., 1941, Quaternary geology of the San Acacia area, New Mexico : Journal of Geology, v. 49, pp. 225-260.

Dobrin, M. B., 1976, Introduction to geophysical prospecting: McGraw-Hill, Inc., 630 p.

Eaton, G. P., 1974, Seismology; in Zohdy, A. R., Eaton, G. P., and Mabey, D. R., Techniques of Water Resources Investigations of the U. S. Geological Survey, Application of surface geophysics to ground-water investigations : Book 2, Chapter D1, pp. 67-84.

Eaton, G. P., and, Watkins, J. S., 1967, The use of seismic refraction and gravity methods in hydrogeological investigations; in Morley, L. W. (ed.), Mining and Groundwater Geophysics : Geological Survey of Canada, Economic Geology Report #26, pp. 544-568.

Evans, G. C., 1963, Geology and sedimentation along the lower Rio Salado in New Mexico : Unpublished M. S. thesis, New Mexico Institute of Mining and Technology, 78 p.

Haeni, F. P., 1986, Application of seismic refraction methods in ground-water modeling studies in New England : Geophysics, v.51, pp. 236-249.

Hatherly, P. J., 1986, Attenuation measurements of shallow seismic refraction data : Geophysics, v.51, pp. 250-254.

Havlena, J., 1988, Hydrologic parameters of an ephemeral stream : the Rio Salado of central New Mexico : Unpublished M.S. thesis, New Mexico Institute of Mining and Technology, 218 p.

Johnson, R. B., 1954, Use of the seismic refraction method for differentiat ing Pleistocene deposits in the Arcola and Tuscola quadrangles, Illinois : Illinois State Geological Survey Report, Inv. 176, 59 p.

Johnson, S. H., 1976, Interpretation of split-spread refraction in terms of plane dipping layers : Geophysics, v. 41, pp. 418-424.

Kjartansonn, E., 1979, Constant Q-wave propagation and attenuation : Jour nal of Geophysical Research, v. 84, pp. 4737-4748.

Knapp, J. S., 1988, Seismic refraction survey in the Rio Salado : Unpublished class report, New Mexico Institute of Mining and Technology.

Machette, M. N., 1978, Geologic map of the San Acacia quadrangle, Socorro County, New Mexico : U. S. G. S., Map GQ-14, scale 1:24,000.

Mazzaferro, D. L, 1984, Groundwater availability and water quality in Southbury and Woodbury, Connecticut : U. S. G. S. Water Re sources Investigations Open-File Report 83-4221.

Morrissey, D. J., 1983, Hydrology of the Little Androscoggin River Valley aquifer, Oxford County, Maine : U. S. G. S. Water Resources Investigations Open-File Report 83-4018.

Northwood, E. J., 1967, Notes on errors in refraction interpretation; in Musgrave, A. (ed.), Seismic Refraction Prospecting : Society of Exploration Geophysicists, pp. 459–465.

Olmsted, F. H., Loeltz, O. J., and Irelan, B., 1973, Geohydrology of the Yuma area, Arizona and California : U. S. G. S. Professional Paper 486–H, 227 p.

Pakisar, L. C., and Black, R. A., 1957, Exploring for ancient channels with the refraction seismograph : Geophysics, v. 22, pp. 32–47.

Stephens, D. B., 1988, Field study of ephemeral stream infiltration and recharge : New Mexico Water Resources Research Institute Technical Completion Report #228.

Warrick, R. E., and Winslow, J. D., 1960, Application of seismic methods to a groundwater problem in northeast Ohio : Geophysics, v. 25, pp. 505–519.

Winograd, I. J., and Thordarson, W., 1975, Hydrogeologic and hydro-chemical framework, south-central Great Basin, Nevada-California, with special reference to the Nevada Test Site : U. S. G. S. Professional Paper 712-C, 126 p.

APPENDIX A

Appendix A includes all of the time distance graphs which were constructed for all seismic refraction lines. The line numbers on the graphs correspond to the numbered locations in Figure 5 of the text. The apparent velocities for the shotpoint from the west (Va1, Va2, and Va3), the apparent velocities for the shotpoint from the east (Vb1, Vb2, and Vb3), the actual velocities, the depth to the first refractor (H1), and the depth from the first refractor to the second refractor (H2) are listed with each graph. Shotpoint offset distances are equal to the geophone spacing unless otherwise indicated.

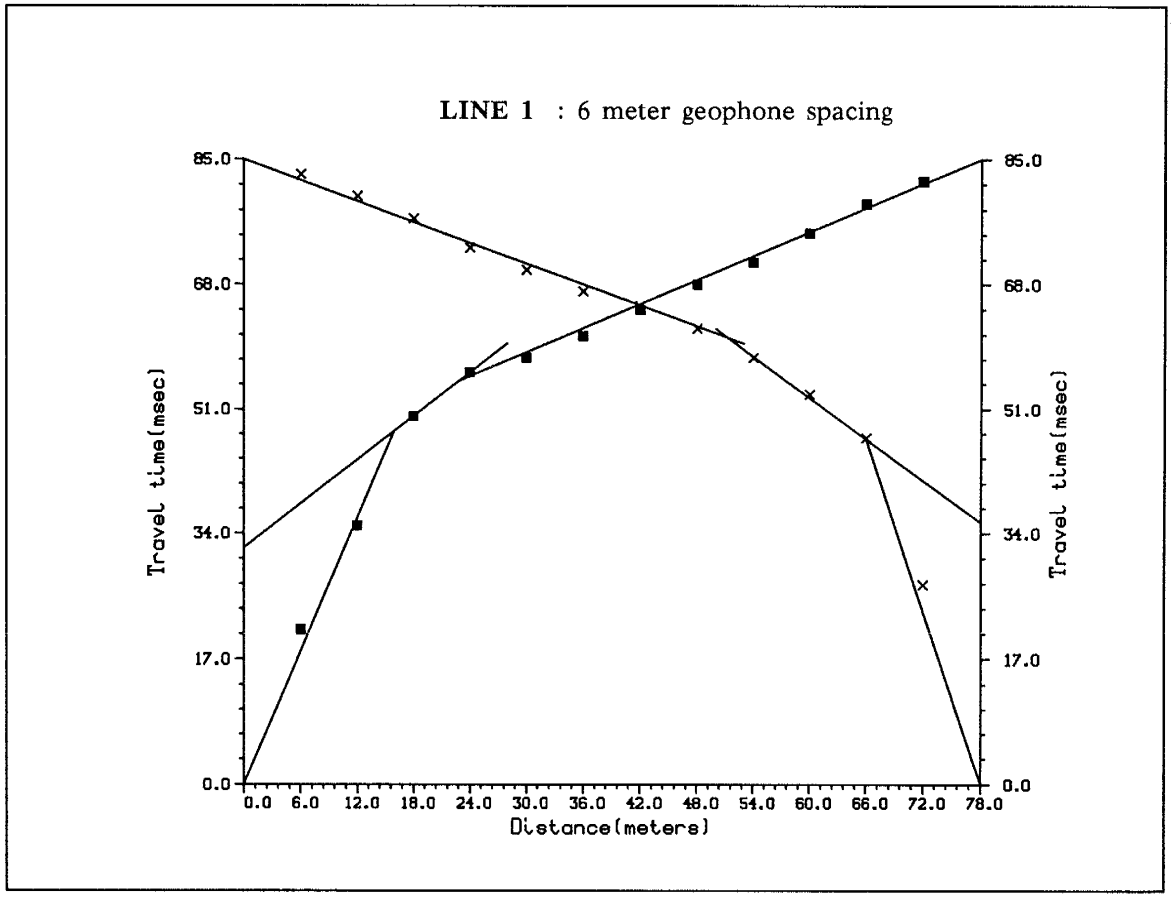

WEST

Apparent

Va1 = 333 m/s
Va2 = 1000 m/s
Va3 = 1833 m/s

EAST

Apparent

Vb1 = 333 m/s
Vb2 = 1059 m/s
Vb3 = 2100 m/s

Actual

V1 = 333 m/s
V2 = 1028 m/s
V3 = 1962 m/s
H1 = 5.9 m
H2 = 6.1 m

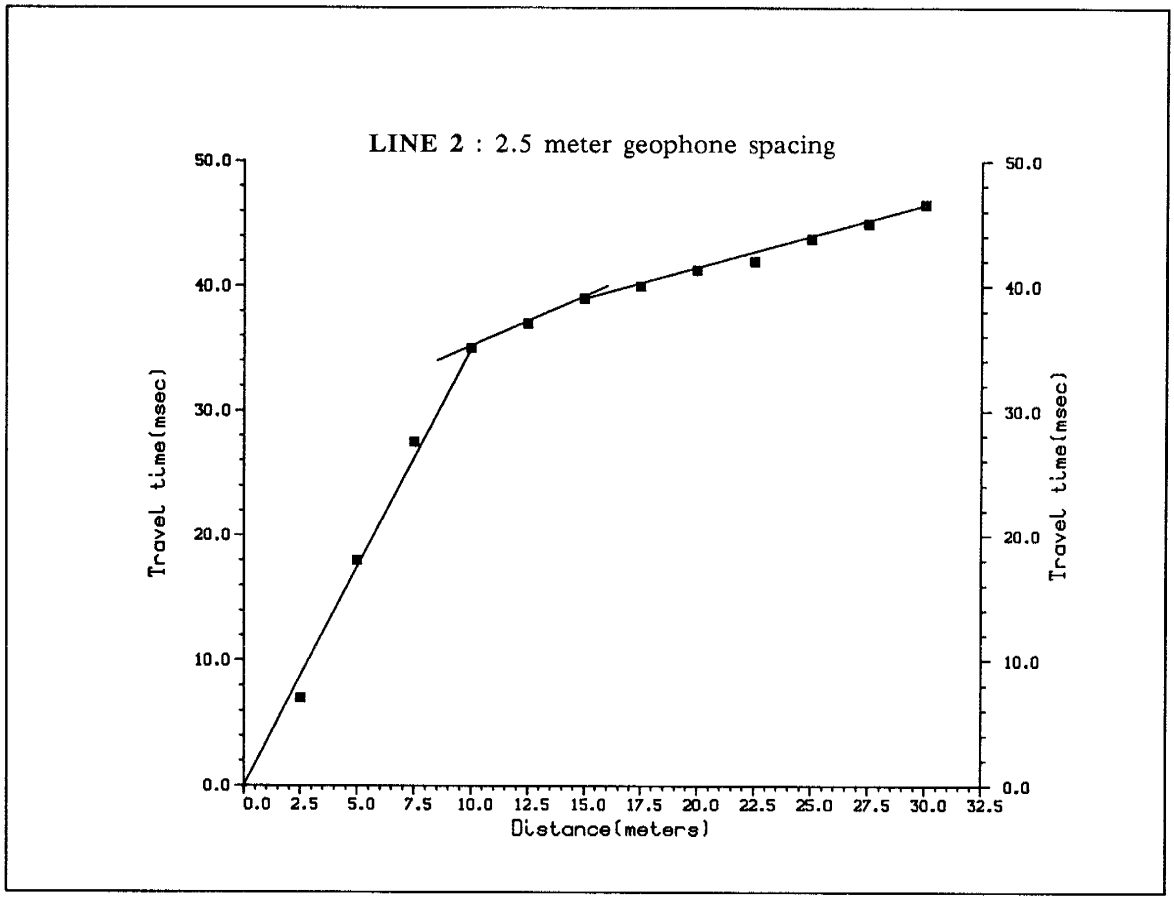

WEST **East**

V1 = 285 m/s
V2 = 833 m/s
V3 = 2000 m/s
H1 = 4.1 m
H2 = 1.2 m

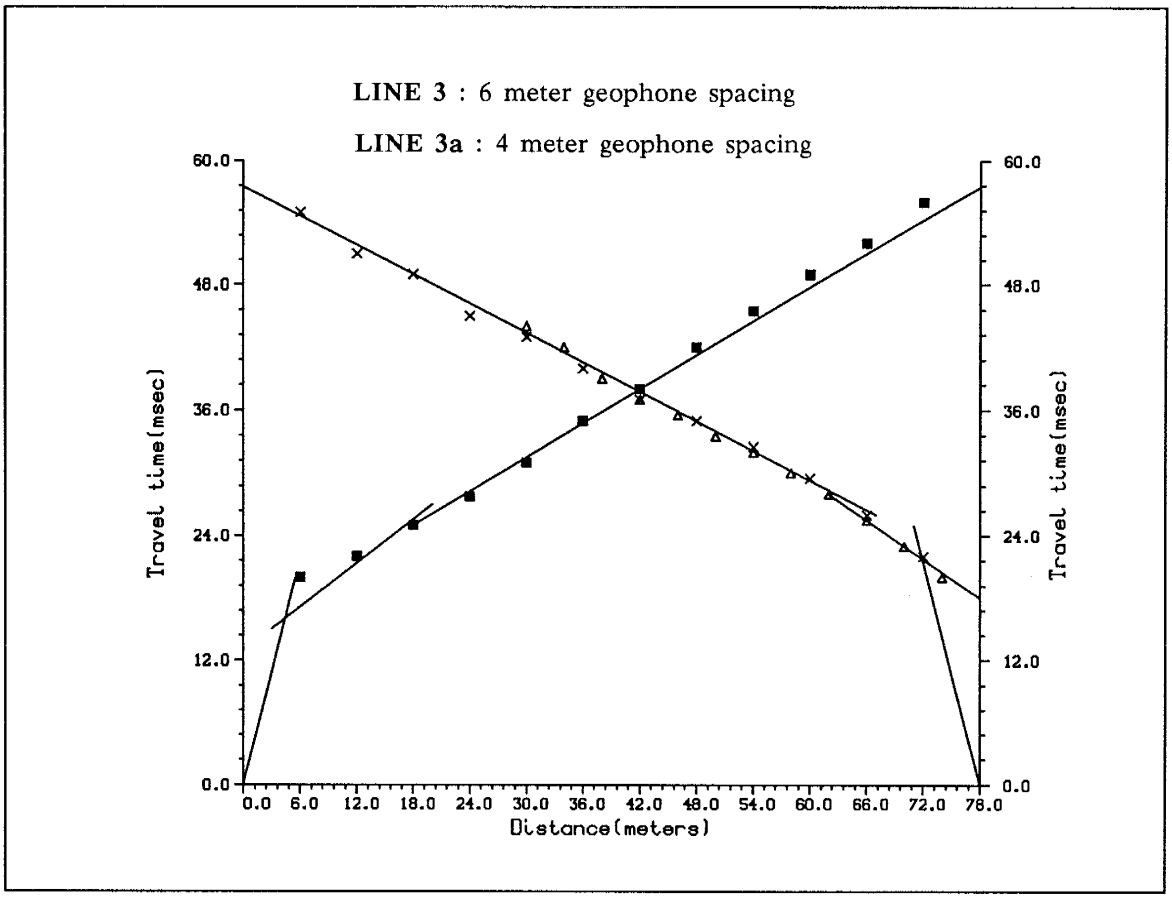

WEST

Apparent

V1a = 275 m/s
V2a = 1400 m/s
V3a = 1850 m/s

EAST

Apparent

V1b = 275 m/s
V2b = 1500 m/s
V3b = 2150 m/s

Actual

V1 = 275 m/s
V2 = 1441 m/s
V3 = 2003 m/s
H1 = 2.1 m
H2 = 2.7 m

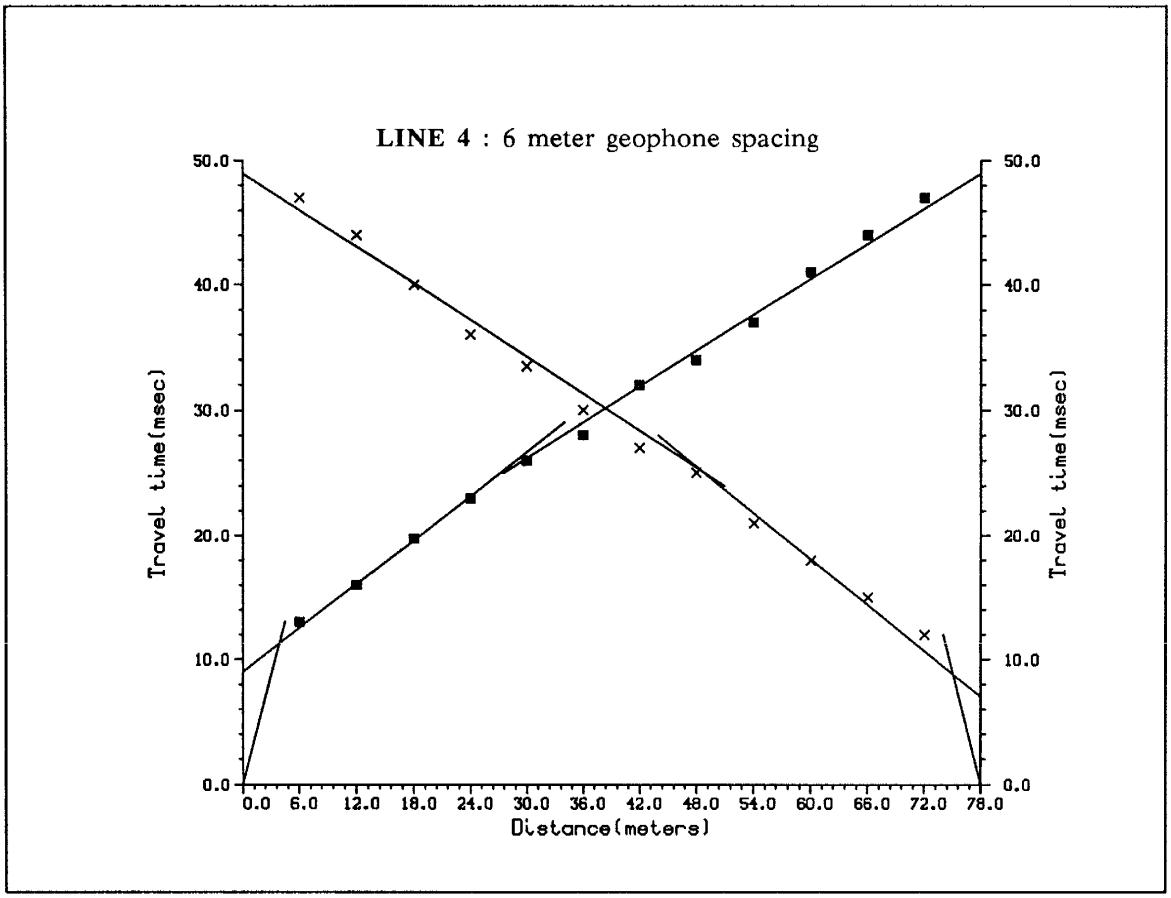

WEST

Apparent

Va1 = 333 m/s
Va2 = 1688 m/s
Va3 = 2125 m/s

EAST

Apparent

Vb1 = 333 m/s
Vb2 = 1607 m/s
Vb3 = 1875 m/s

Actual

V1 = 333 m/s
V2 = 1677 m/s
V3 = 1986 m/s
H1 = 1.4 m
H2= 4.7 m

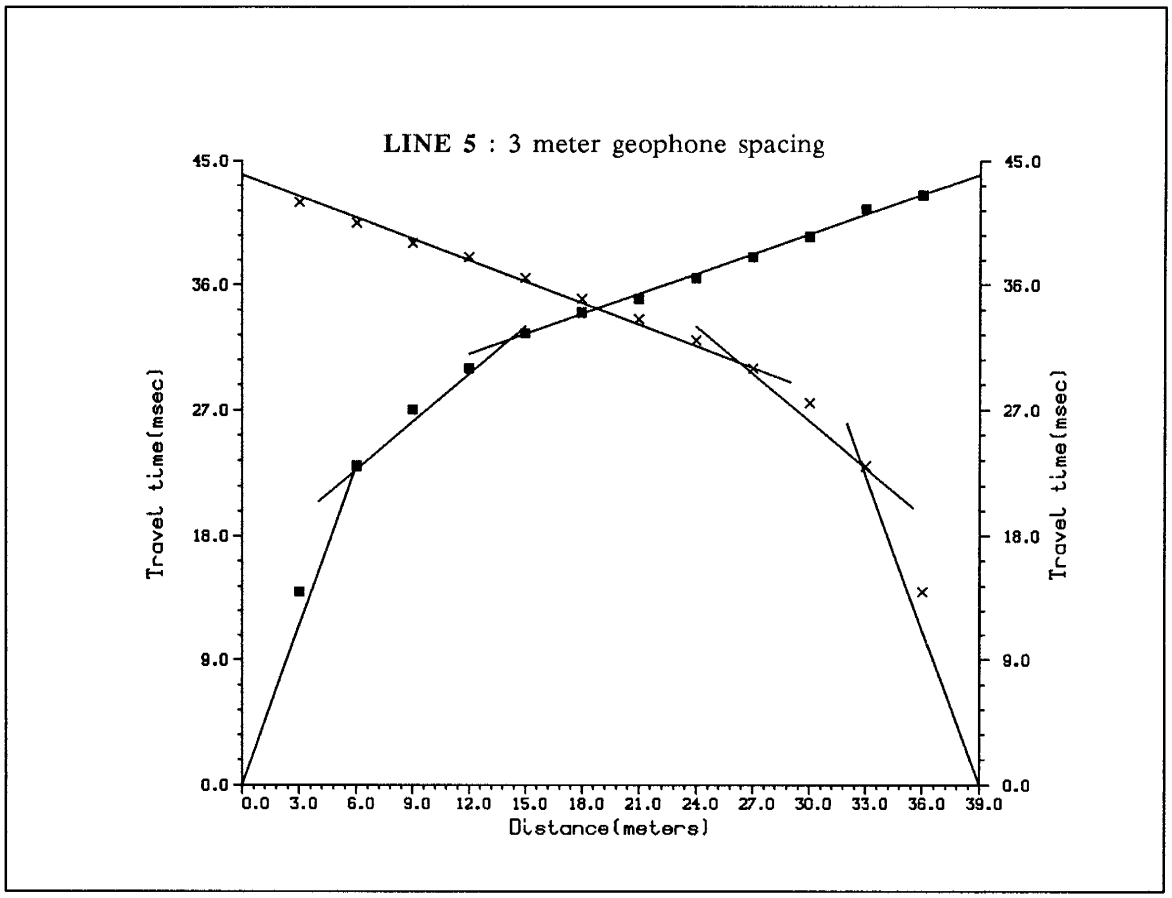

WEST

Apparent

Va1 = 275 m/s
Va2 = 900 m/s
Va3 = 2071 m/s

EAST

Apparent

Vb1 = 275 m/s
Vb2 = 890 m/s
Vb3 = 2000 m/s

Actual

V1 = 275 m/s
V2 = 895 m/s
V3 = 2013 m/s
H1 = 2.3 m
H2 = 4.3 m

LINE 6 : 3 meter geophone spacing

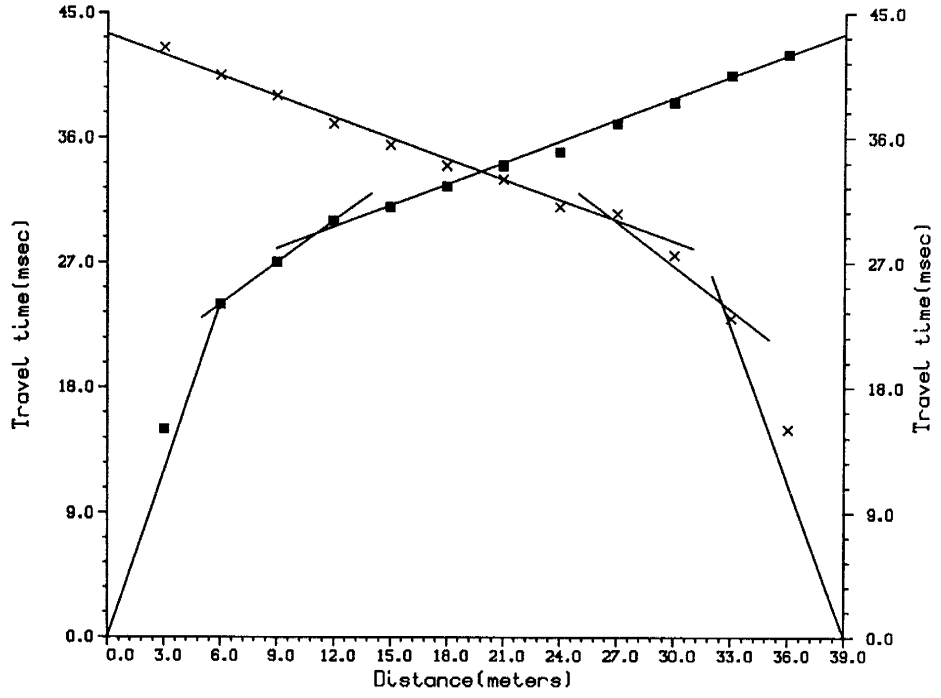

WEST

Apparent

Va1 = 275 m/s
Va2 = 1000 m/s
Va3 = 2000 m/s

EAST

Apparent

Vb1 = 275 m/s
Vb2 = 1000 m/s
Vb3 = 2000 m/s

Actual

V1 = 275 m/s
V2 = 1000 m/s
V3 = 2000 m/s
H1 = 2.5 m
H2 = 3.2 m

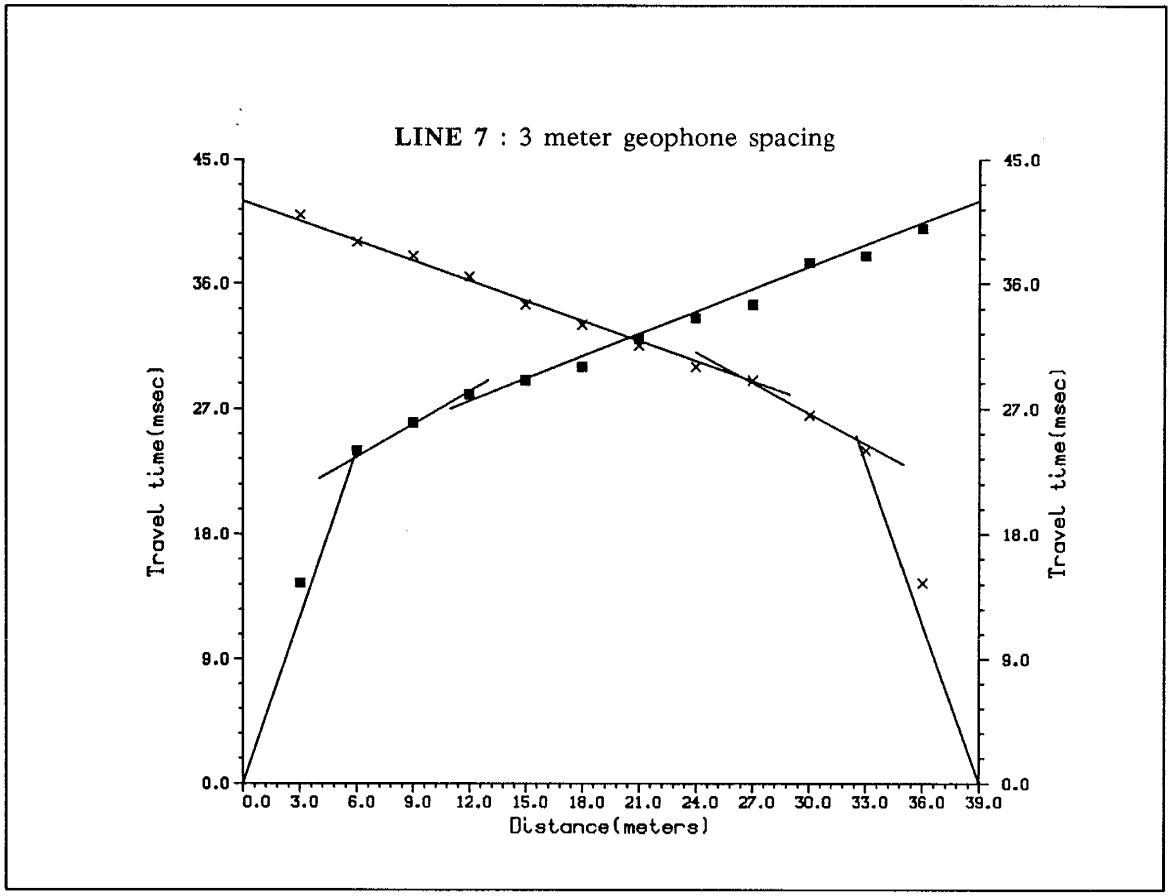

WEST

Apparent

Va1 = 275 m/s
Va2 = 1300 m/s
Va3 = 1889 m/s

EAST

Apparent

Vb1 = 275 m/s
Vb2 = 1333 m/s
Vb3 = 2100 m/s

Actual

V1 = 275 m/s
V2 = 1323 m/s
V3 = 1966 m/s
H1 = 2.7 m
H2 = 2.3 m

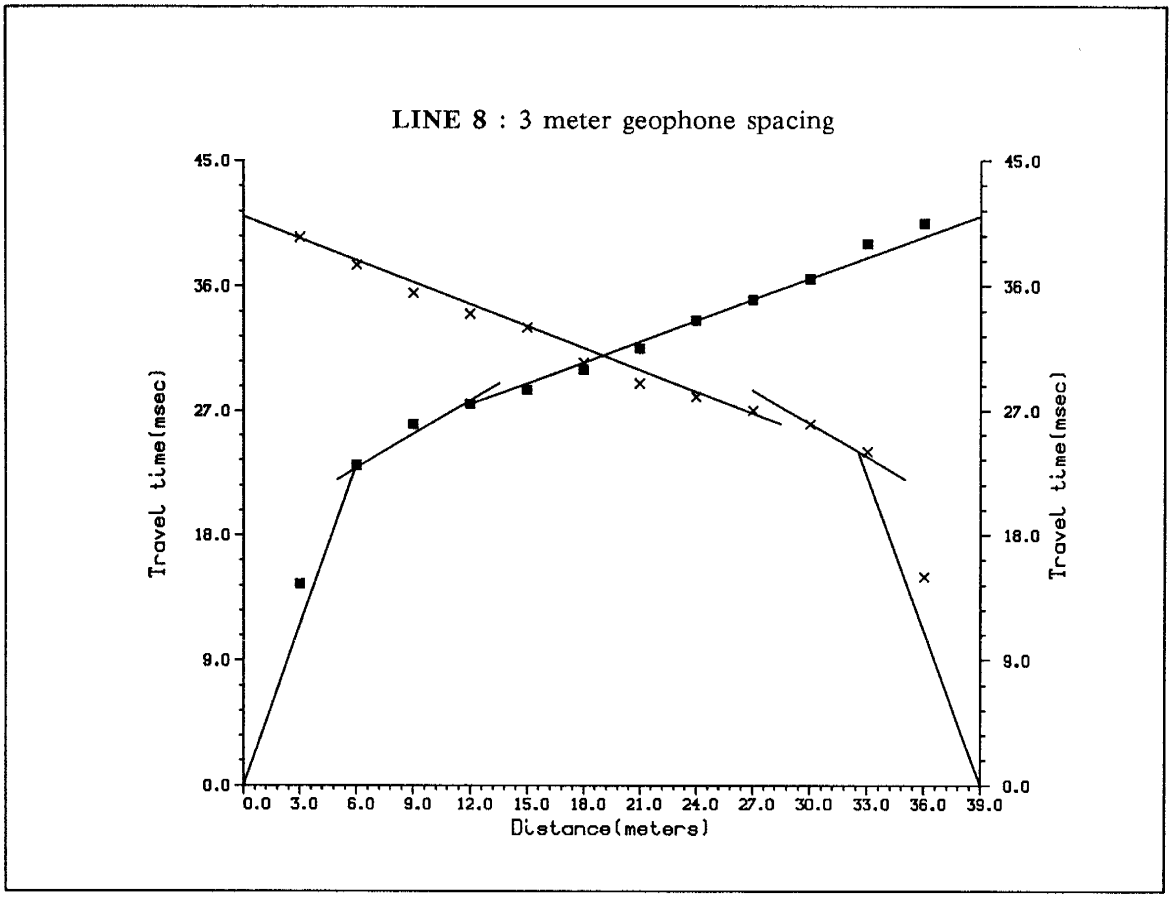

WEST

Apparent

Va1 = 275 m/s
Va2 = 1200 m/s
Va3 = 2000 m/s

EAST

Apparent

Vb1 = 275 m/s
Vb2 = 1250 m/s
Vb3 = 1909 m/s

Actual

V1 = 275 m/s
V2 = 1232 m/s
V3 = 1950 m/s
H1 = 2.6 m
H2 = 1.8 m

LINE 9 : 2 meter geophone spacing

LINE 10 : 5 meter geophone spacing

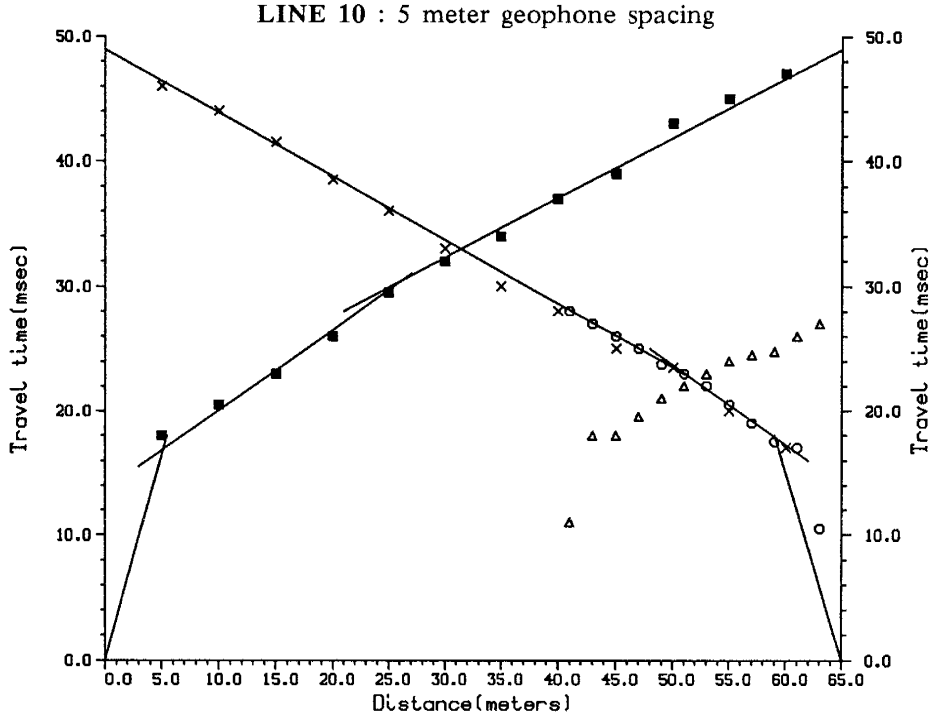

WEST

Apparent

Va1 = 333 m/s
Va2 = 1500 m/s
Va3 = 2125 m/s

EAST

Apparent

Vb1 = 333 m/s
Vb2 = 1600 m/s
Vb3 = 2000 m/s

Actual

V1 = 333 m/s
V2 = 1550 m/s
V3 = 2054 m/s
H1 = 2.4 m
H2 = 3.3 m

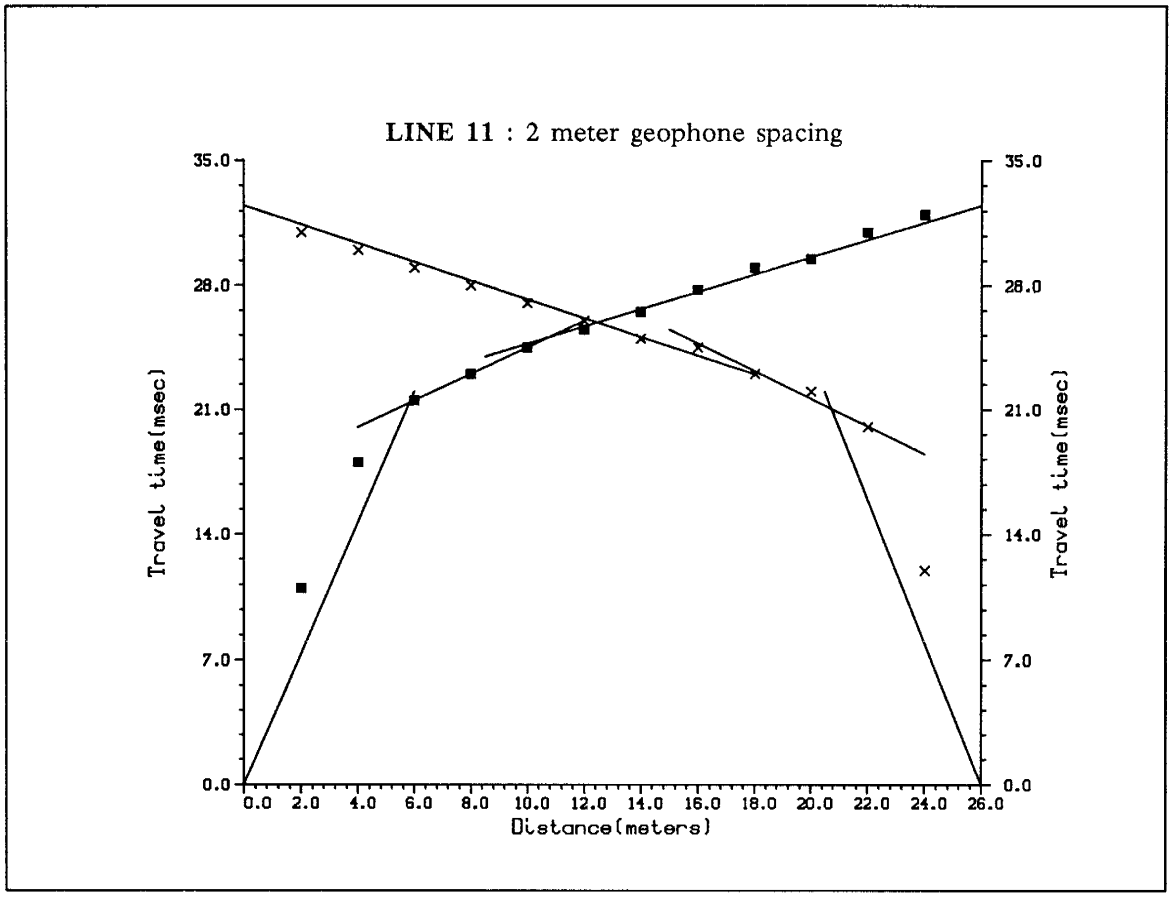

WEST

Apparent

Va1 = 333 m/s
Va2 = 1333 m/s
Va3 = 2000 m/s

EAST

Apparent

Vb1 = 333 m/s
Vb2 = 1333 m/s
Vb3 = 2000 m/s

Actual

V1 = 333 m/s
V2 = 1333 m/s
V3 = 2000 m/s
H1 = 2.9 m
H2 = 1.6 m

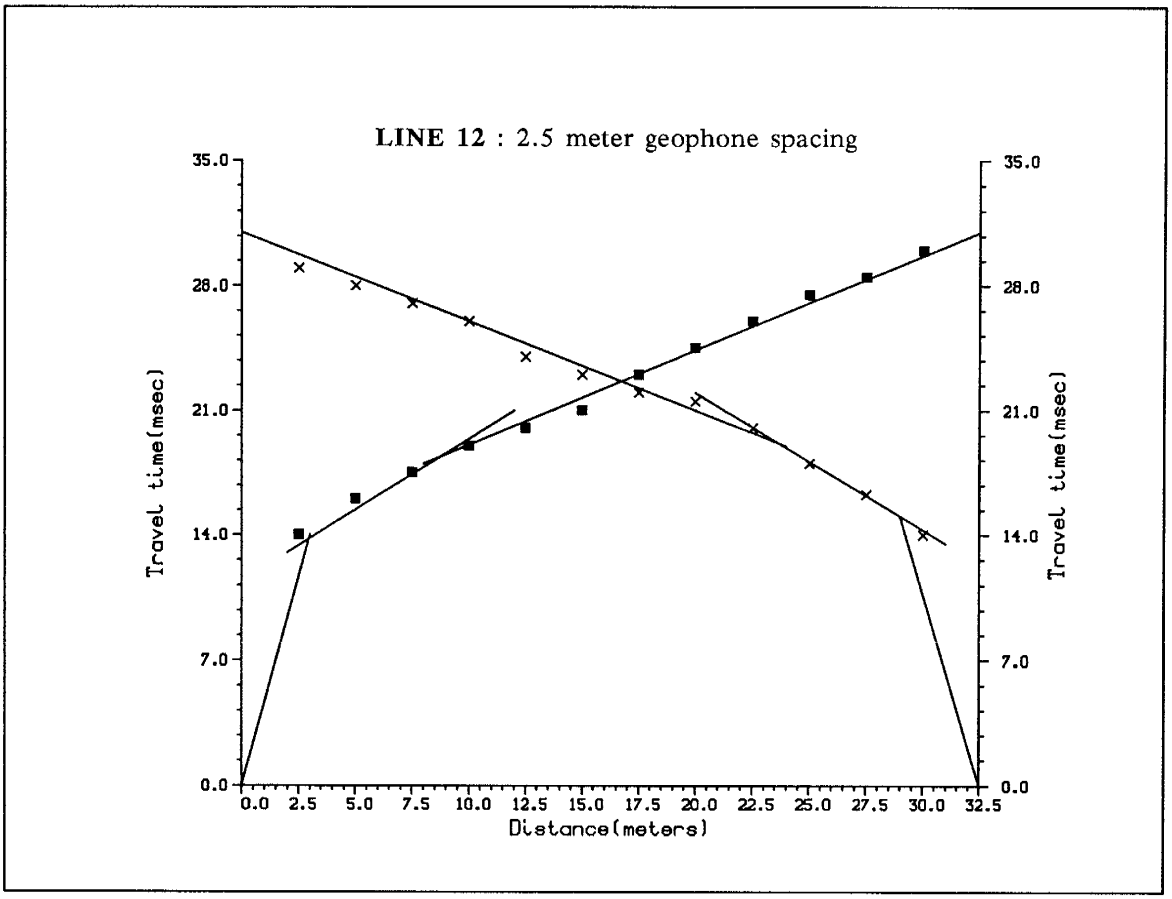

WEST **EAST**

Apparent

Va1 = 250 m/s
Va2 = 1250 m/s
Va3 = 1833 m/s

Apparent

Vb1 = 250 m/s
Vb2 = 1333 m/s
Vb3 = 2000 m/s

Actual

V1 = 250 m/s
V2 = 1287 m/s
V3 = 1916 m/s
H1 = 1.6 m
H2 = 1.5 m

LINE 13 : 3 meter geophone spacing
3 & 6 meter shot offset

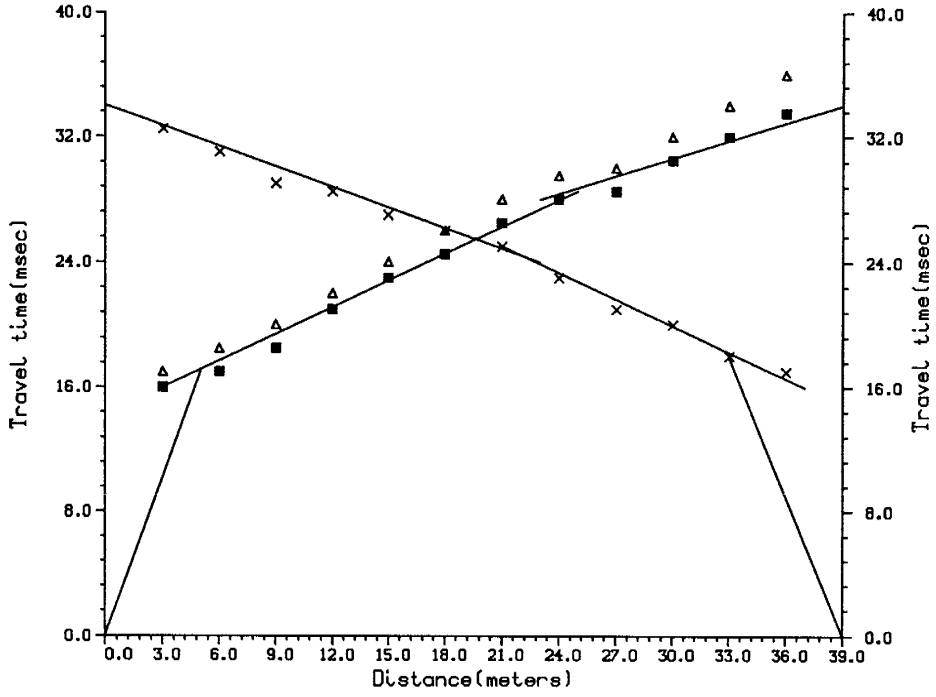

WEST

Apparent

Va1 = 333 m/s
Va2 = 1714 m/s
Va3 = 2250 m/s

EAST

Apparent

Vb1 = 333m/s
Vb2 = 1750 m/s
Vb3 = 2267 m/s

Actual

V1 = 333 m/s
V2 = 1730 m/s
V3 = 2425 m/s
H1 = 2.4 m
H2 = 4.6 m

LINE 14 : 3 meter geophone spacing
LINE 14a : 6 meter geophone spacing

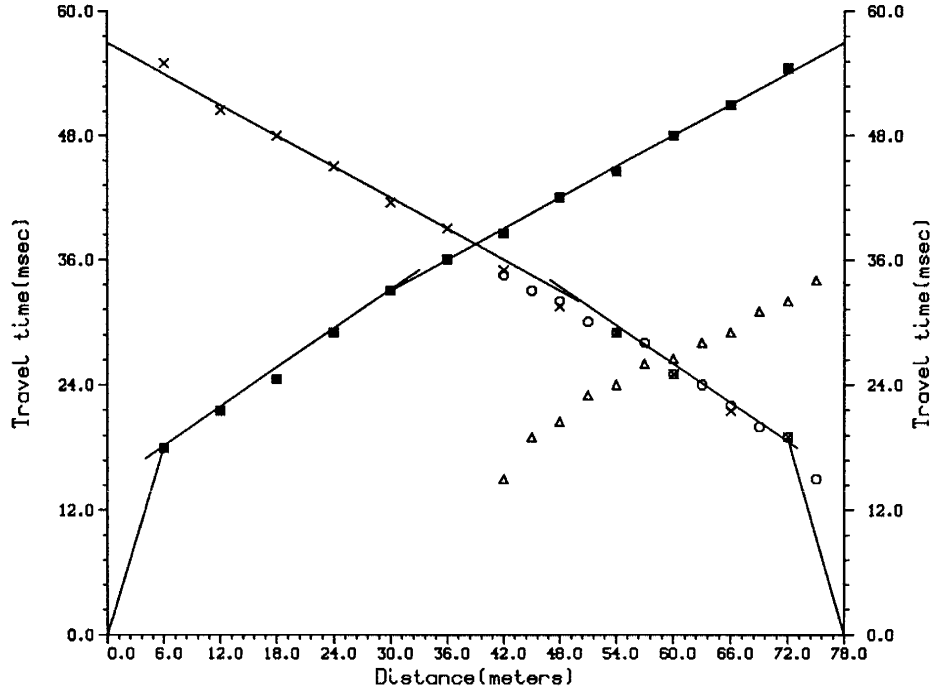

WEST

Apparent

Va1 = 333 m/s
Va2 = 1600 m/s
Va3 = 2000 m/s

EAST

Apparent

Vb1 = 333m/s
Vb2 = 1667 m/s
Vb3 = 2000 m/s

Actual

V1 = 333 m/s
V2 = 1635 m/s
V3 = 1996 m/s
H1 = 2.5 m
H2 = 4.6 m

LINE 16 : 3 meter geophone spacing
3 & 6 meter shot offset

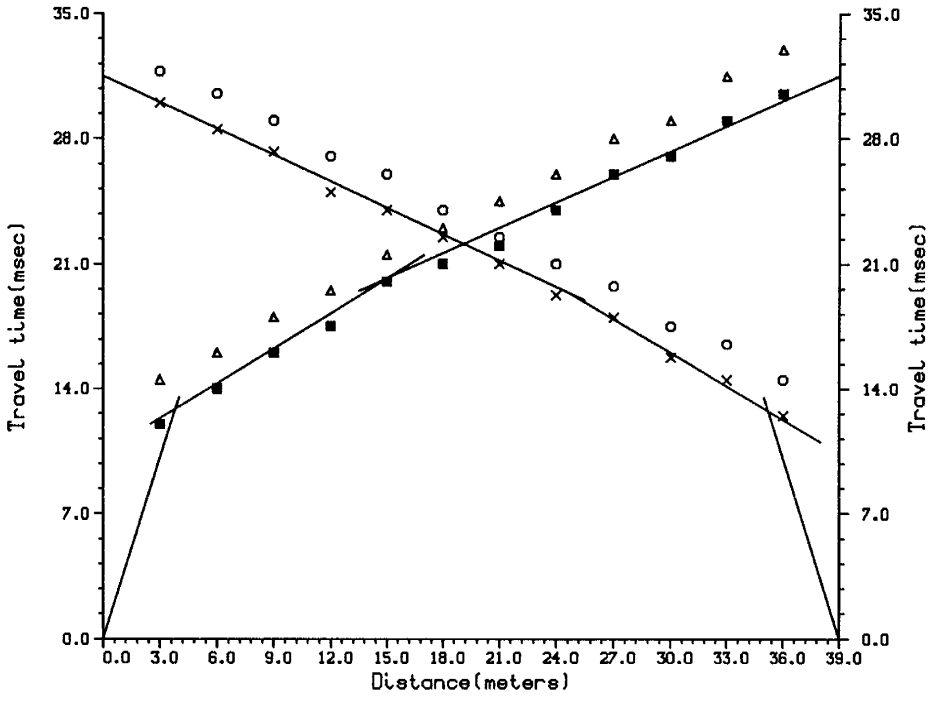

LINE 17 : 2 meter geophone spacing
LINE 17a : 4 meter geophone spacing

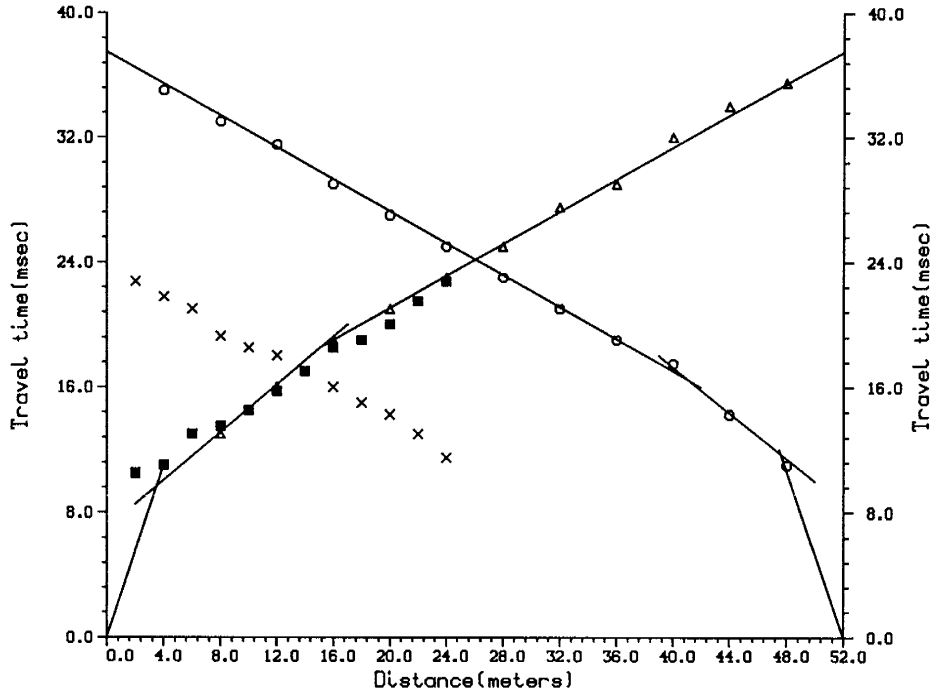

WEST

Apparent

Va1 = 375 m/s
Va2 = 1300 m/s
Va3 = 1960 m/s

EAST

Apparent

Vb1 = 375 m/s
Vb2 = 1333 m/s
Vb3 = 1929 m/s

Actual

V1 = 375 m/s
V2 = 1313 m/s
V3 = 1964 m/s
H1 = 1.5 m
H2 = 2.8 m

LINE 18 : 6 meter geophone spacing
LINE 18a : 2 meter geophone spacing

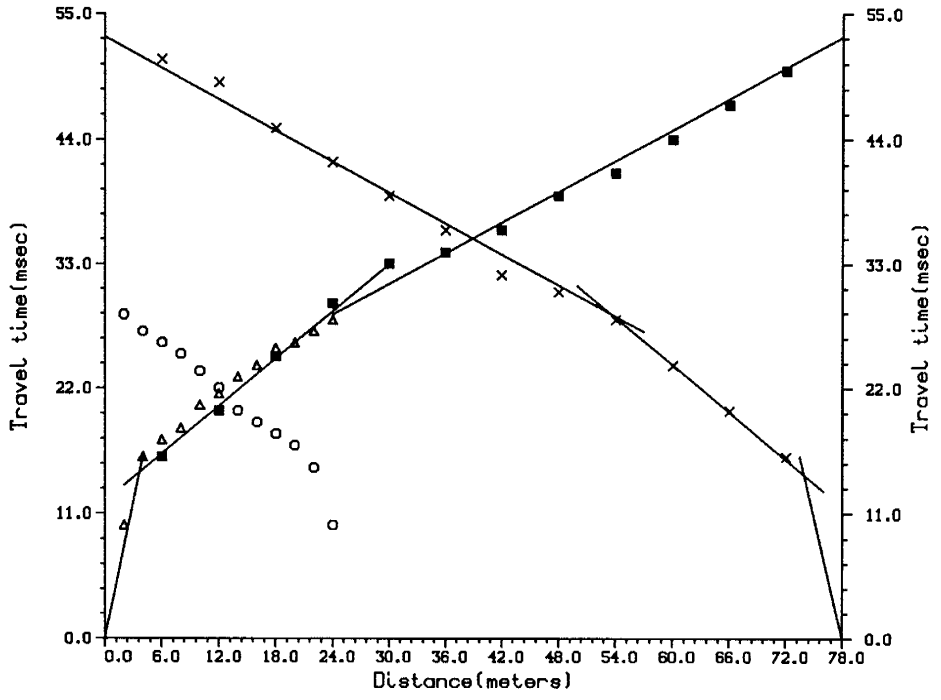

WEST

Apparent

Va1 = 250 m/s
Va2 = 1454 m/s
Va3 = 2250 m/s

EAST

Apparent

Vb1 = 250 m/s
Vb2 = 1444 m/s
Vb3 = 2187 m/s

Actual

V1 = 250 m/s
V2 = 1447 m/s
V3 = 2208 m/s
H1 = 1.5 m
H2 = 5.2 m

LINE 19 : 6 meter geophone spacing
LINE 19a : 2 meter geophone spacing

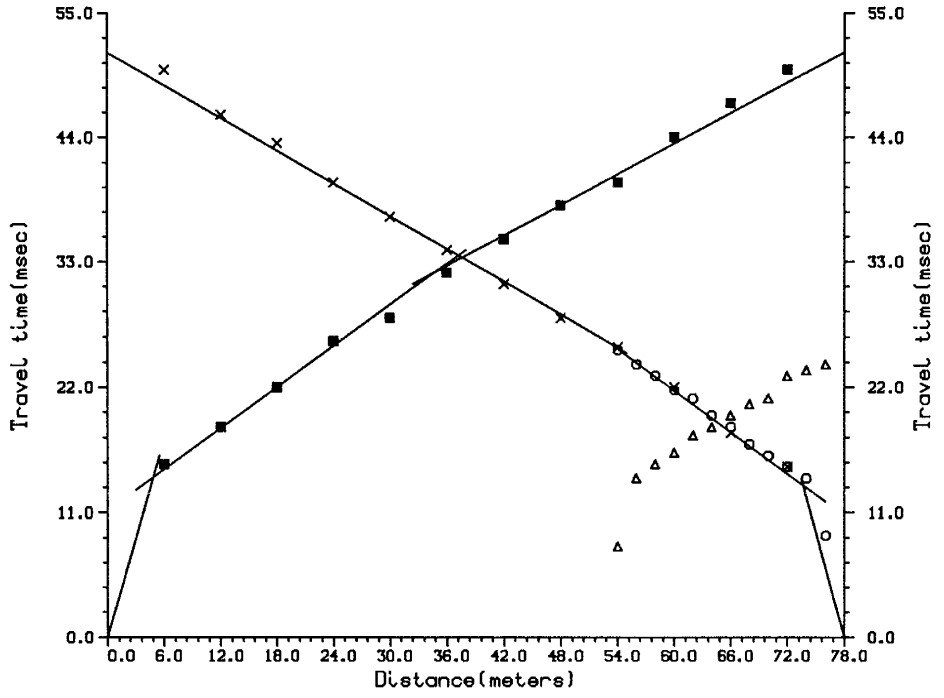

WEST

Apparent

Va1 = 333 m/s
Va2 = 1667 m/s
Va3 = 2200 m/s

EAST

Apparent

Vb1 = 333 m/s
Vb2 = 1667 m/s
Vb3 = 2083 m/s

Actual

V1 = 333 m/s
V2 = 1667 m/s
V3 = 2140 m/s
H1 = 1.9 m
H2 = 5.0 m

LINE 20 : 6 meter geophone spacing
LINE 20a : 1 meter geophone spacing

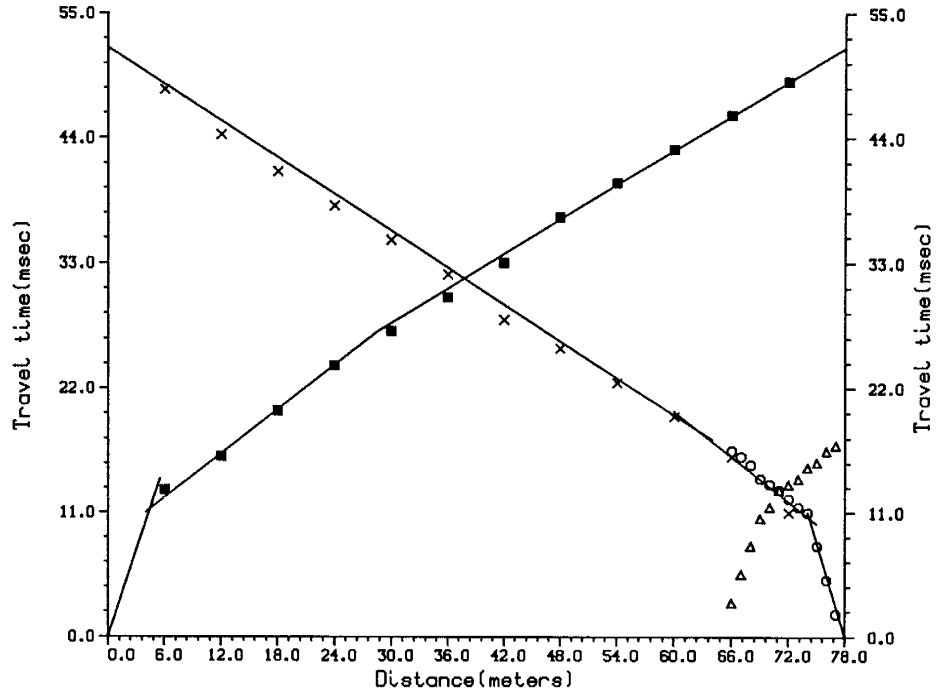

WEST

Apparent

Va1 = 375 m/s
Va2 = 1545 m/s
Va3 = 2000 m/s

EAST

Apparent

Vb1 = 375 m/s
Vb2 = 1545 m/s
Vb3 = 1852 m/s

Actual

V1 = 375 m/s
V2 = 1545 m/s
V3 = 1920 m/s
H1 = 1.5 m
H2 = 4.1 m

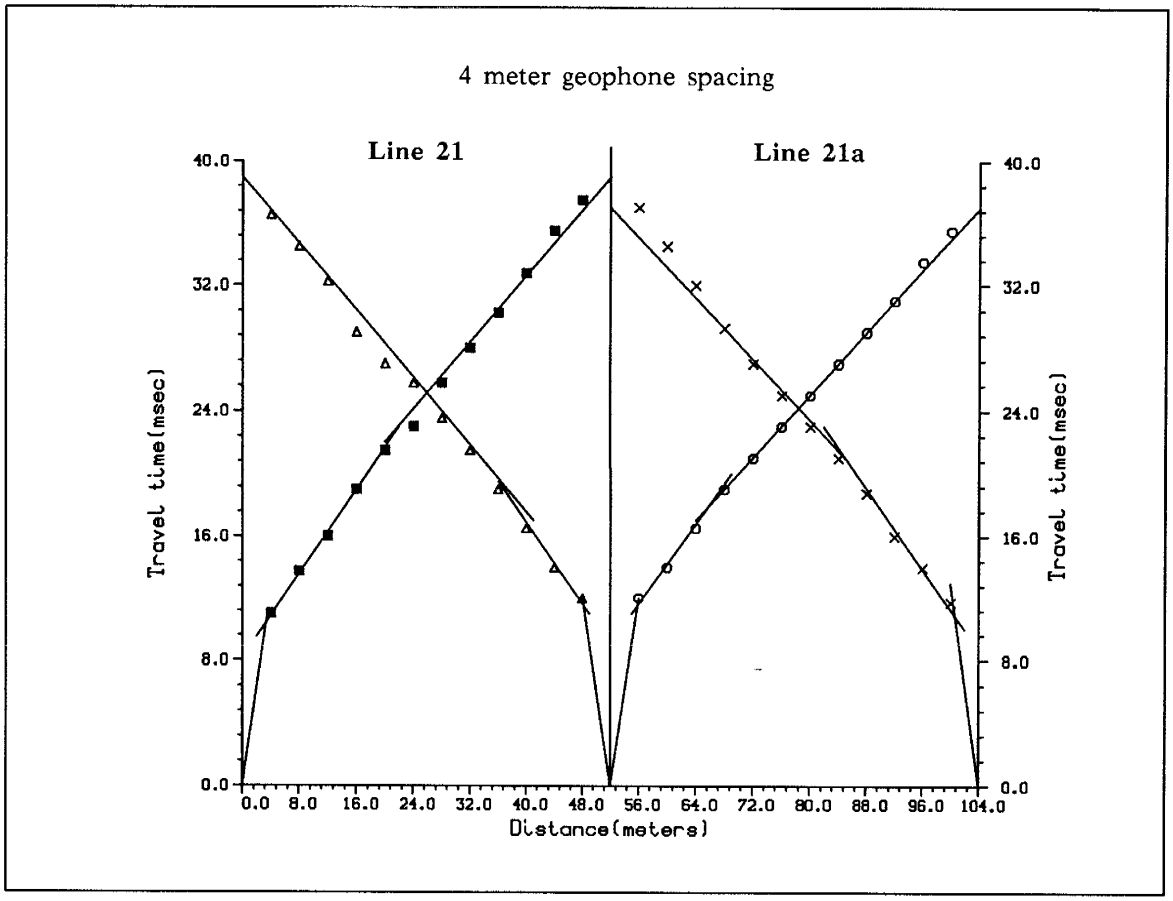

WEST

Apparent

Va1 = 333 m/s
Va2 = 1500 m/s
Vb2 = 1545 m/s
Va3 = 1857 m/s
Vb3 = 1857 m/s

Actual

V1 = 333 m/s
V2 = 1526 m/s
V3 = 1863 m/s
H1 = 1.5 m
H2 = 3.2 m

EAST

Apparent

Va1 = 333 m/s
Va2 = 1555 m/s
Vb2 = 1571 m/s
Va3 = 2000 m/s
Vb3 = 2090 m/s

Actual

V1 = 333 m/s
V2 = 1563 m/s
V3 = 2040 m/s
H1 = 1.5 m
H2 = 3.2 m

LINE 22 : 6 meter geophone spacing
LINE 22a : 2 meter geophone spacing

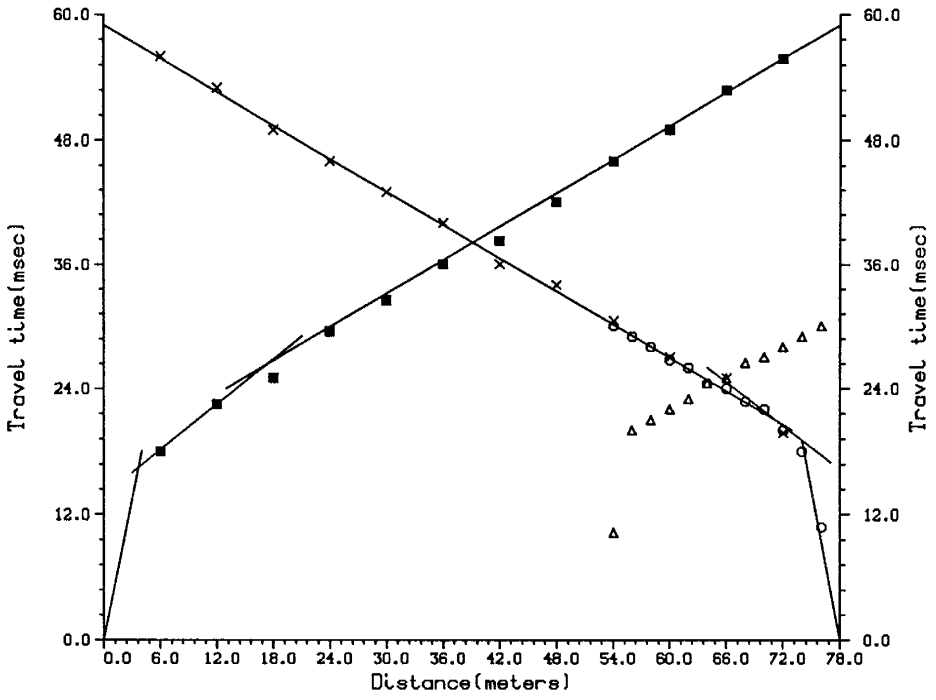

WEST

Apparent

Va1 = 200 m/s
Va2 = 1385 m/s
Va3 = 1860 m/s

EAST

Apparent

Vb1 = 200 m/s
Vb2 = 1580 m/s
Vb3 = 1860 m/s

Actual

V1 = 200 m/s
V2 = 1474 m/s
V3 = 1841 m/s
H1 = 1.5 m
H2 = 3.2 m

LINE 23 : 6 meter geophone spacing
LINE 23a : 2 meter geophone spacing

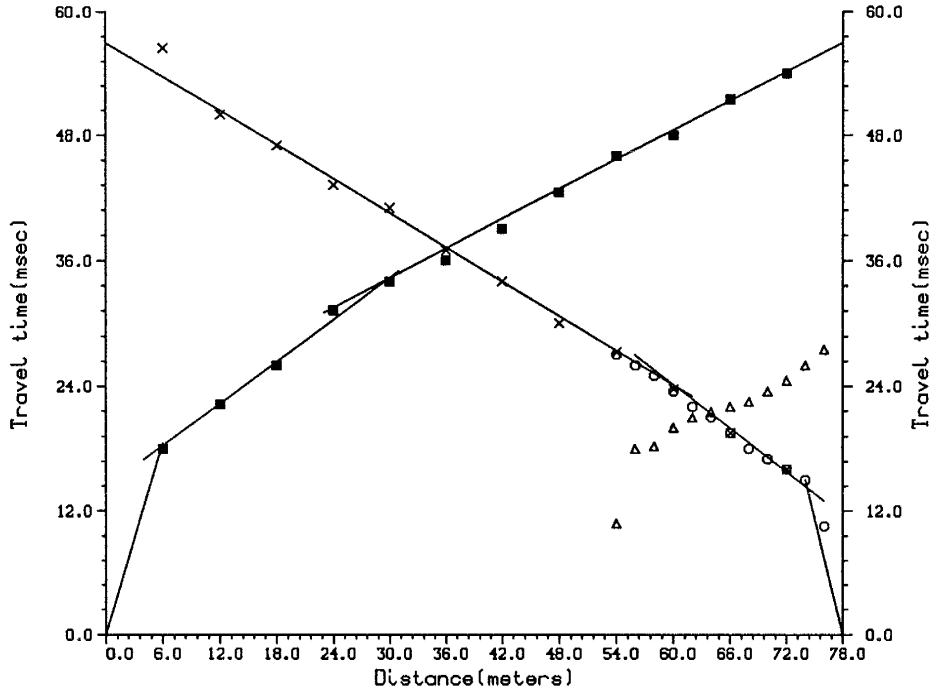

WEST

Apparent

Va1 = 250 m/s
Va2 = 1500 m/s
Va3 = 2125 m/s

EAST

Apparent

Vb1 = 250 m/s
Vb2 = 1444 m/s
Vb3 = 1818 m/s

Actual

V1 = 250 m/s
V2 = 1469 m/s
V3 = 1952 m/s
H1 = 1.6 m
H2 = 4.8 m

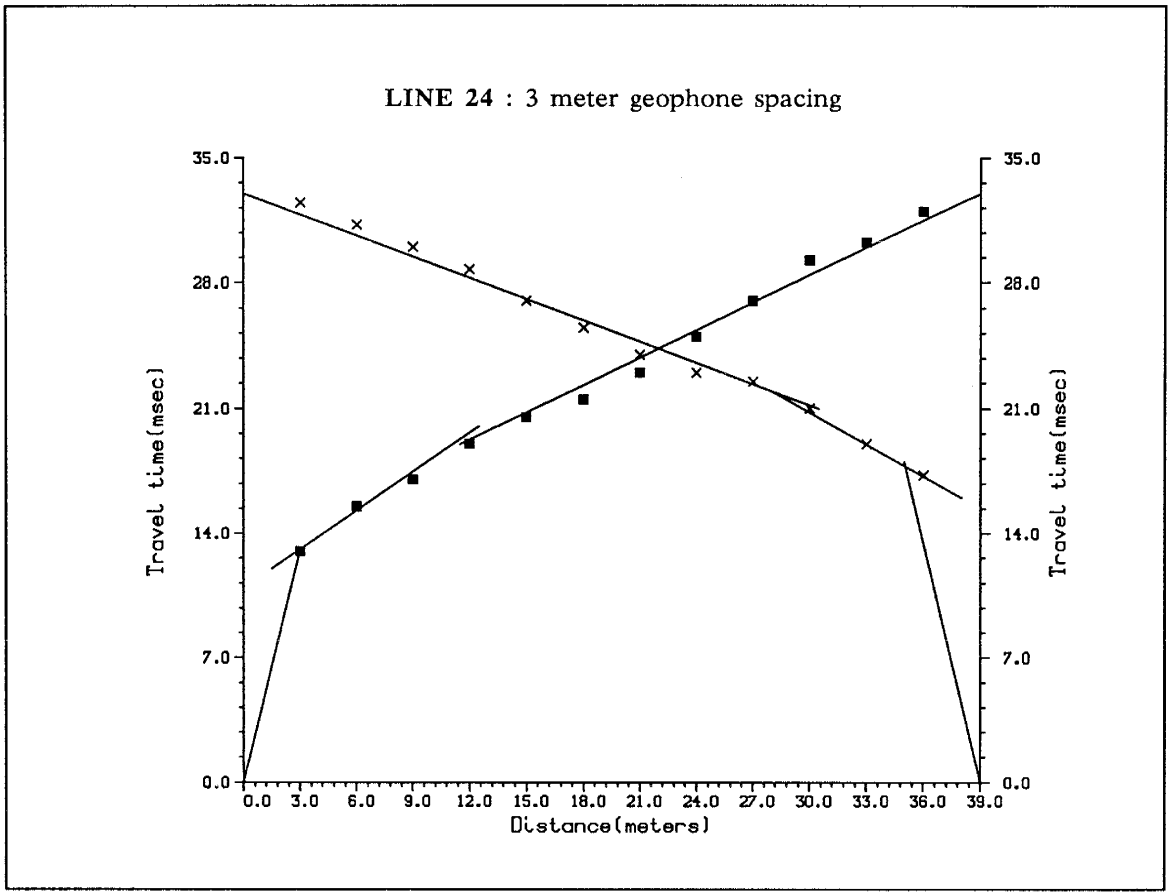

WEST

Apparent

Va1 = 275 m/s
Va2 = 1400 m/s
Va3 = 2000 m/s

EAST

Apparent

Vb1 = 275 m/s
Vb2 = 1650 m/s
Vb3 = 2500 m/s

Actual

V1 = 275 m/s
V2 = 1516 m/s
V3 = 2223 m/s
H1 = 1.9 m
H2 = 3.4 m

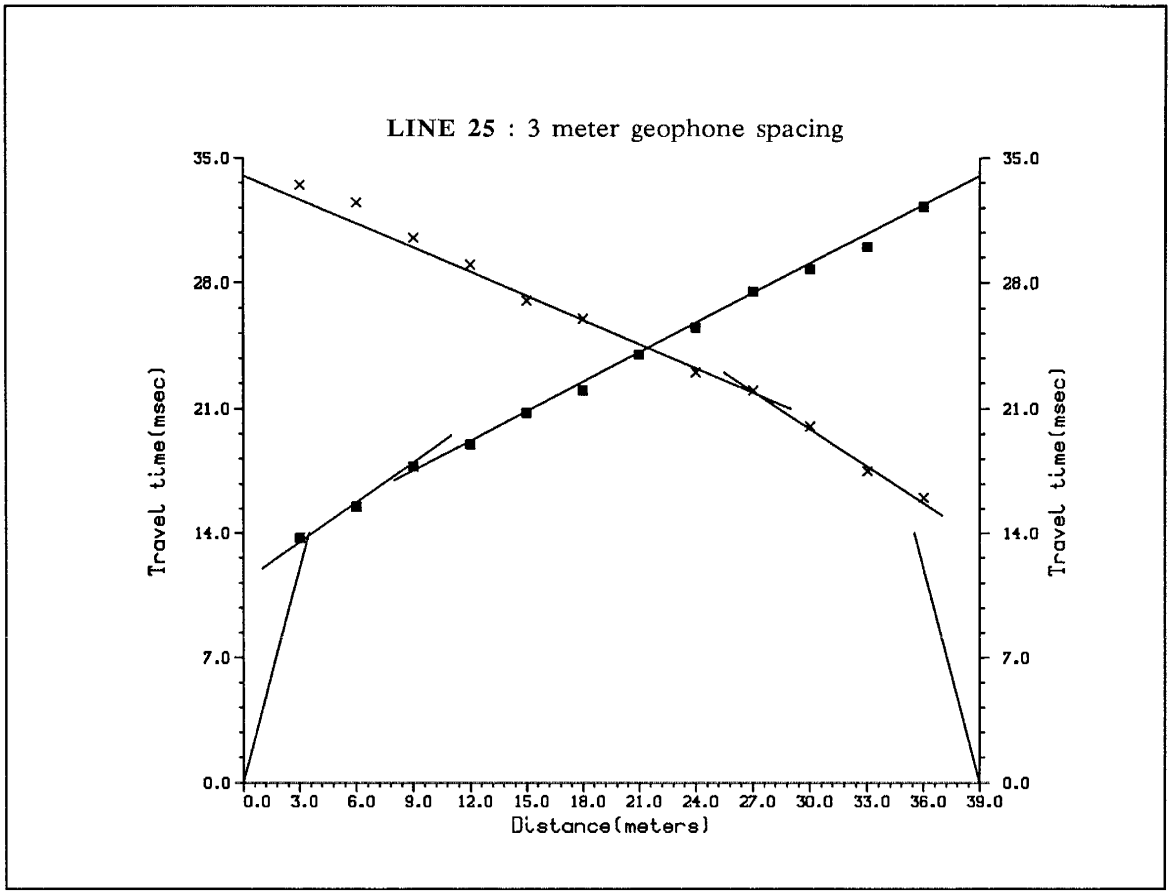

WEST

Apparent

Va1 = 250 m/s
Va2 = 1333 m/s
Va3 = 1860 m/s

EAST

Apparent

Vb1 = 250 m/s
Vb2 = 1444 m/s
Vb3 = 2200 m/s

Actual

V1 = 250 m/s
V2 = 1385 m/s
V3 = 2023 m/s
H1 = 1.6 m
H2 = 1.7 m

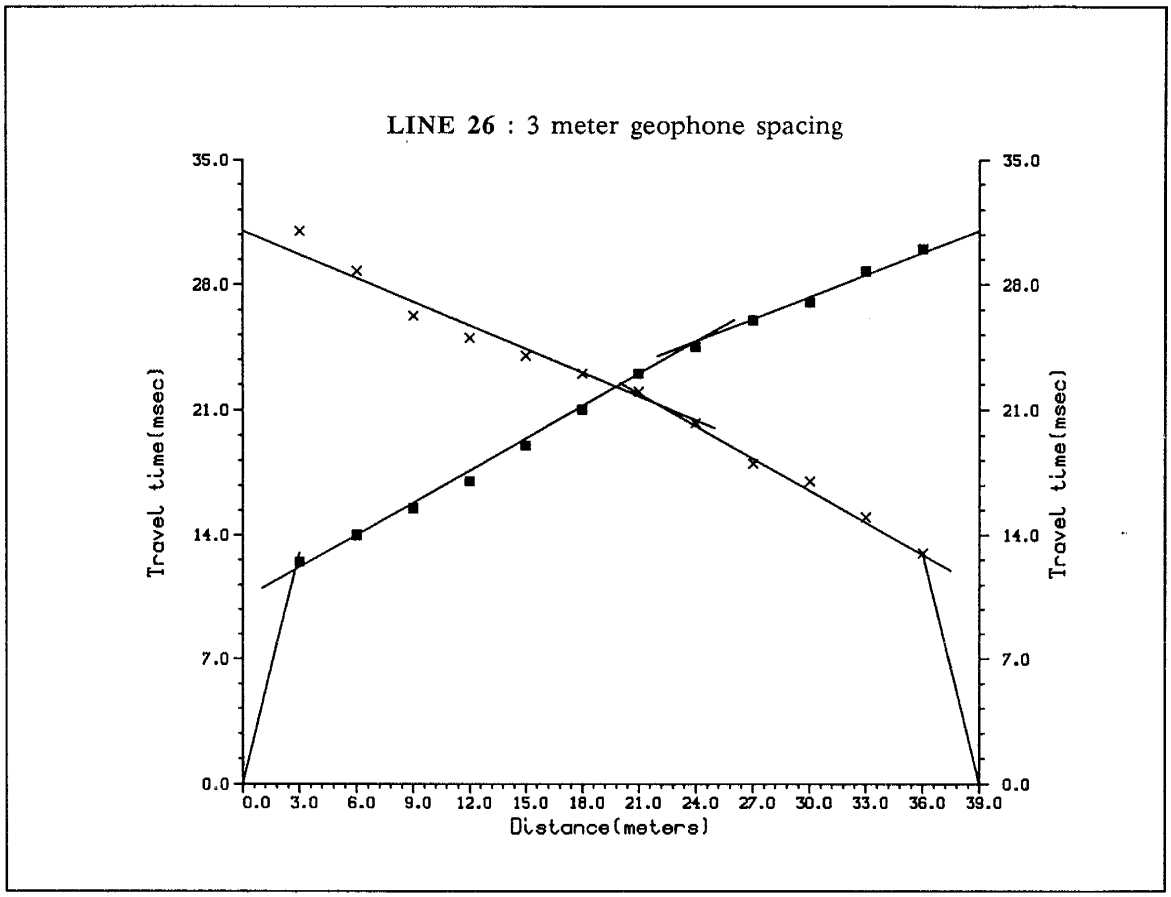

WEST

Apparent

Va1 = 250 m/s
Va2 = 1667 m/s
Va3 = 2500 m/s

EAST

Apparent

Vb1 = 250 m/s
Vb2 = 1667 m/s
Vb3 = 2333 m/s

Actual

V1 = 250 m/s
V2 = 1667 m/s
V3 = 2408 m/s
H1 = 1.4 m
H2 = 3.9 m

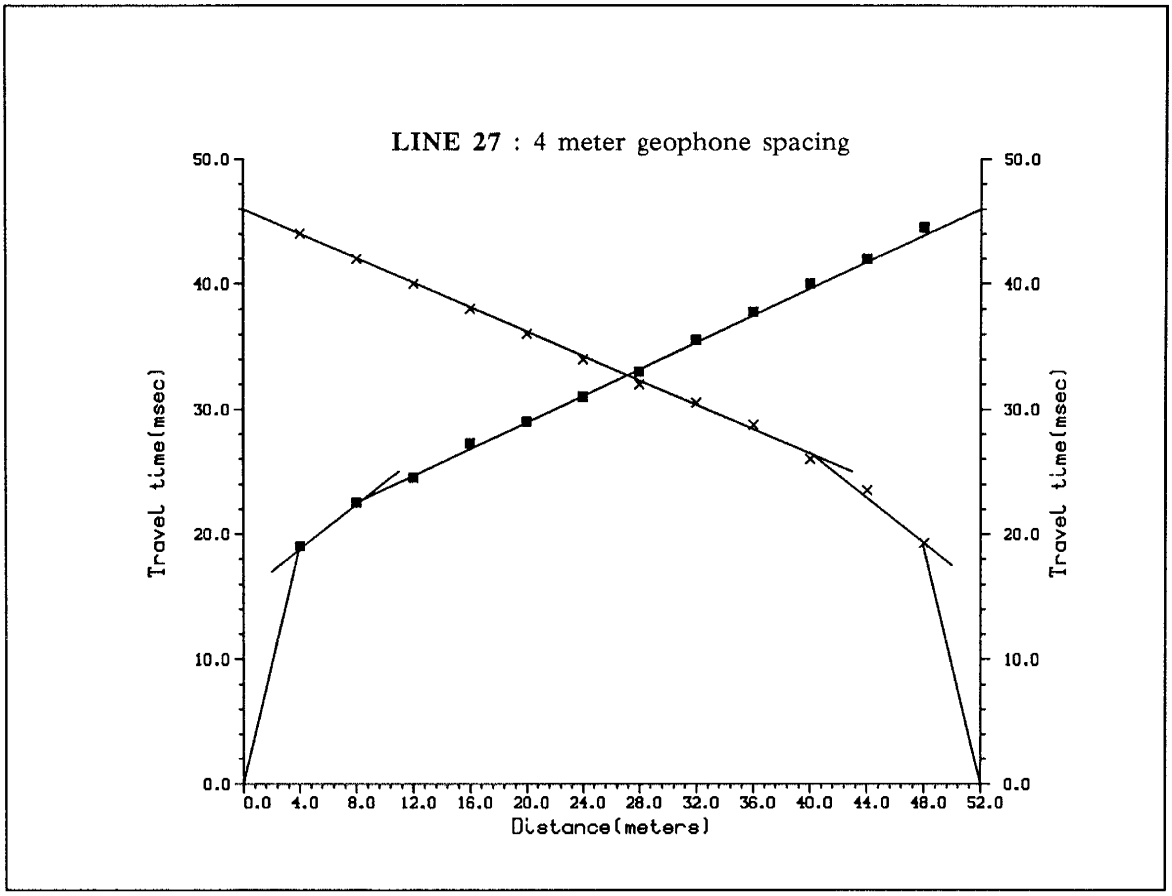

WEST

Apparent

Va1 = 225 m/s
Va2 = 1100 m/s
Va3 = 1900 m/s

EAST

Apparent

Vb1 = 225 m/s
Vb2 = 1111 m/s
Vb3 = 2000 m/s

Actual

V1 = 225 m/s
V2 = 1105 m/s
V3 = 1956 m/s
H1 = 1.8 m
H2 = 2.4 m

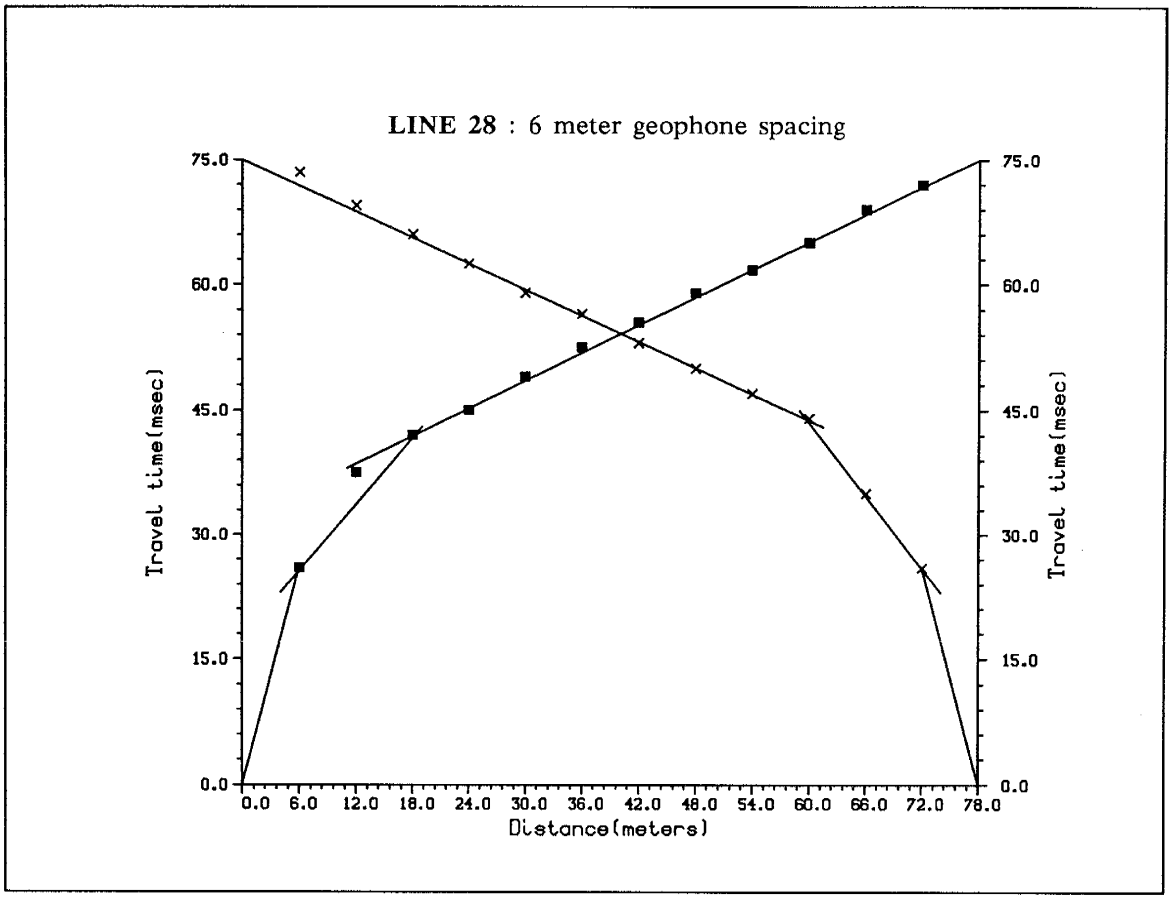

WEST

Apparent

Va1 = 250 m/s
Va2 = 750 m/s
Va3 = 1820 m/s

EAST

Apparent

Vb1 = 250 m/s
Vb2 = 680 m/s
Vb3 = 1930 m/s

Actual

V1 = 250 m/s
V2 = 712 m/s
V3 = 1876 m/s
H1 = 2.3 m
H2 = 5.9 m

APPENDIX B

Seismogram pairs for Line 1, Line 12, Line 13, and Line 17a. Interpretations are shown on the seismograms. Arrivals are labeled for seismograms with a western shotpoint (Va2 or Va3) and seismograms with an eastern shotpoint (Vb2 or Vb3). Secondary arrivals which may represent the V4 layer are also shown by the V4? branch.

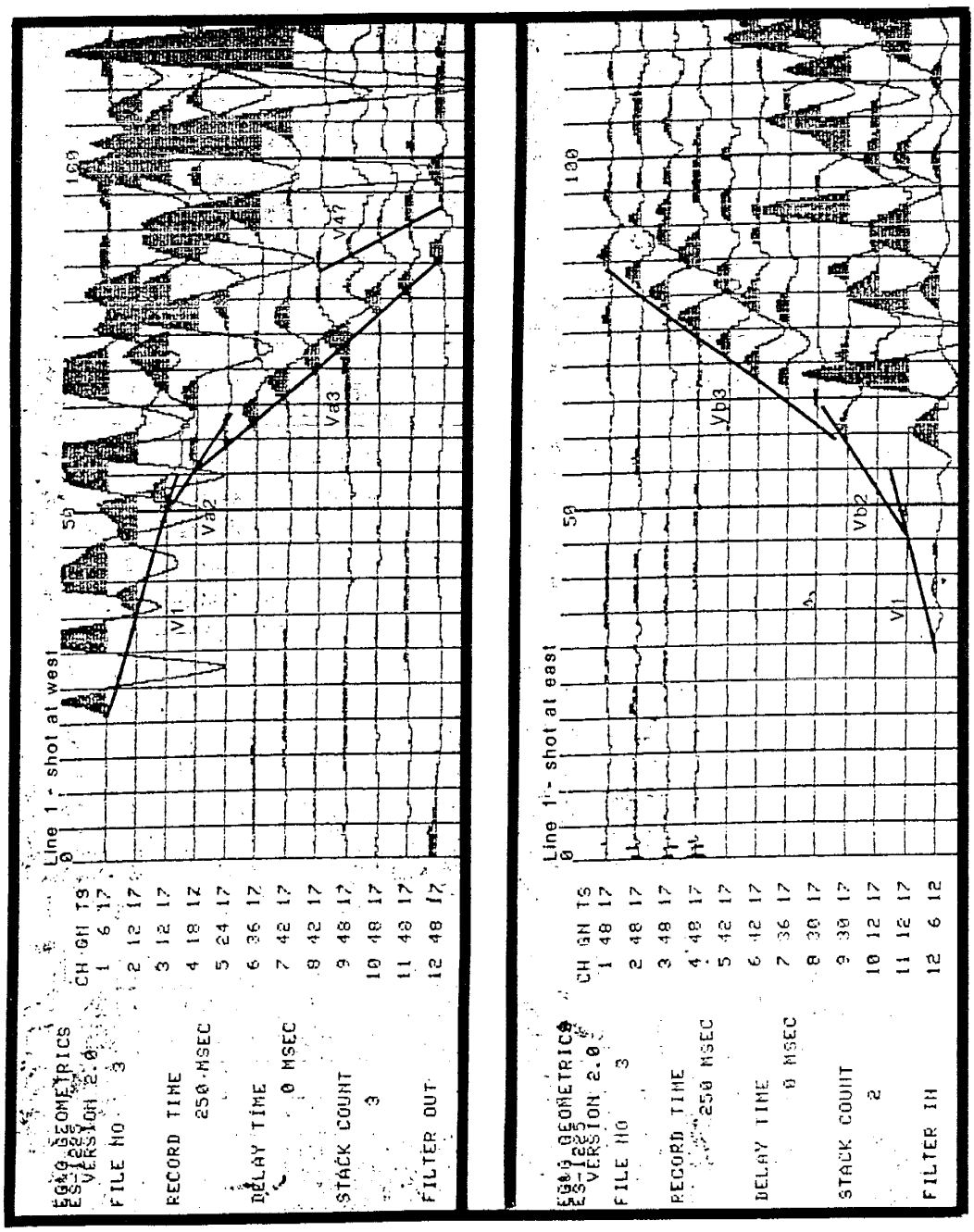
EG&G GEOMETRICS
ES-1225
VERSION 2.0
FILE NO 3
RECORD TIME
250 MSEC
DELAY TIME
0 MSEC
STACK COUNT
3
FILTER OUT
CH GN TS
1 6 17
2 12 17
3 12 17
4 18 12
5 24 17
6 36 12
7 42 17
8 42 17
9 48 17
10 48 17
11 48 17
12 48 17
Line 1 - shot at west
0
50
100
V1
Va2
Va3
V47
EG&G GEOMETRICS
ES-1225
VERSION 2.0
FILE NO 3
RECORD TIME
250 MSEC
DELAY TIME
0 MSEC
STACK COUNT
2
FILTER IN
CH GN TS
1 48 17
2 48 17
3 48 17
4 48 17
5 42 17
6 42 17
7 36 17
8 30 17
9 30 17
10 12 17
11 12 17
12 6 12
Line 1 - shot at east
0
50
100
Vb3
Vb2
V1

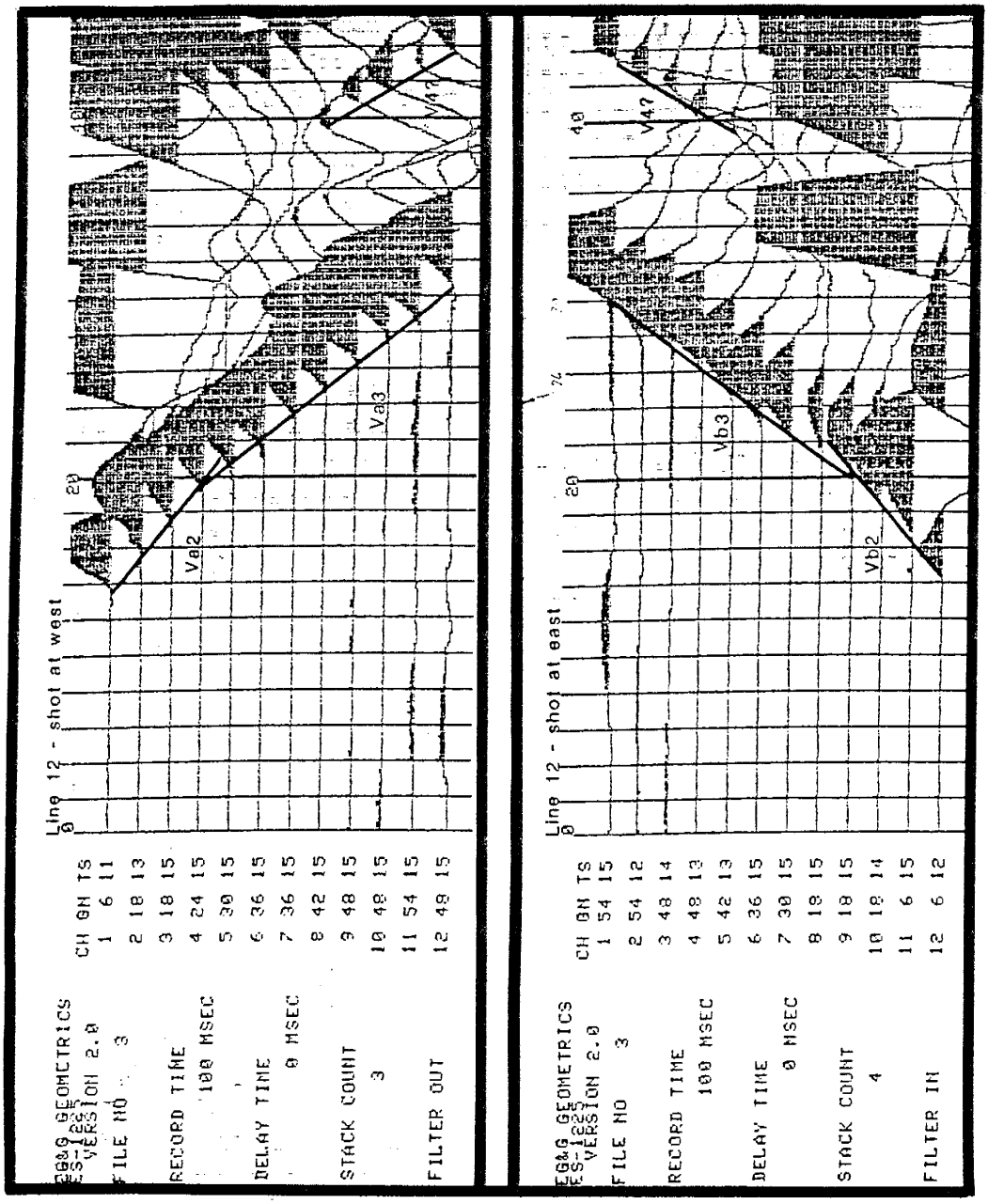
EG&G GEOMETRICS
ES-1225
VERSION 2.0
FILE NO 3
RECORD TIME
100 MSEC
DELAY TIME
0 MSEC
STACK COUNT
3
FILTER OUT
CH ON TS
1 6 11
2 18 13
3 18 15
4 24 15
5 30 15
6 36 15
7 36 15
8 42 15
9 48 15
10 48 15
11 54 15
12 48 15
Line 12 - shot at west
0
20
40
Va2
Va3
Va4
EG&G GEOMETRICS
ES-1225
VERSION 2.0
FILE NO 3
RECORD TIME
100 MSEC
DELAY TIME
0 MSEC
STACK COUNT
4
FILTER IN
CH ON TS
1 54 15
2 54 12
3 48 14
4 48 13
5 42 13
6 36 15
7 30 15
8 18 15
9 18 15
10 18 14
11 6 15
12 6 12
Line 12 - shot at east
0
20
40
Vb2
Vb3
Va4

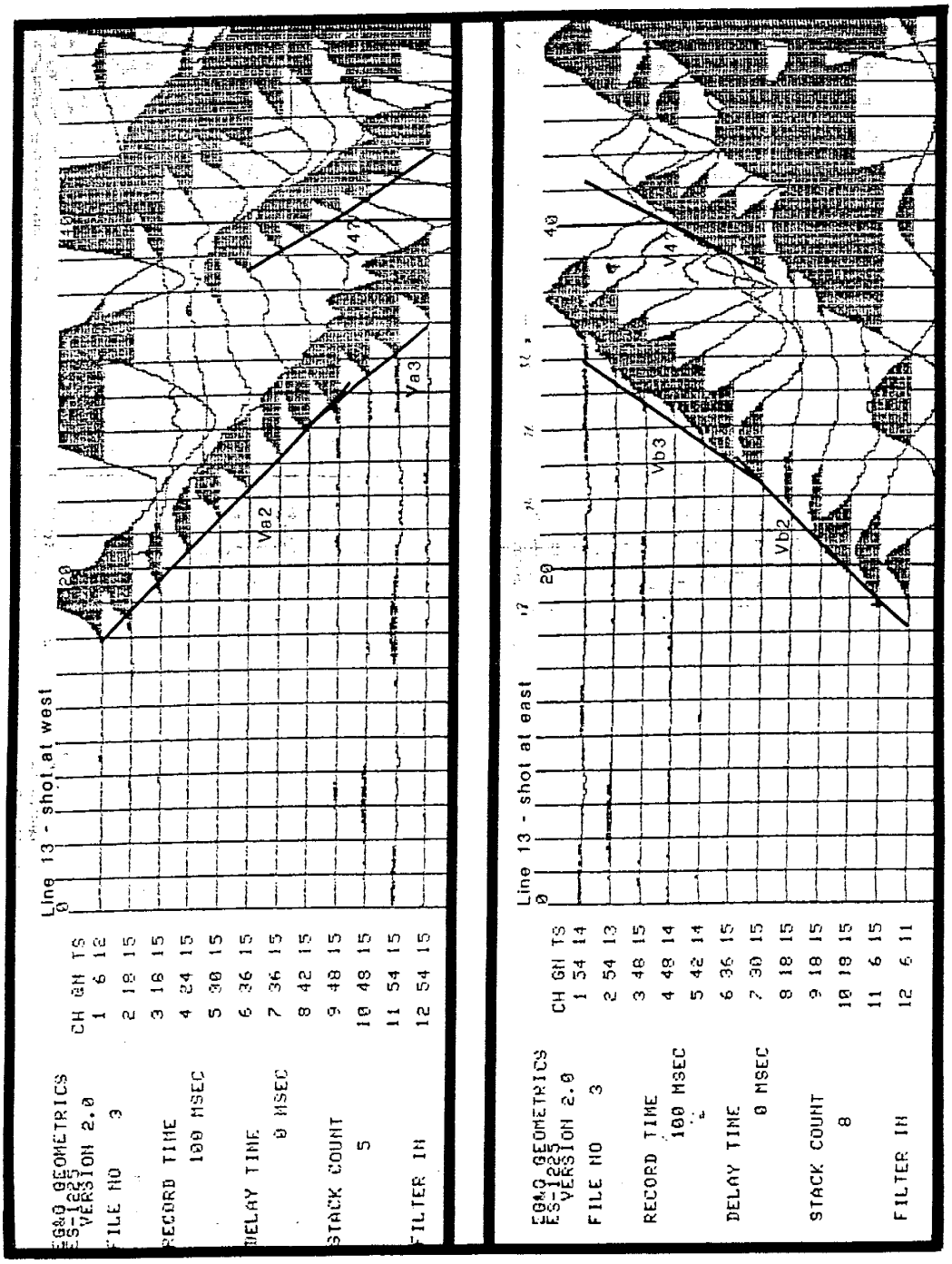
EG&G GEOMETRICS
ES-1225
VERSION 2.0
FILE NO 3
RECORD TIME
100 MSEC
DELAY TIME
0 MSEC
STACK COUNT
5
FILTER IN
CH GN TS
1 6 12
2 18 15
3 18 15
4 24 15
5 30 15
6 36 15
7 36 15
8 42 15
9 48 15
10 48 15
11 54 15
12 54 15
Line 13 - shot at west
Va2
Va3
Va4
EG&G GEOMETRICS
ES-1225
VERSION 2.0
FILE NO 3
RECORD TIME
100 MSEC
DELAY TIME
0 MSEC
STACK COUNT
8
FILTER IN
CH GN TS
1 54 14
2 54 13
3 48 15
4 48 14
5 42 14
6 36 15
7 30 15
8 18 15
9 18 15
10 18 15
11 6 15
12 6 11
Line 13 - shot at east
Vb2
Vb3
Vb4

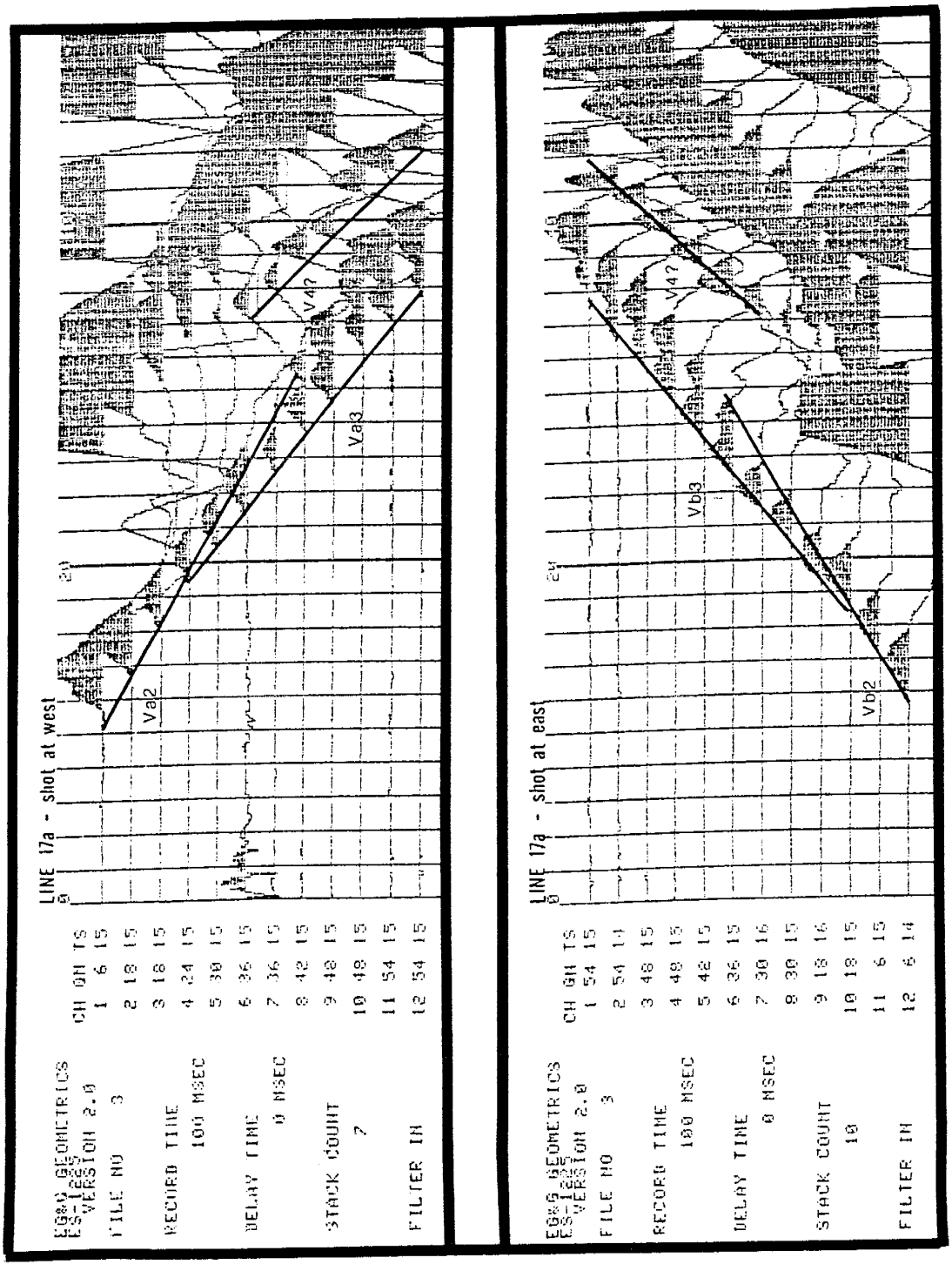
LINE 17a - shot at west
EG&G GEOMETRICS
ES-1225
VERSION 2.0
FILE NO 3
RECORD TIME
100 MSEC
DELAY TIME
0 MSEC
STACK COUNT
7
FILTER IN
CH GH TS
1 6 15
2 18 15
3 18 15
4 24 15
5 30 15
6 36 15
7 36 15
8 42 15
9 48 15
10 48 15
11 54 15
12 54 15
Va2
Va3
V4?
LINE 17a - shot at east
EG&G GEOMETRICS
ES-1225
VERSION 2.0
FILE NO 3
RECORD TIME
100 MSEC
DELAY TIME
0 MSEC
STACK COUNT
10
FILTER IN
CH GH TS
1 54 15
2 54 14
3 48 15
4 48 15
5 42 15
6 36 15
7 30 16
8 30 15
9 18 16
10 18 15
11 6 15
12 6 14
Vb2
Vb3
V4?